

UAV Laser Scanning for DTM Generation in Coastal Areas

Charis Chatzikyriakou

MSc Thesis

Optical and Laser Remote Sensing
Department of Geoscience and Remote Sensing
Delft University of Technology
14 August 2017



Cover illustration: Phoenix's aerial system Alpha AL3-32 is mounted on the minivan of Shore Monitoring & Research B.V. during the first test use of the system in September, 2015. In the background, the study area in Schelphoek, Zeeland, can be seen.

UAV Laser Scanning for DTM Generation in Coastal Areas

by

Charis Chatzikyriakou

to obtain the degree of Master of Science
at the Delft University of Technology,
to be defended publicly on Monday August 14, 2017 at 12:45 PM.

Student Number:	4420292	
Thesis committee:	Prof. dr. Massimo Menenti,	TU Delft, Graduation Professor
	Dr. Roderik Lindenbergh,	TU Delft, Daily supervisor
	Dr. ir. Matthieu de Schipper,	Co-reader and Managing Director of Shore Monitoring & Research B.V.
	Ir. Roeland de Zeeuw,	Managing Director of Shore Monitoring & Research B.V.

An electronic version of this thesis is available at <http://repository.tudelft.nl/>.

Abstract

The Netherlands is a country primarily developed on coastal zones. Coastal zones are very important, since they are a source of valuable living and non-living resources for its population, and they also act as a natural protection against floods. Notably, the natural dynamics driven by the sea as well as the man-made actions on the land change them continuously. As a consequence, the need for systematic coastal protection and management arises, for which coastal monitoring is of paramount necessity. The emergence of remote sensing in this field has been proven to have many advantages, especially due to the large coverage that it offers in a time- and cost-efficient way. Thus, the subject of this study is one of these remote sensing techniques, specifically the UAV Laser Scanning.

UAV Laser Scanning has been introduced in the field of coastal monitoring quite recently, yet it has already proven to be a useful tool, outperforming the other methods used for the same purpose in a number of aspects. Its high accuracy and resolution coupled with flexibility and time efficiency make it a very promising technique. It works on the same principle as all the other laser scanning techniques. Its system components are a platform (drone), a laser scanner, a GNSS receiver and an Inertial Measurement Unit (IMU). The aerial system used in this study Alpha AL3-32, by Phoenix LiDAR Systems, in combination with a DJI Spreading Wings S1000 Octocopter. One of the main aims of this study was to investigate the error budget of that system and its impact on the positioning accuracy.

The sources of error in such a system are its three main components as well as possible misalignments between these components, that cause bore-sight and lever-arm errors, coordinate system transformations and temporal interpolation issues. Herein, an error model was used for the determination of the quantitative impact of them on the positioning accuracy. Using the uncertainties of the instruments that Alpha AL3-32 consists of, the a priori positioning accuracy of the system was estimated equal to 2 cm. In addition, its dependency on the flight parameters was proven. The a posteriori positioning accuracy was derived by investigating a small flat dataset of the UAV Laser Scanning point cloud and was estimated to be 2 cm as well. From the same dataset, the precision was also computed as being equal to 4 cm.

When it comes to the products of this technique, one of the main methods to analyse the morphological changes in coastal zones is by comparing Digital Terrain Models (DTMs) from different epochs. Thus, the generation of accurate DTMs was the other important objective of this study. The standard procedure includes preparation of the dataset, noise removal and above ground analysis. After the ground-only dataset was derived, it was converted into a grid using interpolation, namely the Moving Average or Moving Planes method. The grid size of the DTM can go down to 5 cm. In addition, the RMSE between the UAV Laser Scanning only-ground point cloud and the derived DTM was computed equal to 4 cm, while the DTM accuracy in height was estimated equal to 8 cm by using an empirical formula based on the point density and the slope of the terrain.

Considering the 3D coordinate accuracy that can be achieved with such a system as well as the DTM quality, UAV Laser Scanning was found to be an appropriate technique for coastal monitoring, presenting important advantages over other competing methods. It can reduce the time and cost of surveys at the coastal zones and at the same time maintain high resolution with its high point density.

Acknowledgements

The present Master thesis brings me to the end of my Master programme in the Department of Geoscience and Remote Sensing, but most importantly it brings me to the end of my "career" as a student. It has been a long trip that gave me tons of new knowledge and valuable experiences. But, as it happens with every trip, the thing that I am mostly grateful of is the people that were with me all this time. Therefore, I would like to dedicate the next paragraphs to thank them individually.

I couldn't start with anybody else but my Daily supervisor, Dr. Roderik Lindenbergh. I would like to thank Roderik so much for his kind guidance and support during the whole thesis, his unlimited new ideas for solutions and his understanding. I will truly miss those meeting full of laughter! I would like to thank my Graduation Professor, Prof. dr. Massimo Menenti, for his very useful feedback both on the processing and the writing part. I would also like to thank my Co-reader, Dr. ir. Matthieu de Schipper, for his advice on the improvement of this study and the report. Last but not least, I would like to thank Ir. Roeland de Zeeuw, from Shore Monitoring and Research B.V., for the guidance during the processing of the data and his endless ideas for further improvement.

Next, I would like to say a big thank you to my parents, Apostolis and Voula. They made this "trip" possible for me and their faith and support has always been a source of strength and motivation. A big thank you also to my siblings, Pepi, Tota and Philippos, for keeping me on track and supporting me all this time.

In addition, I want to thank so much my friends, both those that I met here and the ones back home. A big thank you to Elizabeth for her non-stop support, either from Delft or from far away, for her valuable help during my fieldwork and for distracting me for nice strolls. Thank you also to Sonia for supporting me constantly even though she is far, and Jerry and Andrea for their motivation. Finally, a huge thank you to Bartek for his understanding, endless support and motivation these last months.

Not to forget, I would like to thank my dance team for filling this past year with fun and spins!

*Charis Chatzikyriakou
Delft, August 2017*

Table of Contents

List of Figures	xi
List of Tables	xv
List of Abbreviations	xvii
1 Introduction	1
1.1 Motivation	1
1.2 Research objective and questions	2
1.3 Research Methodology	3
1.4 Thesis outline	4
2 Coastal Monitoring	7
2.1 The importance of Coastal Monitoring	7
2.2 Dutch coast characteristics	9
2.3 Data acquisition techniques	11
2.3.1 ARGUS video systems	12
2.3.2 Terrestrial Laser Scanning (TLS)	13
2.3.3 Photogrammetry	13
2.3.4 Airborne Laser Scanning (ALS)	14
2.4 Shore Monitoring & Research B.V.	14
2.5 Summary	15
3 UAV Laser Scanning	17
3.1 Background information on UAV Laser Scanning	17
3.2 The method of UAV Laser Scanning	19
3.3 The system components of a UAV Laser Scanning system.	20
3.3.1 Unmanned Aerial Vehicle (UAV)	20
3.3.2 Laser Scanner	21
3.3.3 GNSS receiver	22
3.3.4 Inertial measurement unit (IMU)	22
3.4 Phoenix's <i>Alpha AL3-32</i> 3D Laser Mapping System	22
3.4.1 UAV: DJI Spreading Wings S1000 Octocopter.	23
3.4.2 Velodyne HDL-32E: High Definition Real-Time 3D LiDAR sensor	23
3.4.3 Navigation System	24
3.4.4 Inertial Measurement Unit (IMU): KVH 1750.	25
3.5 Other available UAV Laser Scanning systems	25
3.5.1 RIEGL Laser Measurement Systems	25
3.5.2 YellowScan.	27
3.5.3 Routescene	28
3.6 Summary	30

4	Fieldwork - Validation Data Acquisition	33
4.1	Description of the study area	33
4.2	Fieldwork preparation and description of instruments	35
4.2.1	Terrestrial Laser Scanning instruments	36
4.2.2	GPS instruments	38
4.3	Acquisition of Terrestrial Laser Scanning data.	39
4.4	Acquisition of GPS data	41
4.5	Summary	41
5	UAV Laser Scanning point quality assessment	43
5.1	Data quality considerations	43
5.1.1	Accuracy and Precision	43
5.1.2	Types of errors	44
5.2	Sources of error in UAV Laser Scanning systems	45
5.2.1	Laser scanner errors	46
5.2.2	GPS errors	47
5.2.3	IMU errors	48
5.2.4	Temporal interpolation errors	48
5.2.5	Instrument misalignment errors	48
5.2.6	Coordinate system transformation errors	49
5.3	Error analysis and accuracy estimation for the Alpha AL3-32	49
5.3.1	Error model for ALS positioning accuracy	50
5.3.2	Error budget	51
5.3.3	Positioning accuracy	52
5.4	Flight planning	56
5.5	Summary	59
6	Post-processing methodologies	61
6.1	Preparation of the point cloud	61
6.2	Noise removal.	62
6.3	Above ground analysis	63
6.4	DTM and DSM generation	63
6.4.1	DTM data redundancy.	65
6.5	Validation.	65
6.5.1	A posteriori errors of the 3D coordinates.	65
6.5.2	Point cloud validation with TLS data	66
6.5.3	DTM quality	66
6.6	Summary	67
7	UAV Laser Scanning post-processing and validation results	69
7.1	Calculation of the vertical accuracy	69
7.2	Preparation of the dataset and noise removal	73
7.3	Above ground analysis	75
7.4	Generation of Digital Terrain Models	78
7.4.1	Grid size	79
7.4.2	Interpolation method	81
7.4.3	Number of neighbours.	84

7.5	Validation	86
7.5.1	Validation of the UAV LS point cloud with TLS data	86
7.5.2	DTM quality estimation	90
7.6	Summary	95
8	Conclusions and recommendations	97
8.1	Conclusions.	97
8.2	Recommendations	100

List of Figures

2.1	The three types of the Dutch coast. Source of the background map: Google Earth	9
2.2	The highest dunes of the Netherlands located in Zoutelande, Zeeland. The shaded area represents the dune area. Source: Google Earth	10
2.3	Cross-section of the coastal zone. Source: [44]	10
2.4	ARGUS video monitoring station at Noordwijk, The Netherlands. Source: [11]	12
3.1	The Aibot X6 hexacopter, manufactured by Aibotix, with the Velodyne HDL-32E laser scanner on board. A characteristic example of an aerial system for UAV Laser Scanning. Source:[28] . . .	17
3.2	Determining types of trees through the resulting waveform (distribution of multiple echoes). Source:[66]	19
3.3	Basic components of a UAV Laser Scanning system. Source:[84]	20
3.4	Left: Fixed-wing drone. Middle and right: Rotary-wing drones (quadcopter and helicopter). Source: [35], [12], [16]	21
3.5	Velodyne VLP-16: Example of a very compact laser scanner used for UAV Laser Scanning. Source:[73]	21
3.6	Roll, Pitch, Yaw (Heading) angles of an aircraft. Source:[41]	22
3.7	Left: The Alpha Series AL3-32 by Phoenix LiDAR Systems. Right: The DJI Spreading Wings S1000 Octocopter. The two images are not in scale. Source: [52], [13]	23
3.8	Dimensions of Velodyne LiDAR HDL-32E. Source: [72]	24
3.9	1750 IMU by KVH. Source: [32]	25
3.10	RiCOPTER equipped with the RIEGL VUX-SYS. Source:[60]	26
3.11	The two laser scanner solutions for the RIEGL VUX-SYS. Left: RIEGL VUX-1UAV and right: RIEGL miniVUX-1UAV. Source:[59], [58]	27
3.12	RIEGL's BathyCopter. Source:[55]	27
3.13	YellowScan's sensors. Left: YellowScan Mapper and right: YellowScan Surveyor. Source: [85], [86]	28
3.14	Routescene's UAV LidarPod. Source:[38]	28
4.1	Left: The location of Schelphoek in the southern part of The Netherlands. Right: A closer look at Schelphoek.	33
4.2	Left: The higher-elevation part of the study area (the dune followed by the bike path and the rock slope). Right: The lower-elevation part (the rock slope followed by the sandy beach and the breakwaters).	34
4.3	Top left: The four breakwaters of the study area. Top right: The parking space. Bottom: The plant that covers the breakwaters. Source of the top images: Google Earth.	35
4.4	Leica ScanStation C10 laser scanner. Source:[20]	37
4.5	Left: Leica round target. Right: Square target	37
4.6	Top left: Trimble R7 GPS receiver. Top right: Trimble Zephyr Geodetic Antenna. Bottom: RTK/GPS Carbon Fibre pole	39
4.7	Left: The three first laser scanning station covering most of the width of the study area. Right: The fourth station in the parking place. The background map comes from Google Earth.	40

4.8	Top: A quick look of the point clouds coming from the three first stations. Bottom: The point cloud coming from the station in the parking place.	40
4.9	RTK/GPS measurements. Right: First set of RTK measurements. Left: Second set of RTK measurements. The background map comes from Google Earth.	41
5.1	Accuracy vs. precision. The four different cases illustrated using round targets.	44
5.2	Accuracy and precision of a normally distributed set of measurements. Source: [79]	44
5.3	The major systematic errors that determine the 3D coordinate accuracy	46
5.4	The effects of the range and the scan angle error on the final position of the laser point. Source:[7]	47
5.5	Discrepancies between the two point clouds due to bore-sight errors. Source: [46]	49
5.6	Positioning diagram of the airborne lidar for a flat terrain. Source: [50]	50
5.7	System components of the Alpha AL3-32 aerial system	51
5.8	Percentage contribution of each one of the three components (laser scanner, GPS and IMU) to the positioning accuracy for different values of the range, 10 m, 20 m, 30 m, 40 m, 50 m and 100 m.	52
5.9	The fluctuating contributions of the laser scanner, the GPS and the IMU to the positioning accuracy.	53
5.10	3D coordinate errors dependency on the range	54
5.11	3D coordinate errors dependency on the roll angle	55
5.12	3D coordinate errors dependency on the pitch angle	55
5.13	3D coordinate errors dependency on the yaw angle	56
5.14	Study area in Schelphoek. For visualisation purposes, the satellite image has been rotated. The symbol in the top right corner shows the North. Source: Google Earth	57
5.15	Flight plan with 11 flight strips and 2 cross strips. The magenta line is the distance that the UAV needs to get steady, the green lines represent the flight strips, the red lines the turns of the UAV and the blue lines are the route of the UAV for the two cross lines.	58
5.16	Flight plan with 7 flight strips and 2 cross strips. The magenta line is the distance that the UAV needs to get steady, the green lines represent the flight strips, the red lines the turns of the UAV and the blue lines are the route of the UAV for the two cross lines.	59
6.1	The 3x3x3 grid of cells that is used in the noise removal algorithm. The green point that falls into the central cell is the query point and the red ones are its neighbouring points.	62
6.2	Axelsson's above ground analysis algorithm. Source: [3]	63
6.3	The difference between a Digital Surface Model (DSM) and a Digital Terrain Model (DTM). Source: [45]	64
7.1	The part of the bike path that was used for the calculation of the vertical accuracy. Source: Google Earth	70
7.2	The locations of the 25 adjacent boxes on the bike path. The colour indicates the elevation in the dataset.	70
7.3	The mean value and the standard deviation for each one of the 25 boxes with varying and with constant number of points (2000 points). The mean value is indicated by the solid line the standard deviation by the shaded area.	72
7.4	The Graphical User Interface of <i>lastile</i> while tiling the dataset into 100x100m tiles	73
7.5	Left: The initial point cloud. Right: Only the points that were classified as noise and later removed. The green boxes around each point cloud represent the bounding boxes. For the visualisation, the GUI of the <i>lasview</i> was used and the point size was increased in order to make it more clear.	74

7.6	Left: Denoised point cloud. Right: Denoised <i>only-ground</i> point cloud.	76
7.7	First example of the above ground analysis results. Top left: Picture of the northern part of the study area. Source: GoogleEarth. Top right: Denoised point cloud, bottom left: Denoised <i>only-ground</i> point cloud and bottom right: Denoised <i>only-nonground</i> point cloud of the same area.	77
7.8	Second example of the above ground analysis results. Top left: Picture of the second region of the study area. Source: GoogleEarth. Top right: Denoised point cloud, bottom left: Denoised <i>only-ground</i> point cloud and bottom right: Denoised <i>only-nonground</i> point cloud of the same area.	78
7.9	DTMs of the selected subregion of the study area with six different grid sizes, 1 m, 0.5 m, 0.20 m, 0.10 m, 0.05 m and 0.01 m.	80
7.10	DTMs of the selected subregion of the study area with four different interpolation methods, Nearest Neighbour, Delaunay Triangulation, Moving Average and Moving Planes.	83
7.11	DTMs of the selected subregion of the study area with five different numbers of neighbours, 5, 10, 20, 50 and 100 using the Moving Planes method.	85
7.12	The three profiles having as background the UAV LS dataset	87
7.13	Histograms of the absolute differences in Z. Top left: for Profile 1, top right: for Profile 2 and bottom: for Profile 3.	88
7.14	Measured distances in the UAV and the TLS point clouds	89
7.15	Point density map of the selected region in points/ m^2	90
7.16	Terrain slope in degrees of the selected area.	91
7.17	DTM vertical accuracy in cm.	92
7.18	Dependency of the vertical DTM accuracy on the point density.	92
7.19	Differences between the only-ground point cloud and the Moving Planes DTM with grid size 5 cm.	93
7.20	Histogram of the differences between the only-ground point cloud and the Moving Planes DTM with grid size 5 cm.	94
7.21	Differences between the GPS validation points and the Moving Planes DTM with grid size 5 cm.	95
8.1	The discrepancies between overlapping strips (blue/orange) and between strips and ground control points (red) are minimised simultaneously by strip adjustment. Source:[23]	100
8.2	Vegetation height map of Monks Wood derived from the ALS data. Source:[25]	101

List of Tables

2.1	Natural and human-induced causes and factors for shore and shoreline variability ([67])	8
2.2	Coastal monitoring methods categorised by space scale. Adapted from: [39]	11
3.1	Specifications of Velodyne's HDL-32. Source: [52]	24
3.2	Comparison of the main specifications of the aerial systems described above	29
4.1	List of instruments and tools needed for the fieldwork	36
5.1	Nominal errors of the instruments that the Alpha AL3-32 consists of	51
5.2	3D coordinate accuracy using the parameters of a typical drone flight	54
7.1	The mean value and the standard deviation for each one of the 25 boxes with varying and with constant number of points (2000 points). δ Mean and δ STD are the differences in the mean and the standard deviation respectively.	71
7.2	Runtime in OPALS for the four interpolation methods	84
7.3	Measured distances in the UAV and the TLS point cloud	89
8.1	Error budget of the Alpha AL3-32	98

List of Abbreviations

3D	3 (three) Dimensional
AHN	Actueel Hoogtebestand Nederland
ALS	Airborne Laser Scanning
AMSL	Above Mean Sea Level
ASPRS	American Society for Photogrammetry and Remote Sensing
DEM	Digital Elevation Model
DGPS	Differential Global Positioning System
DSM	Digital Surface Model
DTM	Digital Terrain Model
FOV	Field of View
GCP	Ground Control Point
GIS	Geographic Information System
GLONASS	Globalnaya Navigazionnaya Sputnikovaya Sistema
GNSS	Global Navigation Satellite System
GPS	Global Positioning System
GUI	Graphical User Interface
IMU	Inertial Measurement Unit
LiDAR	Light Detection and Ranging
MTOM	Maximum Take-off Mass
NOAA	National Oceanic and Atmospheric Administration
OPALS	Orientation and Processing of Airborne Laser Scanning data
POS	Positioning and Orientation System
ppm	parts per million
RMSE	Root Mean Square Error
RPA	Remotely Piloted Aircrafts
RTK	Real-Time Kinematic
TIN	Triangular Irregular Network
TLS	Terrestrial Laser Scanning
UA	Unmanned Aircrafts
UAS	Unmanned Aerial System
UAV	Unmanned Aerial Vehicle
UAV LS	Unmanned Aerial Vehicle Laser Scanning



Introduction

1.1. Motivation

The Netherlands is a densely populated country situated in Western Europe and primarily developed in coastal lowlands. It is bordered by the North Sea and it has an extensive coast of approximately 350 Km long. A large amount of the total population of the country - around nine out of the seventeen million residents - inhabit in the coastal areas and more than half of the country's gross national product - about €400 billion - is generated in these regions [30]. In addition, important international transport infrastructure, like harbours and airports, that serve the movement of the people and the goods are located in these lowlands. However, these areas along the Dutch coast lay below the sea level and thus they are quite vulnerable to flooding and the potential risks of sea level rise as a result of the climate change [62]. Although they are naturally protected by dunes and in certain areas artificially protected by man-made structures (dykes and dams), the future risks create the need for systematic coastal protection and management. For that, the accurate and continuous monitoring is of the highest significance.

With the term coastal monitoring we refer to all these actions needed for the collection, storage and analysis of coastal related information and the impact of the coastal processes on the coastal zones. The protection of the coastal zones against the sea was especially reinforced after the devastating storm surge in 1953. The Delta Committee was set up by the Dutch government right after that in order to prevent any such incidents in the future and it is the one that constructed numerous dykes and dams for the protection of the southwestern part of the country during the second half of the twentieth century [30]. Nowadays, the Dutch Ministry of Transport, Public Works and Water Management (Rijkswaterstaat) is the main body responsible for coastal protection, while at a regional level provincial authorities and water boards determine policies in line with the national objectives.

The methods used for coastal monitoring vary a lot depending on the time scale of the processes and the space scale of the area of interest. There are techniques for the determination of the position of the shoreline or the tideline¹ and the generation of beach profiles, but also for monitoring the topographic and bathymetric changes. However, recently there has been a rapid development in the technologies oriented for this kind of monitoring, which is mostly a result of the rapid development of remote sensing and its emergence in more

¹Tideline is the location of some representation of high water level and low water level [39]

and more new fields. Remote sensing enables us to record different types - from what in-situ measurements do - and quite larger volume of coastal data in short time. One of these technologies is the UAV Laser Scanning, which is also the subject of the current thesis.

Although UAVs are widely used for military applications for some decades now, recently they have been emerging as a very useful tool for surveying purposes, presenting clear time- and cost-efficiency advantages. They are used both with mounted cameras (for photogrammetric measurements) and with mounted laser scanners. The principle of the method of UAV Laser Scanning is quite similar to the one of Airborne Laser Scanning (i.e using a plane as a platform) with the main difference between the two being the flight height. While for a typical ALS survey the flight height can vary between 500 and 1500 m, depending on the application, during a UAV LS survey the flight height is usually around 50 m. The most straight-forward consequence of this low flight height is a much higher point density, which, however, results in a significantly smaller spatial coverage. For coastal monitoring, though, when the study area is restricted to the extent of a beach, a UAV flight of approximately 15 min is enough to scan the entire area of interest.

Currently, there are multiple UAV Laser Scanning systems available in the market and, since it is a very promising technology for surveying applications, there are constantly new ones coming up. During this study, we take a close look at the aerial system *Alpha AL3-32*, manufactured and provided by Phoenix LiDAR Systems, that was chosen and used by Shore Monitoring & Research B.V. in combination with the DJI Spreading Wings S1000 Octocopter. In the chapters that follow, the performance of this system is investigated and evaluated according to the requirements from Rijkswaterstaat for the products intended for coastal monitoring.

For the analysis of morphological changes in coastal zones with the technology of UAV Laser Scanning, Digital Terrain Models (DTMs) of different epochs are generated and compared. In this way, height differences caused by tidal flows, storms, strong winds, and human activities like dredging or deepening of channels, can be detected [61]. Therefore, DTMs are one of the main deliverables of the present study. In addition, Digital Surface Models (DSMs) can also be a very useful product of UAV Laser Scanning in vegetated areas, e.g. in dune areas. More specifically, by subtracting the DTM from the DSM of a study area, the normalised DSM is derived. In vegetated areas, that is actually the vegetation height map. The capability of laser scanning to provide us with information from the top of the vegetation and all the way to the ground is also one of the main advantages of the method when compared to photogrammetry. The vegetation height maps are not an objective of this study though.

1.2. Research objective and questions

The airborne methods that have been used for coastal monitoring up until now are Airborne Laser Scanning and (aerial) Photogrammetry. Nowadays, though, the use of UAVs in diverse applications is ever-increasing. Thus, the scope of this Master thesis is to focus on UAV Laser Scanning as an innovative tool for coastal monitoring purposes and to investigate its potential, since it possibly presents advantages when compared to the other methods. The aerial system that is looked into as an example of such a UAV LS system is the Alpha AL3-32 by Phoenix LiDAR Systems. The main research question that is raised is thus:

What is the potential of UAV Laser Scanning for monitoring coastal zones?

To reach to conclusions about the main research question, we divided it into several secondary questions. By elaborating and giving answers to each one of these sub-questions, the main research objective of the

project will also be achieved. The sub-questions, that form also the different phases of the study, are related to technical characteristics of UAV Laser Scanning, the added-value products that can be generated from such point clouds as well as validation methods and they are the following:

1. ***What are the sources of error introduced in a point cloud coming from UAV Laser Scanning and what is the error budget of such a system?*** A UAV Laser Scanning system consists of three main components. These are the laser scanner, the GPS and the IMU. Each one of these components introduces some errors in the measurements, which have to be determined and quantified in order to know the accuracy of the final computed coordinates of the point cloud. Along with that, systematic errors may be introduced due to misalignments between the instruments, but also through the transformation into other coordinate systems.
2. ***How can the a priori and a posteriori quality of a UAV LS point cloud be derived?*** One of the most critical criteria for the selection of a UAV LS system is the 3D coordinates accuracy of the derived point cloud. That is directly connected to the errors that are introduced by the components of the system, but also to all the actions performed till the derivation of the final 3D coordinates. In general, the a priori accuracy is determined based on the specifications of the instruments used, while the a posteriori accuracy is determined based on the measurements. The quality of the 3D coordinates influence further the quality of the products generated from a point cloud. The answer to this question is needed also in order to determine whether the quality requirements set by Rijkswaterstaat can be met or not.
3. ***How can an accurate Digital Terrain Model (DTM) be generated from such a point cloud?*** A Digital Terrain Model is a very useful product that somebody can derive using the method of UAV Laser Scanning, when it comes to the monitoring of coastal zones. For their generation, the points that lay above ground have to be extracted and excluded, since a DTM is a representation of only the ground surface. Apart from the so-called *above ground analysis*, the parameters for the grid creation can, also, vary depending on the objectives of the survey, i.e. the grid size, the interpolation method etc.
4. ***How can the results derived from the processing of the UAV Laser Scanning dataset be validated with external measurements?*** Validation is an essential step of every surveying study and it is performed in order to check the accuracy of the results through the use of ground-truth data. In the case of UAV Laser Scanning, the ground-truth data are GPS measurements realised in the study area, but they may also be laser scan data obtained, for instance, with Terrestrial Laser Scanning or even AHN data.

1.3. Research Methodology

In order to find the answers to the sub-questions stated above, and indirectly to reach to the main research objective, different methodologies were used and combined throughout this study. It was initiated with a literature review on UAV Laser Scanning and with the delivery of the UAV LS dataset that was acquired by Shore Monitoring & Research B.V. Since the method is quite new and related studies have only recently started to be carried out, there is not much literature yet available. However, the principles of UAV LS are quite similar to the ones of Airborne Laser Scanning and therefore ALS studies - which have been taking place for a long time now - were very useful for its understanding. In addition, because UAV Photogrammetry has been used prior to UAV LS, literature related to that contributed as well to getting an insight into the topic. This literature review gave the answer to the first sub-question.

Apart from that, this initial phase of the thesis was dedicated also to getting familiar with the provided dataset

and its format as well as trying different tools, i.e. software, in order to conclude to what would be useful for the processing later on.

The next period was focused on the used aerial system, Alpha AL3-32. More specifically, after the first look at the given data, it was necessary to understand exactly how the system performs each measurement, so that we could also understand why certain errors or unexpected features exist in the dataset. For that purpose, the system was decomposed into all the different components that it consists of and each one of them was looked closely. These components were the laser scanner, Velodyne HDL-32E, the GPS and the IMU, KVH 1750. Additional information and advice was also provided, when needed, from the company that manufactured it, Phoenix LiDAR Systems. That resulted to conclusions regarding the sources of error introduced into the measurements - and thus into the derived point clouds and the final error budget of the system. So, consequently the second question could be answered.

To determine the accuracy of the 3D coordinates of the derived point cloud, so thus to answer the third question, the quantitative impact of the different errors on them was investigated by using an error model that was based on the geometry of the UAV LS measurements. The contribution of each source of error to the total error budget was also determined. In this way, we concluded to the a priori positioning accuracy that can be achieved with this specific aerial system. The a posteriori positioning accuracy was later determined by performing a statistical analysis on a flat part of the study area.

What followed was the creation of a standard processing chain for the generation of a DTM. Starting from the raw point cloud and by performing all the necessary processing steps, such as the selection of the study area, the filtering of the dataset for the removal of possible outliers and the above ground analysis, the final clean and only ground point cloud was derived. Then, some important parameters that need to be specified for the DTM creation were investigated, having as a result a method to derive a DTM according to the nature of the study. Through that procedure, the fourth question was answered.

Finally, the validation of the derived point cloud and the DTMs was performed. At first, for the validation of the point cloud, TLS measurements were carried out at the study area several months after the UAV flight. The TLS point clouds of the stable parts of the study area could be compared with the UAV LS point cloud and in this way the accuracy of the latter could be determined. In the same way, AHN3 data were also used. For the validation of the resulted DTMs, GPS measurements obtained by Shore Monitoring & Research B.V. at the same day of the UAV flight were used. After the completion of these tasks, the fifth and last research sub-question was also answered.

1.4. Thesis outline

The present document is the final report of a Master thesis conducted in the Department of Geoscience and Remote Sensing, TU Delft, and in collaboration with the coastal engineering company Shore Monitoring & Research B.V. The theoretical background of its topic was combined with the description of the methodologies used throughout the study and the derived results and they are presented in the following chapters.

The structure of the report is the following:

- in *Chapter 2*, some background information on coastal monitoring is given
- *Chapter 3* focuses on the method of UAV Laser Scanning and UAV LS aerial systems.

-
- the first part of *Chapter 4* is dedicated to the description of the study area and the provided UAV LS dataset, while the second one to the fieldwork that took place for the acquisition of validation data.
 - in *Chapter 5*, all the methodologies that were used during this study are explained.
 - *Chapter 6* contains the results of all these methods and their discussion.
 - and finally *Chapter 7* gives an overview of the conclusions of this study and the recommendations for future research on this topic.

2

Coastal Monitoring

The Netherlands is a country that, due to its location and its very low elevation, has always been vulnerable to dangers coming from the sea, such as floods that have caused a large number of human lives and extensive damages in the past. For that reason, monitoring the coastal processes and their impacts on the coastal zones for the determination of appropriate management and policies is of high significance. This chapter provides some background information on coastal monitoring, and more specifically on its importance, on the Dutch coast characteristics and the current data acquisition techniques. In addition, the coastal engineering company Shore Monitoring & Research is introduced.

2.1. The importance of Coastal Monitoring

Coastal zones are the interfaces where landmasses, oceans and the atmosphere interact. They extend from coastal plains, which are the flat, low-lying pieces of land adjacent to the seacoast, across the continental shelves. They present high environmental and ecological variability and provide valuable living and non-living resources, which are nowadays often being exploited by humans on a non-sustainable basis [29]. Although coastal zones represent a relatively small system, it is highly profitable and diverse, including a variety of ecosystems, from coastal terrestrial habitats to deep water regions approaching 200 m in depth [37].

The human interventions on the coastal areas have caused major environmental changes directly and indirectly. However, the environmental problems that many of the coastal ecosystems worldwide are currently facing are so critical that they threaten the sustainability of the goods and services that they provide to human beings. In developing countries, such problems are particularly severe, since the rapid population increase is coupled with requirements of economic growth, which implies that the pressure on coastal areas and their resources is only rising [29]. Accordingly, the appropriate regional but also global management and use of coastal zones is necessary, and the prediction and reaction to potential geomorphological changes is of high significance when considering the threats to human life. This may only be accomplished with accurate and current monitoring data [40].

The term coastal monitoring refers to all these actions needed for the collection, storage and analysis of information related to coastal processes and their impact on the coastal zones. This information is highly important, since it enables us to detect changes, rates of change and trends in the evolution of a large number

of phenomena that take place in the coastal zones [4]. Coastal monitoring is used for a wide range of factors, such as the response of beaches, seabed, cliffs, structures and ecological systems. However, the coastal forcing factors, i.e. the waves, tides, wind and currents, are the most critical due to their high influence on the evolution of the coastal zones.

Apart from getting insight into the coastal processes, though, the data collected with coastal monitoring is also used to inform strategic studies and decide on management intervention thresholds. In addition, it is a very useful input for predicting the timing of future problems and determining the design conditions as well as the timing of the necessary engineering works. For that, sufficient data collection, management and analysis is needed and therefore the monitoring of the same system is often carried out using different methods which have different characteristics [19].

The coastal evolution is driven by both natural and human-induced causes. To understand the effects of these factors on the coastal system, long-term monitoring is required. Furthermore, to assess the need for constructing sea defences, maintaining/ improving the existing ones, or even letting nature to take its course, authorities need access to reliable good quality coastal data.

Table 2.1 gives an overview of the main natural and human-induced causes and factors that contribute to the coast variability.

Table 2.1: Natural and human-induced causes and factors for shore and shoreline variability ([67])

<i>Scale</i>	<i>Natural causes/factors</i>	<i>Human causes/factors</i>
Very long term (time scale: centuries to millennia; space scale: ~ 100 km and more)	<ul style="list-style-type: none"> - sediment availability - relative sea-level changes - differential bottom changes - geological setting - long-term climate changes - paleomorphology (inherited morphology) 	<ul style="list-style-type: none"> - human-induced climate change - major river regulation - major coastal structures - major reclamations and closures - structural coastal (non)management
Long term (time scale: decades to centuries; space scale: ~ 10 – 100 km)	<ul style="list-style-type: none"> - relative sea-level changes - regional climate variations - coastal inlet cycles - sand waves - extreme events 	<ul style="list-style-type: none"> - river regulation - coastal structures - reclamations and closures - coastal (non)management - natural resource extraction(subsidence)
Middle term (time scale: years to decades; space scale: ~ 1 – 5 km)	<ul style="list-style-type: none"> - wave climate variations - surf zone bar cycles - extreme events 	<ul style="list-style-type: none"> - surf zone structures - shore nourishments
Short term (time scale: hours to years; space scale: ~ 10 m – 1 km)	<ul style="list-style-type: none"> - wave, tide and surge conditions - seasonal climate variations 	<ul style="list-style-type: none"> - surf zone structures - shore nourishments

In the table above, the natural and the human-induced causes and factors for the shore and the shoreline variability are categorised in four different scales in terms of time but also space. Depending on the scale - very long term, long term, middle term and short term - different monitoring methods are suitable and different fields of study are involved. For example, while for the very long term coastal monitoring geological tools are necessary, since the processes are slower, for the shorter term monitoring coastal engineering tools and technologies are used in order to determine the effects of the natural factors, such as waves, winds or extreme weather events, as well as the effects of the human interventions on the natural environment (shores) but also on the man-made structures. Later in this chapter, these different coastal monitoring techniques are discussed.

2.2. Dutch coast characteristics

The Netherlands is bordered by the North Sea and it is located in the deltas of the three rivers: Rhine, Meuse and the Scheldt. The Dutch coast, which is entirely along the North Sea, is approximately 350 Km long [30] and it is divided into three main parts [64], as shown in Fig. 2.1:

- the Delta coast: it is an estuary¹ coast in the south-western part of the country. The Delta coast actually consists of a number of former islands, separated by tidal basins², inlets and an estuary formed by the three aforementioned rivers. After the major flood disaster of 1953 most of the tidal basins were closed or semi-closed by large constructional works (the Delta works). The Delta coast is also where the study area of the present study is located [62].
- the Holland coast: it is an uninterrupted coastline in the central part of the country, between the Hook of Holland (south) and Den Helder (north), with major city areas close to the sea [62]. It has a length of 120 Km and there are no tidal inlets, sea arms or islands. The beaches along the Holland coast have a width of 100-200 m from the dune foot to the low water line and they are usually multi-barred [64].
- the Wadden coast: it is a barrier island coast in the northern part of The Netherlands. The Wadden coast consists of barrier islands alternating with tidal inlets and their related ebb-tidal deltas³ at the seaward side. The lagoon area, widely known as Wadden sea, between the barrier islands and the mainland consists of several connected tidal basins with extensive tidal flats [62].



Figure 2.1: The three types of the Dutch coast. Source of the background map: Google Earth

The Dutch coast consists over its whole length of wide sandy beaches and - the bigger part of it - of extensive, usually low-vegetated, dunes (see example in Fig. 2.2). More specifically, 290 Km of the coast is protected by

¹An estuary is a partially enclosed coastal body of brackish water with one or more rivers or streams flowing into it, and with a free connection to the open sea [80].

²The term tidal basin implies a shallow coastal inlet or bay that fills and empties with water as the tide rises and falls, often characterised by tidal flats and marshes.

³An ebb-tidal delta is a bulge of sand formed at the seaward mouth of tidal inlets as a result of interaction between tidal currents and waves.

dunes, which act as a natural defence to the North Sea, while the remaining 60 Km is protected by man-made structures, such as dikes and dams [64]. A characteristic example of this is the Delta Works. The geomorphological features of such a coast are highly dependent on the transport of the sediments, driven mainly by the water but also the wind [17]. Therefore, the Dutch coast is characterised as a wave dominated coast.



Figure 2.2: The highest dunes of the Netherlands located in Zoutelande, Zeeland. The shaded area represents the dune area. Source: Google Earth

Typically, the Dutch coast looks like the sketch in Fig. 2.3. Where the polder area finishes, the coastal zone starts, which is the subject of coastal monitoring. Within the coastal zone, the dunes, the beach and the shoreface can be distinguished. The width of the dunes vary from less than one hundred metres to several kilometres. The first lines of the dunes (foredune), the beach and the near shore zone (going down to about 8 m) together form the coastal system that serves as a defence against the sea. In this part of the coastal zone, most of the sediment transport takes place [44]. The deeper foreshore (going down to more than 8 m) is not that easily affected by the forcing factors and thus the changes in it are slower and more gradual.

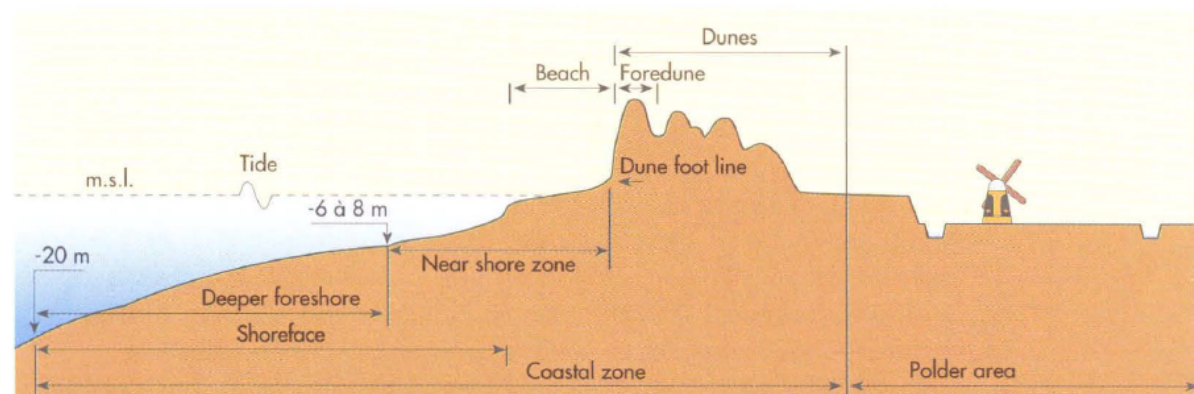


Figure 2.3: Cross-section of the coastal zone. Source: [44]

The Dutch coast is low-lying and therefore the danger of flooding and the potential risks of the sea level rise due to the climate change is increased. The fact that 60% of the total population of the country lives in these lowlands, but also the fact that 65% of the Gross National Product is generated in these areas imply how vital they are and how significant the coastal protection and management are [30].

However, these areas can be quite unfriendly for coastal monitoring purposes when using certain remote sensing techniques, especially if they are located in intertidal zones. Either the tide (regularly) or the weather conditions (irregularly) cause the water to move towards the shore, leaving parts of it muddy and with puddles. In addition, if rocky structures are present, they are very often covered with algae or seaweed. This fact implies that a monitoring technique that requires the least possible physical presence at the study area would be preferable.

2.3. Data acquisition techniques

Coastal monitoring provides useful information about the state of the coastal zones and significant data for the statistical descriptors and numerical models of their behaviour. This section focuses on the equipment and the technologies that are available and used for that purpose. Table 2.2 gives an overview of some of the main coastal monitoring methods and technologies categorised according to the space scale of the type of monitoring that they are used for. To achieve a link between Table 2.2 and Table 2.1 - that described the factors that contribute to the coastal changes - although they contain different kind of information, we can correspond the full range of spatial scales of the former to the *short* and *middle* terms of the latter. That is due to the large scale of Table 2.2, which describes the monitoring of tidelines and shorelines in a time scale from a few years to decades and spatial scale of a few kilometres.

Table 2.2: Coastal monitoring methods categorised by space scale. Adapted from: [39]

Monitoring type	Description	Method/Instrument
<i>Small scale</i>		
Underwater acoustic measurements of the seabed	An acoustic backscatter device is used to detect the level of the seabed and give information about sediment in suspension, provided that both the seabed and the instrument are fully submerged.	- Autonomous Sand Ripple Profiler (ASRP)
<i>Medium scale</i>		
Cross-shore profile surveys and topographic surveys	Beach profiles and topographic surveys are typically carried out using a large range of methods, usually of remote sensing nature.	- Total station - Real-Time Kinematic GPS (e.g. mounted on a quad bike) - Laser scanning systems - Repeated digital photography (Argus video system) - X-band radar
<i>Large scale</i>		
Mapping of tidelines and shorelines	The position of the shoreline or tideline ⁴ is commonly marked on maps. Different editions of the same map series are used to determine long term changes to the position of the shoreline.	- Orthorectified aerial or satellite photos - Topographic LiDAR - Bathymetric LiDAR - Synthetic Aperture Radar (SAR) - Bathymetric surveys from ships

⁴Tideline is the location of some representation of high water level and low water level.

The small scale monitoring of the table above refers to the monitoring of seabed changes that can be observed in a time scale of hours - in the case of extreme weather phenomena - to a few years, when a more gradual evolution occurs. The medium scale monitoring is used for the derivation of cross-shore profiles with a spatial scale of a couple of hundreds of metres and a time scale again of some hours to years. Finally, the large scale monitoring of the table refers to the mapping of tidelines and shorelines, where changes take place in larger time and spatial scales. While for small scale monitoring, there is the need in certain cases for acquisition of in situ measurements, as it can also be concluded from Table 2.2, the majority of the methods used for coastal monitoring are remote sensing techniques and they cover larger space scales. Remote sensing is, thus, a valuable field of study for coastal monitoring, since it can provide information about the coastal evolution in a time- and cost-efficient way. In the following paragraphs, details on some of the most frequently used techniques are given.

2.3.1. ARGUS video systems

With the emergence of digital imaging technology, shore-based remote video techniques, like the ARGUS system (see Fig. 2.4), have increasingly been used for the monitoring of coastal processes in support of coastal management and engineering. The ARGUS system was initially developed at Oregon State University (USA), in 1992 - and installed for the first time in the Netherlands in 1995 - and it can provide us with high resolution video data at spatial scales of decimetres to kilometres and temporal scales of hours to years by using unmanned, automated video stations [10].



Figure 2.4: ARGUS video monitoring station at Noordwijk, The Netherlands. Source: [11]

An ARGUS monitoring system typically consists of four to five video cameras, spanning a 180° view, and allowing full coverage of about four to six kilometres of beach. The cameras are mounted on a high location along the coast and they are connected to a computer on site. The data sampling is typically hourly, although it can be specified according to the needs, and continues even during rough weather conditions. Each hourly collection usually consists of three types of images [10]:

1. a snapshot image, that serves as simple documentation of the ambient conditions but offers little quantitative information.

2. a time exposure image, which is the result of the averaging out of the natural modulations in wave breaking and it reveals a smooth pattern of bright image intensities.
3. a variance image, which are used for distinguishing the regions that change in time (sea surface) from those that remain unchanged (dry beach).

In addition, geo-referencing the images enables us to carry out measurements of length scales of morphological features, like breaker bars, and detect rip currents. The applications that it is mostly used for is the quantification of storm-driven shoreline changes, the detection of intertidal morphological changes at a nourished beach, the measurement of surf zone bathymetry and the quantification of wave run-up on coastal structures [10].

2.3.2. Terrestrial Laser Scanning (TLS)

Terrestrial laser scanning is a ground-based active remote sensing technique, following the principles of LiDAR. The term ground-based implies that the scanning instrument is mounted on a tripod positioned over the ground for capturing, at street view, the surface of objects in the surroundings, such as bridges, dams, building facades, trees or cultural heritage sites [33].

The direct measurement of distances and angles between the sensor and reflecting targets provides highly accurate 3D point clouds [26] of all the beach features and of the existing human interventions [15]. For coastal monitoring purposes, 3-dimensional models of the coastal zones are generated in this way, on a regular basis, so that the volume of sediments that has been eroded or built up can be determined.

During a TLS survey, the laser scanner is usually placed in multiple stations and thus multiple scans (or point clouds) are derived. In order to register these scans together into a common coordinate system, targets that can be identified in the laser point cloud need to be placed in the acquisition area and Ground Control Points (GCP) must be measured for the geo-referencing of the point cloud into a mapping frame. Therefore, it is considered to be a quite time-consuming and costly method for measuring wide areas, especially when high resolution is required.

2.3.3. Photogrammetry

Photogrammetry is the field of study and the scientific tool of extracting topographic information about physical objects and the environment by recording and performing measurements on photographic images, as well as interpreting them, particularly for the recovery of the exact positions of surface points. Typically the recording instrument (camera) is mounted on moving platforms, such as satellites, aircrafts, helicopters, UAVs etc., but for certain applications, e.g. in archaeology, it can be also ground-based, which means that the camera is stationed on or close to the Earth's surface - usually on a tripod. In the most common form of photogrammetry - when it comes to coastal monitoring, multiple overlapping photos of the ground are taken as the platform (aircraft or UAV) flies along a flight path. These photos are referenced to ground control surveys. The main products of photogrammetry are DTMs, DSMs, orthoimages, 2D and 3D reconstruction and classification of objects for mapping or thematic applications and visualisation [6].

When photogrammetry is used for coastal monitoring purposes, aerial photographs are used to illustrate the geomorphological features of the coasts. By processing such photographs derived from different time periods, it is possible to detect the changes in the features of interest and produce datasets depicted, e.g. the changes in the shoreline position. Beach profiles can also be obtained from photogrammetry [68]. In addition, the geo-referenced - and orthorectified - aerial photographs can be incorporated within a GIS to

provide the basis for displaying these features. This method presents, however, some important drawbacks for coastal monitoring. The quality of aerial photographs depends a lot on the light available and thus it can create contrast problems in the images. Problems appear also in wet or flat metal. Furthermore, this technique requires the collection of Ground Control Points (GCPs) which can be a quite demanding task in specific areas (e.g. muddy or high vegetated areas).

2.3.4. Airborne Laser Scanning (ALS)

Airborne Laser Scanning is a rapid, highly accurate and efficient method of capturing 3D data of large areas, such as agricultural or forestry sites, urban areas, industrial plants, etc. As it is implied by its name, the scanning device is typically mounted at the bottom or below a moving platform, e.g. an aeroplane, a helicopter or more relevantly a UAV.

The instruments that are used during an ALS survey are the airborne laser scanners, which are active sensing systems using a laser beam as the sensing carrier. That means that two optical beams - the emitted laser beam and the received portion of that beam - must be considered. The laser scanner system consists of the laser scanner itself and a Position and Orientation System (POS), realised by an integrated differential GPS (DGPS) and an inertial measurement unit (IMU) and the control unit [77]. The laser scanners measure the distance between the sensor and the illuminated spot on ground and the remaining components are used for the determination of the 3D-coordinates.

The short time needed for the production of data and the detail and high accuracy of the derived Digital Terrain Models make it a useful tool to monitor and map areas susceptible to changes, an characteristic example of which is the coastal zones. Various applications demonstrated that when using ALS it was possible to depict subtle features in relief, which are hardly detectable and comprehensible when surveying terrestrially [14].

In addition, the latest development in the method of ALS, which is the use of a drone as a moving platform, is considered to be very promising and that is a fact that can be easily concluded by the amount of UAV Laser Scanning systems that have been emerging recently. The flexibility and the agility of such a system make it suitable for surveying even large study areas in a fast and cost-efficient way. More details of this method are provided in the chapters that follow.

2.4. Shore Monitoring & Research B.V.

Shore Monitoring & Research B.V. is both a consulting and a measuring company in the field of Coastal Engineering, founded in 2009, and it is located in the Hague, the Netherlands. It focuses on the collection, analysis and visualisation of hydrological, topographical, sedimentological and hydraulic measurements.

More specifically, they perform sediment samplings and wave, tidal, water, salinity and flow measurements. In addition, they carry out topographic measurements for the volumetric investigation in landfills, dune areas etc. Finally, they specialise in bathymetric surveys for the underwater mapping. Among many other methods of measuring, they use UAVs with high resolution and geometrically calibrated cameras on board to map coastal areas. That enables them to map even more difficult areas, like dunes and transshipment areas (areas where shipment logistics are handled). For the detection of the changes, they generate DTMs out of a large number of overlapping aerials photographs. Their most recent innovation though is the use of a drone LiDAR system for monitoring, which is the subject of the present study.

Considering Table 2.1 as a reference in order to specify the scales of the present study, Shore Monitoring & Research B.V. mainly focuses on the monitoring of coastal changes due to short and middle term processes. The temporal scale of such processes ranges from hours to years and decades, while the spatial scale ranges from tens of metres to a few kilometres. The company investigates mostly the changes that are caused by human interventions such as surf zone structures and shore nourishments. In order, though, to have a full view of the problem, the natural causes should be investigated, too. The natural causes and factors that lead to short and middle term coastal changes are, among others, the wave, tide and surge conditions, the seasonal climate variations and the possible extreme events that can modify the coastal zones very rapidly.

2.5. Summary

In this first literature chapter, background information on coastal monitoring and the techniques that are used for that purpose was given. More specifically, at first, the significance of coastal zones was highlighted as a source of valuable living and non-living resources for human beings. Although they represent a relatively small system, it is highly profitable and thus its evolution, driven by natural and human-induced factors, has to be monitored. In this way, the prediction - or even the prevention - of future problems and the determination of the design condition of the necessary engineering works can be achieved. The Netherlands, in particular, is a country with a quite long coastline (~ 350 Km), the larger part of which is protected by dunes, acting as a natural defence to the North Sea. The fact that 60 % of the total population of the country lives in the coastal lowlands and that 65 % of the Gross National Product is generated in these areas imply the high importance of their monitoring. However, since the coastal processes differ a lot in time and space scale, depending on the nature of the process, different monitoring techniques are used. Small scale processes usually require in situ measurements, while for larger spatial scale processes remote sensing is a valuable tool, since it is time- and cost-efficient. Among all the remote sensing methods used for coastal monitoring, the ARGUS video system, Terrestrial Laser Scanning (TLS), Photogrammetry and Airborne Laser Scanning (ALS) can be distinguished as the most commonly used techniques. The ARGUS video system is mostly suitable for long-term monitoring, since it can provide valuable coastal information, but it is not flexible. TLS offers us high resolution data, but it is time-consuming, since the scanner has to change multiple positions in order to cover the whole study area. Photogrammetry is a quite suitable technique for coastal monitoring, able to cover large areas in a short time. However, it cannot provide us with data through vegetated areas and also GCPs are required. That leads us to the conclusion that ALS is the most preferable technique. It can provide us with high resolution data, it can cover large areas in short time and there is no need for GCPs. UAV Laser Scanning, in particular, is the latest development of ALS and it is proven to be an efficient and cost-effective survey tool for topographic mapping and measurement in the coastal zone. UAVs are flexible and durable platforms. When combined with a laser scanning system, they can provide us with dense and accurate data, due to the much lower flight height. In addition, they only require a single operator to safely deploy in the field, removing the need for separate and time-consuming on-ground surveying of ground control points (GCPs). These together with the general advantages of the laser scanning, such as its capability to penetrate through vegetation, its weather- and light-independent nature etc. raise the interest for further investigation of the method and its potential.

3

UAV Laser Scanning

UAV Laser Scanning is a surveying technique that has emerged quite recently, but it is considered to be one of the most promising methods for various applications, such as forestry, agriculture, coastal monitoring, archaeology and others. The first part of this chapter is focused on the principles of the method and the description of the main components of such an aerial system. In the second part, the chosen by Shore Monitoring & Research B.V. aerial system, Alpha AL3-32 by Phoenix LiDAR systems, is discussed. Finally, an overview of the most competitive aerial systems that are currently available in the market is given.

3.1. Background information on UAV Laser Scanning

Laser Scanning or LiDAR (Light Detection and Ranging) is a remote sensing technique that uses light in the form of laser pulses for measuring ranges to the Earth. Using these measurements in combination with other data recorded by the airborne system, accurate 3D information about the shape of the Earth and its surface characteristics are derived [42]. The term UAV Laser Scanning implies that the platform used is a UAV (see an example of such a platform in Fig. 3.1). A UAV, which stands for Unmanned Aerial Vehicle, also can be referred to as drone, Unmanned Aerial System (UAS), Unmanned Aircrafts (UA), or Remotely Piloted Aircrafts (RPA), is an unmanned aircraft or ship guided by remote control or onboard computers. Sometimes the term UAV is purposely changed to UAS to reflect the complex systems that are involved in drone operations [70].



Figure 3.1: The Aibot X6 hexacopter, manufactured by Aibotix, with the Velodyne HDL-32E laser scanner on board. A characteristic example of an aerial system for UAV Laser Scanning. Source:[28]

The early development and fast evolution of UAVs has been strongly motivated in the past by military applications. More specifically, after World War II, there was the need by some nations to construct aerial vehicles that would be capable of providing surveillance, reconnaissance and penetration of hostile terrains without the deployment of human beings in areas of high danger. Later on, in 1979, Przybilla and Wester-Ebbinghaus used for the first time a UAV experimentally in photogrammetric applications [18]. Since that time, drones, of various shapes, sizes, and functionalities, have been used for reconnaissance, but their recent application to remote sensing was exceptionally rapid and their civilian applications are becoming increasingly appealing. Flexible, cost-efficient and high-resolution remote sensing systems that use UAVs as platforms are being currently used for filling data gaps and supplementing the capabilities of crewed/manned aircraft and satellite remote sensing systems [70].

However, they present also some limitations that have to be taken into account before their use. At first, a professional (certified) drone operator is required for any non-personal use of a drone. In addition, there are restrictions regarding the flight permission, the flight height, the maximum distance from the operator and other such regulations, that are specified by laws that vary from country to country, but also change on a regular basis. Someone has, thus, to be well-informed about all the relevant restrictions before carrying out a survey. The poor battery issues can also be a problem and it is something that has yet to be further developed.

Currently, UAV Laser Scanning is found in a variety of fields, the main of which are listed below [34], [8], [1]:

- **AGRICULTURE:** UAV LiDAR can be very effectively used to determine the slopes and the sun exposure on a farm land. In addition, we can generate blend topography maps with crop yield data in order to get information on the health of the soil.
- **FORESTRY MANAGEMENT AND PLANNING:** One of the most useful properties of LiDAR is its ability to penetrate through vegetation and thus to measure the entire vertical structure of forest canopies. Apart from being able to map the ground beneath the forest, with LiDAR we can also calculate the canopy bulk density and canopy base height. Carrying out these kinds of LiDAR surveys with UAVs, the level of time- and cost-effectiveness is significantly increased.
- **METEOROLOGY:** LiDAR systems mounted on UAVs can provide us with important meteorological information, such as cloud profiles, wind speed measurements and useful data regarding other atmospheric components.
- **ARCHAEOLOGY:** Drone LiDAR facilitates significantly the surveying and the planning of field campaigns in archaeological sites, especially when it comes to mapping features beneath forest canopies. Archaeologists can generate high-resolution Digital Elevation Models (DEMs) of archaeological sites, that are otherwise hidden by vegetation, and study their micro-topography.
- **URBAN PLANNING:** UAV LiDAR is a very suitable technology for obtaining Digital Surface Models (DSMs) of the earth's surface, which when combined with digital orthophotos can result to highly detailed Digital City Models. These are typically used for land use planning in the level of municipalities, cities or provinces. Furthermore, urban objects, such as buildings, can be extracted from them for further processing.
- **MINING:** Precise ore volume calculations - with a few centimetres accuracy - are feasible with periodic UAV flyovers and scanning of the quarry areas. In addition, UAV LiDAR is used for surveying the land around the possible mining areas to check its suitability and to give an accurate indication of environmental impact.

- **ENVIRONMENTAL CONSERVATION:** UAV LiDAR has many applications in flooding modelling, coastal management, pollution modelling, natural hazards as well as climate change studies, all together contributing to the environmental conservation.

3.2. The method of UAV Laser Scanning

As implied by its name, LiDAR is based on the light transit time estimation. More specifically, light waves travel with a known velocity in a given medium. By recording the time delay that it takes for the light to travel from a source to a reflective target surface and back to the light detector - which is referred to as round trip, τ - the distance (or range) can be estimated in a very convenient way. These systems are also known as time-of-flight due to the principle of their operation [74].

The propagation velocity of the light is its fundamental property and thus it is quite often used for determining related parameters. In a given medium, this velocity is finite and constant and therefore by using the measurement of the time delay of the round trip τ according to formula 3.1, the range ρ is evaluated:

$$\rho = \frac{c \tau}{n 2} \quad (3.1)$$

where c is the speed of light. The current accepted value for the speed of light in a vacuum is $c = 299,792,458 m/s$. When the light waves travel in the air, the refractive index n , which depends on the air temperature, pressure and humidity, is equal to $n \approx 1.00025$. But usually it is assumed that the speed of light is $c = 3 \times 10^8 m/s$ and the refractive index of the air is $n = 1$ [74]. So, the previous formula can be transformed into:

$$\rho = c \frac{\tau}{2} \quad (3.2)$$

A very important fact about laser scanning is that one single pulse can generate more than one echoes. That is due to the multiple returns caused by the varying site characteristics. Airborne systems capture certainly the first returned pulse (or echo) and the last echo for each emitted pulse, when that exists. Some airborne systems are capable of capturing four to five separate echoes or even more, as for example the RIEGL laser scanners that can usually capture up to seven echoes. This is a very useful property, used in various applications, since it enables us to calculate the height of the scanned objects, either these are e.g. buildings or vegetation. In some cases, especially when scanning forest canopies, it even enables us to distinguish different kinds of trees [66], as illustrated in Fig. 3.2.

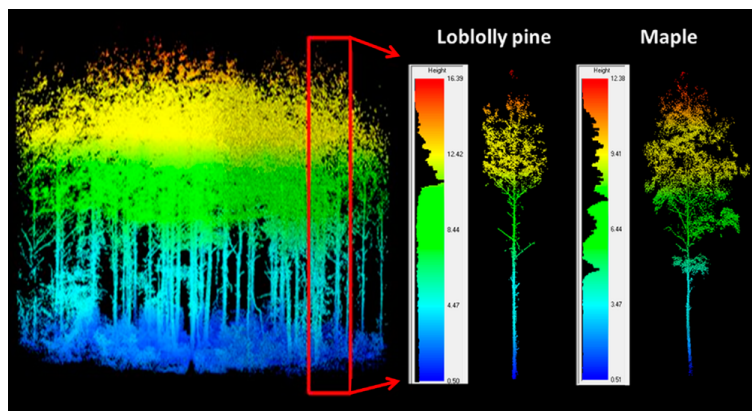


Figure 3.2: Determining types of trees through the resulting waveform (distribution of multiple echoes). Source:[66]

3.3. The system components of a UAV Laser Scanning system

A UAV Laser Scanning system, like every other airborne laser scanning system, consists of four main components [84]. As shown in Fig. 3.3, these are:

1. the platform (drone)
2. the laser scanner
3. the GNSS receiver
4. and the Inertial Measurement Unit (IMU)

These are the basic, and always necessary, components of such a system. Optionally, more sensors can be mounted as well, if the total takeoff weight is within the limits. Quite often, for instance, a camera is also on board. In the following paragraphs, information on each one of these four components is given.

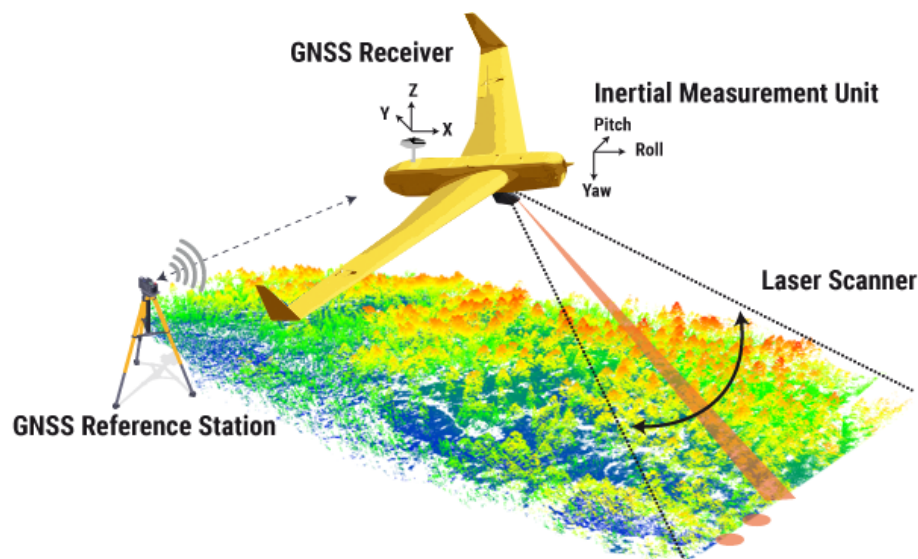


Figure 3.3: Basic components of a UAV Laser Scanning system. Source:[84]

3.3.1. Unmanned Aerial Vehicle (UAV)

As it was mentioned earlier, the first drones were developed in the early 20th century and since the 1950s, their main use has been for aerial reconnaissance. However, as of 2005, drones started emerging into other fields as well, apart from the military purposes for what they are most commonly used [70]. These applications vary from environmental applications to archaeology and urban planning. There are two major types of drones based on takeoff and landing techniques: *horizontal* takeoff and landing and *vertical* takeoff and landing.

The first type, the one that operates with horizontal takeoff and landing, is typically the fixed-wing drones (airplanes), whereas the second type, that operates with vertical takeoff and landing, are the rotorcrafts or rotary-wing drones (helicopters and autogyros), ships, and balloons. All the aforementioned types of drones are illustrated in Fig. 3.4. For the development of drones specifically for remote sensing applications, stability and flight range are two parameters that have to be taken seriously into account. Depending on the characteristics

of the drones, they perform differently in terms of stability and range and thus they are suitable for diverse kinds of surveys [70].



Figure 3.4: Left: Fixed-wing drone. Middle and right: Rotary-wing drones (quadcopter and helicopter). Source: [35], [12], [16]

More specifically, fixed-wing drones are preferable for surveys where the study area is large, since they offer higher field coverage than the other types in the same amount of time. In addition, this is the type for which the minimum experience is required in order to operate them. However, large fixed-wing drones need a runway for their takeoff and their landing, which means that they cannot be launched at any location, whereas smaller ones can be taken off manually or by using ground stands or vehicles. On the other hand, rotary-wing drones should be chosen when there is the requirement for high spatial resolution measurements. Furthermore, they present the advantage of less system crashes [70]. The larger the number of the rotor blades, the lower the risk, since when a rotor blade is destroyed, the drone can continue operating unaffected. Two other very important elements of the drone equipment are the power source and the maximum payload weight. The former is very critical because it affects directly the flight endurance and the latter since it determines the maximum weight of the sensor(s) that can be mounted on the platform. This maximum payload weight can vary from tens of grams to hundreds of kilograms, depending on the drone. Finally, they drones can fly autonomously, but they can also be pre-programmed so that the flight plan suits the characteristics of the terrain to study [70].

3.3.2. Laser Scanner

The sensors that the UAVs carry on board are laser scanners. Laser scanners utilise opto-mechanical scanning assemblies that comprise of the laser, the scanning mechanics and the optics. The laser system, mounted at the bottom of the UAV, continuously sends laser pulses towards the terrain as the drone flies [74]. Depending on the drone's velocity and survey height, the measurement density varies. Since there is a limitation on the weight that UAVs can carry on board, these laser scanners are small and light.



Figure 3.5: Velodyne VLP-16: Example of a very compact laser scanner used for UAV Laser Scanning. Source:[73]

3.3.3. GNSS receiver

The GNSS receiver is always mounted at an exposed position on the top of the UAV so that it will have an undisturbed view to GPS satellites and it records GPS signals at a specified sampling rate. It is typically a dual frequency antenna, although recently triple frequency antennas - so receiving also L5 frequency apart from L1 and L2 - have started emerging into the market. Except for the rest of the products, by analysing the recordings, which are coordinates in a selected coordinate system, the trajectory of the drone can be retrieved.

3.3.4. Inertial measurement unit (IMU)

An Inertial Measurement Unit (IMU) is an electronic device that measures and reports a body's specific force, angular rate, and sometimes the magnetic field surrounding the body, using a combination of accelerometers and gyroscopes, sometimes also magnetometers [81]. In the case of UAV Laser Scanning, IMUs are typically used to maneuver the drones. An IMU is either fixed directly to the laser scanner or close to it on a stable

survey platform. Typically, it records acceleration data and rotation rates at a sampling rate of up to 1000 Hz. Acceleration data can be used to support the interpolation of the platform position on the GPS trajectory, while rotation rates are used to determine platform orientation. The platform orientation is expressed in three rotation angles, the *roll*, *pitch* and *yaw*. Roll is called the rotation around the front-to-back axis, pitch is the rotation around the side-to-side axis and yaw - or *heading* - is the rotation around the vertical axis, as shown in Fig. 3.6. The combination of GPS and IMU data allows one to reconstruct very accurately the flight path (air trajectory) [74]. The former is necessary for the determination of the coordinates of the drone, while the latter for the determination of its orientation angles.

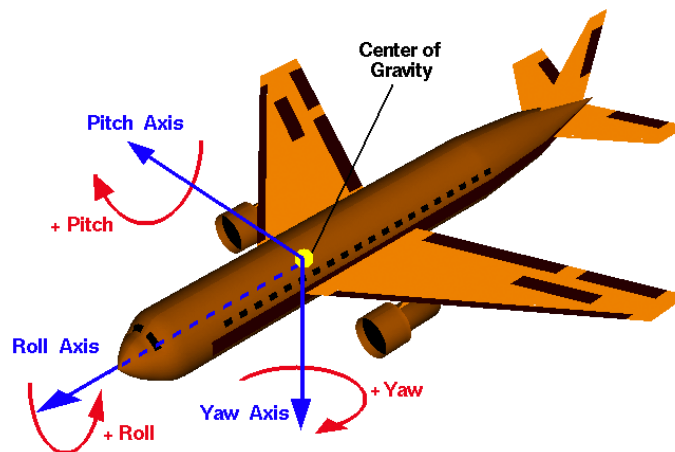


Figure 3.6: Roll, Pitch, Yaw (Heading) angles of an aircraft. Source:[41]

3.4. Phoenix's *Alpha AL3-32* 3D Laser Mapping System

For the present study, Shore Monitoring & Research B.V. chose to use one of the aerial systems offered by Phoenix LiDAR Systems, the *Alpha AL3-32*, in combination with the DJI Spreading Wings S1000 Octocopter. Phoenix LiDAR Systems is an American company that specialises in the construction of compact, multi-vehicle compatible, survey-grade ¹ laser mapping and photogrammetry solutions [53]. The Alpha AL3-32, presented

¹With the term survey-grade, a cm-level accuracy is implied.

in Fig. 3.7, is considered to be at the moment one of the lightest, highest density and most accurate 3D laser mapping systems globally. It provides survey-grade accuracy with 105 m laser range and high-quality intensity calibration. In addition, it is fully autonomous and it can be mounted on any drone, car, boat and/or even backpacks, while it can be easily upgraded with the following modular options: Dual LiDAR Sensors, DSLR, GeniCam, GigEVision, thermal, multispectral, hyperspectral and custom sensors [53]. In the paragraphs that follow, more information on this aerial system and its components is provided.



Figure 3.7: Left: The Alpha Series AL3-32 by Phoenix LiDAR Systems. Right: The DJI Spreading Wings S1000 Octocopter. The two images are not in scale. Source: [52], [13]

3.4.1. UAV: DJI Spreading Wings S1000 Octocopter

The platform that was used for the survey was the DJI Spreading Wings S1000 Octocopter. Generally, octocopters are much faster and more agile when compared to quadcopters or hexacopters, they can reach exceptionally high elevations (e.g. 1000 m) and they are very powerful. In addition, they can carry larger loads on board (close to 10 Kg) and at the same time they can remain stable. From that, it is concluded that for the case study the choice of an octocopter was necessary, when considering the weight of a laser scanner, which typically weighs a couple of kilograms, combined with the rest of the required components and the cabling. On the contrary, though, octocopters are bigger in size, more expensive and, most importantly, the battery life is often far less.

The S1000 was originally designed for professional aerial photography and cinematography, but as it was also proven in practise, it is a good choice for remote sensing applications as well. It weighs 4.2 Kg, and with a maximum takeoff weight of about 11Kg, which means that it can carry extra 6.8 Kg, it could easily carry the Alpha AL3-32 payload for up to 15 minutes. The flight controller that it includes helps it to remain stable even with the loss of a rotor. All eight arms can be completely folded down and the folding propellers can be tucked away, minimising the S1000's size for transportation. Its operating temperature range spans from - 10° C to +40° C [13].

3.4.2. Velodyne HDL-32E: High Definition Real-Time 3D LiDAR sensor

The LiDAR sensor that is included in the Alpha AL3-32 aerial system is the HDL-32E by Velodyne LiDAR. The HDL-32E creates 360° 3D images by using 32 lasers/detector pairs, aligned from +10.67° to -30.67° (the vertical field of view (FOV) is 41.3°), whose housing rapidly spins to scan the surrounding environment. This design allows each one of the lasers to fire thousands of times per second, providing a point cloud of up to 695,000

points per second with a range from 1 m and up to 100 m and a typical 3D coordinates' accuracy of ± 2 cm at 10 Hz. It can provide up to two different returns (echoes), e.g. in case of vegetated areas, from which usually the first one is the strongest. Its operating temperature range spans from -10°C to $+60^{\circ}\text{C}$ and the wavelength of the laser beam is 903 nm [52].

At the same time, HDL-32E measures only 149.86 mm high by 85.3 mm in diameter (Fig. 3.8) and weighs 1.0 Kg (plus 0.3 Kg for cabling), which makes it suitable for many different applications, in particular those with constrained form factors and pricing requirements but still demand high performance, such as autonomous vehicle control, mobile mapping, aerial mapping, security, and surveillance [52].

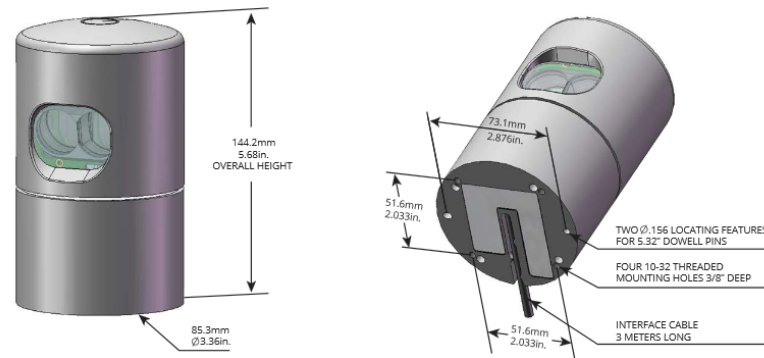


Figure 3.8: Dimensions of Velodyne LiDAR HDL-32E. Source: [72]

The sensors can synchronise their data with precision, GPS-supplied time pulses. Synchronising to the GPS pulse-per-second (PPS) signal provides users the ability to compute the exact firing time of each data point [72].

Table 3.1: Specifications of Velodyne's HDL-32. Source: [52]

Laser Properties	Class 1 (eye safe), 905 nm
Range Min / Max / Resolution	1.0 m / 120 m / 2mm
RMS Ranging Error	20 mm
Scan Rate	700k shots/s, up to 1.4 mio points/s
Field Of Range	+10° to -30° Vertical / 360° Horizontal FOV
Number Of Returns	2
Number Of Lasers/Planes	32
Recommended Scanning Height (AGL)	20 - 60 m

3.4.3. Navigation System

The navigation system of Alpha AL3-32 consists of a dual-frequency antenna that supports GPS, GLONASS, Galileo and BeiDou. Real-time Kinematic as well as post-processing is possible [51]. In addition, the accuracy of the horizontal positioning is $1\text{cm} + 1\text{ppm}^2$.

²That means that for every kilometre of distance to the GNSS reference station, called the baseline, an additional millimetre of error is to be expected.

3.4.4. Inertial Measurement Unit (IMU): KVH 1750

The Inertial Measurement Unit (IMU) that was used in this case study was the *Fiber Optic Gyro (FOG) 1750 IMU*, which is one of the latest developments of KVH on the field of miniaturised advanced navigation and stabilisation system sensor products (see Fig. 3.9). Its 3 high-precision FOGs provide high reliability and stable performance, while its 3 MEMS (Micro-Electro-Mechanical Systems) accelerometers provide highly accurate 6-degrees-of-freedom angular rate and acceleration data [32]. These six degrees of freedom correspond to the motion along 3 perpendicular linear axes and to the rotation around of each of these axes. In numbers, the accuracy in the Pitch and Roll angle is 0.015° RMS, while in the Heading it is 0.035° RMS.



Figure 3.9: 1750 IMU by KVH. Source: [32]

3.5. Other available UAV Laser Scanning systems

The integration of UAVs and LiDAR is considered to be one of the most useful developments in the surveying profession. Apart from the value of its products, this fact can also be proven by the variety of the solutions for UAV Laser Scanning that is being available the last couple of years. In the paragraphs that follow, the main available UAV Laser Scanning systems are going to be presented and a comparison of their main specifications is going to be given.

3.5.1. RIEGL Laser Measurement Systems

RIEGL Laser Measurement Systems, located in Horn, Austria, is a leading company for more than 30 years now in the research, development and production of terrestrial, industrial, mobile, bathymetric, airborne and UAS-based laser scanners and laser scanning systems.

RiCOPTER

The RiCOPTER is the first UAV developed and manufactured by a provider of laser scanners and scanning systems. It consists of a lightweight carbon fibre main frame, foldable propeller carrier arms and shock-absorbing undercarriage, which enable stable flight, safe landings and handy transportation. The RiCOPTER can be equipped with different sensors, e.g. photogrammetric cameras, thermal-infrared cameras, hyper-spectral cameras, magnetometers, radiation sensors, and gas leak detectors, up to an overall maximum payload of 16 kg (sensors and power supply). For surveying missions, the RiCOPTER is equipped with the airborne laser scanning system RIEGL VUX-SYS, which is further described below. Its Maximum Take-off Mass (MTOM) is 25 kg, its flight endurance with maximum load is 30 minutes and its maximum operating altitude AMSL (Above Mean Sea Level) is up to 4000 m (12,000 ft) [56].

RIEGL VUX-SYS

The RIEGL VUX-SYS is a complete miniaturised airborne laser scanning system solution of low weight (approximately 3.5 Kg) and compact size (298 x 180 x 125 mm) for flexible use in UAVs, helicopters, gyrocopters and ultra-light aircraft installations. The system consists of a RIEGL laser scanner, an IMU/GNSS system (fiber optic gyroscope and GPS/GLONASS receiver), a control unit with various interfacing options and up to two optional cameras [57]. The laser scanner solutions for the RIEGL VUX-SYS are the following:

- RIEGL VUX-1UAV (former VUX-1)
- RIEGL miniVUX-1UAV

The combination of the RiCOPTER and the RIEGL VUX-SYS, carrying the suitable laser scanner for each application, can result to the acquisition of high-accuracy and high-resolution laser scan and image data. Its structure and its components are shown in Fig. 3.10.

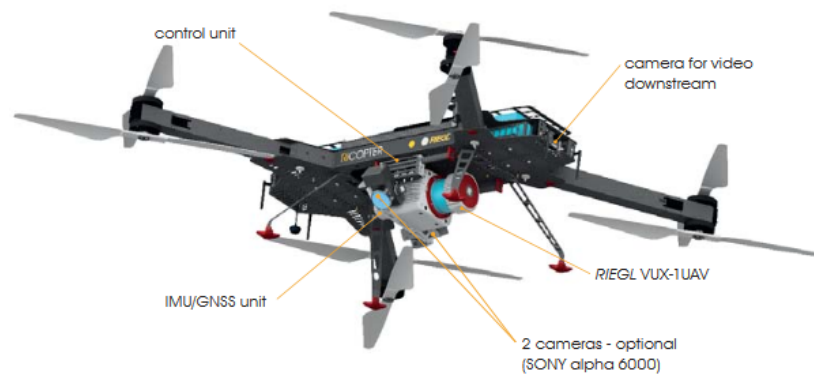


Figure 3.10: RiCOPTER equipped with the RIEGL VUX-SYS. Source:[60]

RIEGL VUX-1UAV

The RIEGL VUX-1UAV (former VUX-1) (see Fig. 3.11) is a lightweight and compact laser scanner that provides highspeed data acquisition using a narrow infrared laser beam and a fast line scanning mechanism. More specifically, with a scan speed up to 200 scans/second and measurement rate up to 500,000 meas./sec, a 10 mm survey-grade accuracy can be achieved. The operating flight altitude is up to more than 300 metres and the field of view is up to 330°. It provides also the opportunity for online waveform processing and multiple target capability [59].

RIEGL miniVUX-1UAV

The RIEGL miniVUX-1UAV (see Fig. 3.11) is the new release of RIEGL and it is an extremely compact, lightweight (1.55 kg) and cost-efficient, yet robust, device to acquire survey-grade measurement data by use of remotely piloted helicopters and unmanned aircrafts for a variety of applications. It provides a 360° field of view and multiple target capability – up to 5 target echoes per laser shot - with a scan speed up to 100 scans/sec (around 100,000 measurements/sec). In addition, it enables the online waveform processing, just like the RIEGL VUX-1UAV [58].



Figure 3.11: The two laser scanner solutions for the RIEGL VUX-SYS. Left: RIEGL VUX-1UAV and right: RIEGL miniVUX-1UAV. Source:[59], [58]

BathyCopter

Apart from the previous, RIEGL has combined the RiCOPTER with another system, the RIEGL BDF-1, creating the BathyCopter (see Fig. 3.12) for hydrographic applications ideally suited for generating profiles of inland water bodies. RIEGL BDF-1 is a bathymetric depth finder comprising of tilt compensator, an IMU/GNSS unit with antenna, a control unit and up to two external digital cameras - and optionally a miniVUX-1UAV LiDAR sensor. It sends out laser pulses at a rate of 4 kHz and the echo signal of each laser pulse is digitised and recorded for the entire range gate of 50m. That means, that predetection averaging of the waveforms can be performed in post processing, increasing the depth performance [55].



Figure 3.12: RIEGL's BathyCopter. Source:[55]

3.5.2. YellowScan

YellowScan is another world-famous company that designs, develops and produces aerial drone imaging sensor systems for professional applications. It is located in Montpellier, in the South of France and it offers two main products (sensors) to be mounted on a UAV, the YellowScan Mapper and the YellowScan Surveyor. Details about the two systems follow in the next paragraphs.

YellowScan Mapper

YellowScan Mapper was the first sensor created by YellowScan and thus the base for the development of YellowScan Surveyor. As shown in Fig. 3.13, it is lightweight (2.1 Kg) surveying solution for drones and other ultra-light aircrafts that finds wide application in corridor mapping, environment studies, archaeology as well as forestry. It offers a precision of 10 cm and an absolute accuracy of 15cm, while having a laser scanner

frequency of 40 kHz. it includes a high-end Attitude and Heading Reference System (AHRS), which allows precise measurements of the attitude and Dual-frequency GNSS receiver [85].

YellowScan Surveyor

YellowScan Surveyor is an improved version of YellowScan Mapper, offering a subscale-decimeter accuracy for highest density level data in demanding survey applications. More specifically, its precision is increased to 4 cm and its absolute accuracy to 5cm with a measurement rate around 300,000 per second. In addition, it is smaller and even lighter (1.6 Kg). The battery autonomy is the same as for the YellowScan Mapper (2 hours) [86].



Figure 3.13: YellowScan's sensors. Left: YellowScan Mapper and right: YellowScan Surveyor. Source: [85], [86]

3.5.3. Routescene

Routescene's solution for UAV Laser Scanning is the so-called UAV LidarPod (see Fig. 3.14). It is a turnkey product, which means that it includes the sensor, GPS/INS, radio telemetry, data storage and power management and thus no external components are necessary. The laser scanner that is integrated here is the same as the one used by Shore Monitoring & Research B.V. (Velodyne HDL-32E) and the GNSS receiver is a triple-frequency GNSS receiver that provides up to 1 cm accuracy positioning and supports all of the current and future satellite navigation systems. The whole system weighs 2.5 Kg, enabling a 20-minute flight duration and offers an absolute position accuracy of 6 cm at 40 m range [38].

Recently, Routescene collaborated with Hanseatic Aviation Solutions and came up with the integration of a fixed-wing UAV, the Hanseatic S360, with the Routescene LidarPod. That is an unmanned aerial 3D mapping solution capable of flying long-distances, particularly for use in large countries with great expanses of remote land. The applications of this integrated solution are diverse from long distance surveys such as powerline inspections in the utilities sector, biomass mapping of forests to geophysical surveys [21].



Figure 3.14: Routescene's UAV LidarPod. Source:[38]

In the table that follows, the main specifications of the aforementioned aerial systems are compared.

Table 3.2: Comparison of the main specifications of the aerial systems described above

	 Phoenix LiDAR Systems	 Riegl Laser Measurement Systems	 Riegl Laser Measurement Systems	 YellowScan	 YellowScan	 RouteScene
Manufacturer	Phoenix LiDAR Systems	Riegl Laser Measurement Systems	Riegl Laser Measurement Systems	YellowScan	YellowScan	RouteScene
Model	AlphaAL3-32	RIEGL VUX-SYS with VUX-1UAV	RIEGL VUX-SYS with miniVUX-1UAV	Mapper	Surveyor	LidarPod
Wavelength (nm)	905	905	905	905	905	905
Waveform processing	No	Yes	Yes	No	No	No
Maximum range (m)	107 at 60% Reflectivity	920 at 60% Reflectivity	250 at 60% Reflectivity	100	50	107 m @ 60% Reflectivity
Positioning accuracy XY (cm)	2.5-3.5 at 50 m range	10	15	10 + 1% x altitude for XY and 0.5% for Z	5 + 1% x altitude for XY and 0.5% for Z	6 cm at 40 m range
Precision (cm)	-	5	10	10	3	-
Field of view horiz. (deg)	360	330	360	100	360	360
Field of view vertical (deg)	+30/-10	single layer	single layer	single layer	single layer	+30/-10
Laser scanner frequency (kHz)	5-20	up to 550	100	40	300	5-20
Maximum number of returns	2	4	5	3	2	2
Type of GNSS Receiver	Dual-frequency, GPS, GLONASS, RTK-ready	no info available	no info available	Dual-frequency, GPS, GLONASS, RTK-ready	Dual-frequency, GPS, GLONASS, BeiDou, RTK or PPK mode	Triple-frequency, GPS, GLONASS, GALILEO and BeiDou, RTK-ready
Weight (Kg)	3.2	5.4	3.2	2.1	1.5	2.8
Size (mm)	L296 x W225 x H197 mm	L298 x W209 x H129	L243 x W111 x H85	L172 x W206 x H147	L100 x W150 x H140	L320 x D100
Power consumption (W)	40	95	16	10	15	28
Year of launch	2015	2015	2016	2014	2016	2014

According to Table 3.2, the six aerial systems that were chosen to be compared here have certain common specifications, but also some significant differences. At first, the wavelength is the same for all of them and equal to 905 nm (Near-Infrared), but only the RIEGL systems provide the opportunity of full-waveform processing. The maximum range of the laser scanners is quite different, with the largest being the one of the RIEGL VUX-SYS with VUX-1UAV system (920 m at 60 % reflectivity), while the other RIEGL system presents also large range (250 m at 60 % reflectivity). The rest three scanners have a range of approximately 100 m and finally the YellowScan Surveyor has the smallest one, of only 50 meters. As far as the positioning accuracy is concerned, the highest one is presented by the Phoenix aerial system (~ 3 cm at 50 m range). The rest of the systems can provide a positioning accuracy of about 5 to 10 cm, with the exception being the RIEGL VUX-SYS with miniVUX-1UAV system whose positioning accuracy is 15 cm. In addition, the horizontal field of view is 360 deg for all of them, apart from the RIEGL VUX-SYS with VUX-1UAV system (330 deg) and YellowScan Mapper (100 deg). At the same time, the Phoenix system and the LidarPod are the only systems that offer a wide vertical field of view (+30/-10 deg), while the rest have a single layer. The scanning frequency is quite high for the RIEGL systems (up to 550 kHz and 100 kHz for VUX-1UAV and miniVUX-1UAV respectively) and for the YellowScan Surveyor (300 kHz), while for the other systems is 20-40 kHz. In addition, the highest number of returns is provided by the RIEGL systems (4 and 5 returns for VUX-1UAV and miniVUX-1UAV respectively), YellowScan Mapper provides 3 returns and the other two systems only 2 returns. Regarding, the GNSS receivers of the systems, the one included in the LidarPod system is the only one that is triple-frequency receiver, while all of them can operate in RTK-mode. When it comes to the weight and the size of the systems, the lightest and smallest at the same time are the YellowScan systems (2.1 and 1.5 Kg for Mapper and Surveyor respectively), while the heaviest is the RIEGL VUX-SYS with VUX-1UAV system (5.4 Kg). All the other systems weigh approximately 3 kg. Finally, regarding the year of launch of the systems, the oldest ones are the YellowScan Mapper and the LidarPod, launched in 2014, the Phoenix system and the RIEGL VUX-SYS with VUX-1UAV system followed in 2015 and most recently, in 2016, the RIEGL VUX-SYS with miniVUX-1UAV system and the YellowScan Surveyor were launched as well.

3.6. Summary

Laser Scanning is a remote sensing technique that uses light in the form of laser pulses for measuring ranges to the Earth, and by combining them with other data recorded, the 3D coordinates of points on the target surface can be derived. UAV Laser Scanning is the latest development in the field of laser scanning and uses a UAV as a platform for this kind of measurements. It has already found application in a variety of fields, such as in agriculture, in forestry management, in archaeology, in mining etc. Its principle is based on the known propagation velocity of the light. Using this information together with the recorded time delay of the round trip of a pulse, the range can be evaluated. The system components of a UAV Laser Scanning system are the platform (drone), the laser scanner, the GNSS receiver and the IMU. Although the first drones were developed in the early 20th century and they were used for military purposes, as of 2005, drones started emerging into other fields as well and recently they have proven to be really useful in surveying. Laser scanners are responsible for the range measurements and when combined with the GPS and IMU observations, which determine the position and the orientation of the platform, 3D coordinates can be derived. In this study, the aerial system that was used is the Alpha AL3-32, by Phoenix LiDAR Systems, in combination with the DJI Spreading Wings S1000 Octocopter. This system is currently considered to be one of the lightest, highest density and most accurate 3D laser mapping systems globally. However, more and more such systems are being constantly developed. One of the most important companies in this field is RIEGL Laser Measurement Systems, which offers two UAV Laser Scanning systems, RIEGL VUX-SYS with VUX-1UAV and RIEGL VUX-SYS with miniVUX-1UAV. In addition, the French company YellowScan has developed two such systems for surveying purposes as well, which are the YellowScan Mapper and the YellowScan Surveyor. Finally, using the same

Velodyne laser scanner, Routsene has created the LidarPod, which is a high accuracy system, also due to its advanced GNSS receiver. The specifications of these systems differ when it comes to the range, the positioning accuracy, the number of returns, the weight etc.

4

Fieldwork - Validation Data Acquisition

One of the most important steps during the post-processing of a point cloud is the validation of it and its after-products. When we particularly speak about a point cloud that comes from UAV Laser Scanning, its validation can be realised by carrying out Terrestrial Laser Scanning and GPS measurements in the study area or by using AHN data. The latter is available online, however it was decided to go on a fieldwork to Schelphoek in order to acquire additional validation data, TLS and GPS data. It should be mentioned that Shore Monitoring & Research B.V. had already provided a GPS dataset from the day of the UAV flight. So, the aim was to measure different parts of the study area and use them in combination. The fieldwork took place on April 23, 2016 and lasted approximately 8 hours. This chapter starts with a description of the study area and its characteristics, it continues with the instruments and the methods that were used at the field and finally there are

4.1. Description of the study area

The study area, depicted in Fig. 4.1 is located in Schelphoek, which is the coastal part of Serooskerke. Serooskerke is a small village on the island - and municipality - of Schouwen-Duiveland, in the province of Zeeland, The Netherlands.



Figure 4.1: Left: The location of Schelphoek in the southern part of The Netherlands. Right: A closer look at Schelphoek.

As shown in Fig. 4.2, when looking at Schelphoek from the higher to the lower elevations, the study area consists of a low-vegetated dune that ends to an almost flat bike path and a rock slope (covered with asphalt)

that follows. Where the slope ends, a sandy beach starts. There, four breakwaters are constructed, one after the other. Since Schelphoek is situated in an intertidal zone ¹, the breakwaters are sometimes above and sometimes below the water level, depending on the tide.



Figure 4.2: Left: The higher-elevation part of the study area (the dune followed by the bike path and the rock slope). Right: The lower-elevation part (the rock slope followed by the sandy beach and the breakwaters).

Because we are looking at the study area from a coastal monitoring point of view, we need to distinguish the variable and non-variable elements in it. The reason for that is because only the non-variable elements can be used for the acquisition of validation data on a different date than the one on when the ALS measurements were carried out.

In these terms, the bike path, the rock slope and potentially the breakwaters are considered to be stable structures that do not change over time, especially when speaking about a time period of several months. The breakwaters are potentially - and not fully - suitable, however, because of the fact that they are covered with a type of plant (see in Fig. 4.3 the bottom image) that makes them relatively variable over time as well. If it is possible to take measurements of only the actual structure (through the plant), then it should not be a problem. In addition, at the middle of the gulf, there is a parking space (see in Fig. 4.3 the top right image), which is essentially a flat asphalt area, with no sand, and it can also be a very good source of validation data.

¹Intertidal zone is the area that is above water at low tide and under water at high tide [78]



Figure 4.3: Top left: The four breakwaters of the study area. Top right: The parking space. Bottom: The plant that covers the breakwaters. Source of the top images: Google Earth.

On the other hand, though, the area of the beach can not be used for validation purposes, unless the measurements take place at the same time of the UAV flight. The weather phenomena and the interaction with the water can rapidly change the sandy surface of the beach, even in one day.

4.2. Fieldwork preparation and description of instruments

One of the most important parts of a fieldwork is the preparation of the equipment that is going to be needed when being at the field. A good planning of all the necessary instruments and tools helps a lot for the prevention of unexpected mistakes. In the case of the Schelphoek fieldwork, the instruments that would be used both for the TLS and the GPS measurements are listed in Table 4.1 according to relevance and a brief description of them follows in the next paragraphs.

Table 4.1: List of instruments and tools needed for the fieldwork

Laser Scanning	Leica ScanStation C10 4 Batteries Tripod Tripod road stand Leica round targets Square targets
GPS	2 Trimble R7 receivers 2 Trimble Zephyr Geodetic antennas Tripod RTK Range pole 8 Batteries Measurement tape
Other	Camera USB stick Hammer Safety vests

4.2.1. Terrestrial Laser Scanning instruments

The laser scanner that was used during the fieldwork was the one that is available in the Department of Geoscience and Remote Sensing, TU Delft, and that is the Leica ScanStation C10 (see Fig. 4.4). This instrument includes the scanner, the batteries, a graphic-controller (interactive screen), the data storage and a video camera, thus it is more accurately described as a platform that carries all the necessary components. Its main specifications are [20]:

- Accuracy of single measurement:
 - Position: 6 mm
 - Distance: 4 mm
 - Angle (horizontal/vertical): 60 μ rad/ 60 μ rad
- Target acquisition: 2 mm
- Laser type: Green, wavelength = 532 nm visible
- Range: 300 m
- Scan rate: up to 50,000 points/sec
- Field-of-view:
 - Horizontal: 360°
 - Vertical: 270°
- Scanning Optics: Vertically rotating mirror on horizontally rotating base
- Data storage capacity: 80 GB onboard
- Duration: 3.5 hours, with 2 batteries
- Dimensions (D x W x H): 238 mm x 358 mm x 395 mm
- Weight: 13 kg (w/o batteries)



Figure 4.4: Leica ScanStation C10 laser scanner. Source:[20]

During its operation, the scanning data are saved automatically in its internal storage and after the end of the measurements they can be easily exported to a USB stick.

For the registration of the point clouds that come from different stations, the use of targets is necessary. Therefore, during the fieldwork two different types of targets were used. The first one is the target shown on the left of Fig. 5.1 and it is provided also by Leica. That consists of a six inch diameter paddle, which can be rotated both horizontally and vertically, and a magnetic base. The latter is very useful, especially when scanning in urban areas, where the target can be easily mounted on any metal object. The second type of target is essentially a 20-cm labelled square pattern mounted on wooden plates (see Fig. 5.1 on the right). For some of them, the wooden plates are attached to wooden stakes (of varying length) so that they can be placed into the ground when possible.



Figure 4.5: Left: Leica round target. Right: Square target

In addition to the previous, a heavy stable tripod as well as a tripod road stand was necessary. The stand is used only in case the scanning station is on the road, or generally on a hard surface, so that the stability is as good as possible.

4.2.2. GPS instruments

For the GPS measurements, two pairs of GPS receivers and antennas (base and rover station) were used. These were the Trimble R7 GPS receivers and Trimble Zephyr Geodetic antennas (see Fig. 4.6), which were also available at the Department of Geoscience and Remote Sensing, TU Delft. Their specifications are presented below [43]:

- Trimble R7 GPS receiver
 - Static and Fast Static GPS Surveying
 - ◊ Horizontal: ± 5 mm + 0.5 ppm RMS
 - ◊ Vertical: ± 5 mm + 1 ppm RMS
 - Real-time and Post-processed Kinematic Surveys
 - ◊ Horizontal: 10 mm + 1 ppm RMS
 - ◊ Vertical: 20 mm + 1 ppm RMS, 0.02 seconds latency
 - Dual-frequency (L1 and L2) receiver and tracking of the L2 Civil Signal (L2C)
 - Channels: 24
 - Greater than 10 hours data logging or 7 hours of RTK operation
 - Front panel for control of power, data logging, ephemeris etc.
 - LED indicators for satellite tracking, radio link operation data logging and power monitoring
 - Data Storage: up to 128 MB
 - Operating temperature: -40 °C to $+65$ °C
 - Dimensions: 13.5 cm W x 8.5 cm H x 24 cm L
 - Weight: 1.4 Kgs

- Trimble Zephyr Geodetic antenna
 - Dimensions: 34.3 cm diameter x 7.6 cm maximum depth
 - Weight: 1.0 Kgs
 - Operating temperature range: -40 °C to $+70$ °C
 - Integral Low Noise Amplifier
 - 50 dB antenna gain
 - Trimble Stealth™ Ground Plane for reduced multipath



Figure 4.6: Top left: Trimble R7 GPS receiver. Top right: Trimble Zephyr Geodetic Antenna. Bottom: RTK/GPS Carbon Fibre pole

When carrying out an RTK survey, the rover station is movable and therefore the antenna should be mounted on a pole. During the fieldwork, a 2-m carbon fibre pole, which can be disassembled into two parts, was used. So, the usual practise is that the GPS receiver is in a backpack, carried by the surveyor who moves together with the pole.

4.3. Acquisition of Terrestrial Laser Scanning data

The first type of measurements that were carried out at Schelphoek was Terrestrial Laser Scanning. Performing TLS measurements at the same region as the UAV LS data were collected would enable us to make a comparison between Terrestrial and UAV Laser Scanning for coastal regions. Since the procedure and the properties of the measurements differ a lot, it was expected that the two methods would show certain advantages and disadvantages (which are discussed later), especially when taking the nature of the study area into account. Thus, it was interesting to discover them and make a conclusion about the most suitable method for such a survey. In addition, these TLS data would be used for the validation of the point cloud that comes from the UAV flight as well as the DTM derived from it. In the following paragraphs the procedure for the data collection that was followed is described.

According to what is aforementioned, the main goal regarding the TLS measurements was to scan stable parts of the study area and these were decided to be the rock slope, the breakwaters and the parking space. The exact locations of the different stations had to be at first determined in such a way that the objects of interest are included in the scan and there are overlapping areas for the later registration of the point clouds. For the realisation of the registration, targets are needed and therefore they should be put in these overlapping areas. So, the next decisions had to do with the location of the targets. After checking the features of the area, it was concluded that three stations would be used for the coverage of almost the entire width of the study area (not to its full length, just part of it) and one extra for scanning the parking place. The locations of these stations are shown in Fig. 4.7.



Figure 4.7: Left: The three first laser scanning station covering most of the width of the study area. Right: The fourth station in the parking place. The background map comes from Google Earth.

At every station, the laser scanner was mounted and levelled on the tripod, and we had to make sure that at least some of the already placed targets were visible. In addition, the resolution of the scans was always set the same in order to have the same point density in the derived point clouds. Fig. 4.8 shows these four point clouds, in an RGB visualisation derived from the pictures that were taken at the same time as the scanning.

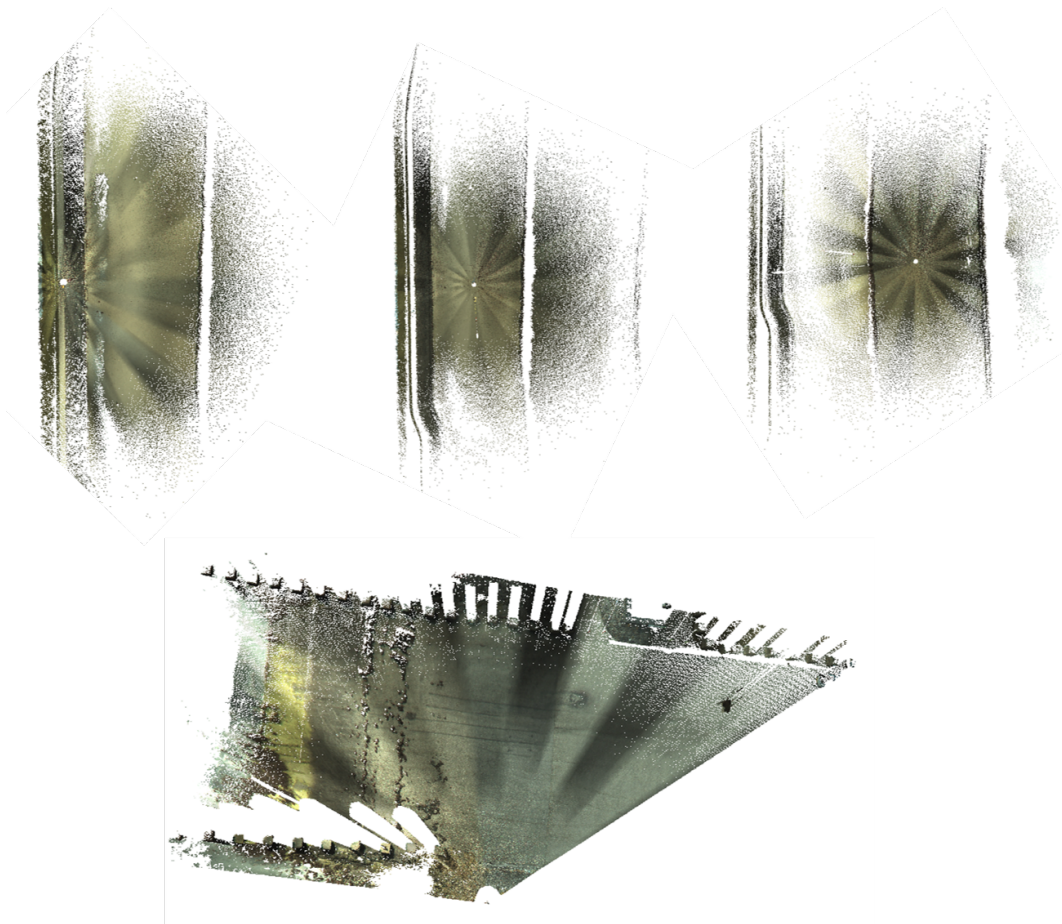


Figure 4.8: Top: A quick look of the point clouds coming from the three first stations. Bottom: The point cloud coming from the station in the parking place.

4.4. Acquisition of GPS data

Since the exact locations of the laser scanning stations had to be known for geo-referencing purposes, after the operation of the laser scanner at each station was finished, the GPS system was placed on the same tripod (without moving it), recording data for about half an hour each time. That was the first type of GPS measurements. The second one was using the Real-Time Kinematic method.

More specifically, when the one GPS was placed on the tripod of the third station and it was recording data of its location, it was also used as a base and at the same time the spare GPS was used as a rover. The second antenna was mounted on the RTK pole and the corresponding receiver was placed in a backpack. The goal was to take measurements of the stable objects. So, the first dataset contains measurements mainly from the breakwaters (with the RTK pole penetrating the plant) and the second dataset from the bike path and the rock slope. For each measurement, the pole was levelled and kept still for about 10 seconds. The route that was followed during the two sessions is depicted in Fig. 4.9.

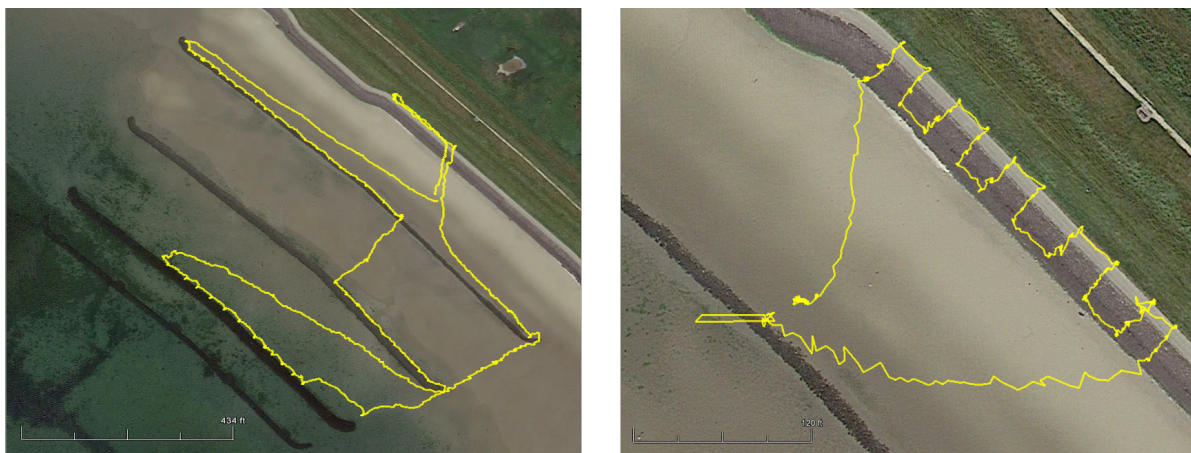


Figure 4.9: RTK/GPS measurements. Right: First set of RTK measurements. Left: Second set of RTK measurements. The background map comes from Google Earth.

4.5. Summary

This chapter was focused at first on the description of the study area in Schelphoek. It lays in an intertidal zone and therefore it is usually a quite muddy area and unfriendly for in situ measurements. The area consists of a low-vegetated dune that ends on a flat bike path. Where the bike path finishes, there is a slope that leads to the sandy beach. There somebody can find four breakwaters made out of rocks and covers with seaweed. In April, 2016 a fieldwork was carried out in this region in order to get some more insight in the study area and most importantly to get some extra validation data. More specifically, Terrestrial Laser Scanning measurements were performed in four different stations. The strategy for the TLS survey was to gather validation data from stable objects of the region, e.g. the asphalt slope, the breakwaters and a parking area that exists there, so that they could be used for the validation of our UAV LS dataset that was derived in another epoch. For these measurements, the laser scanner Leica ScanStation C10 was used together with two different types of targets, Leica round target and 20-cm labelled square pattern mounted on wooden plates. In addition to the TLS, GPS observations were also acquired from the field. For that, two Trimble R7 GPS receivers and two Trimble Zephyr Geodetic antennas were used. Having the same strategy as for TLS, two GPS datasets were acquired, the first one containing measurements mainly from the breakwaters and the second one from the bike path and the rock slope.

5

UAV Laser Scanning point quality assessment

UAV Laser Scanning is considered to be a promising surveying technique and its evolution in the coming years is expected to be rapid. Apart from the time- and resources-saving nature of the UAV Laser Scanning, though, the accuracy level of the 3D coordinates of the derived point cloud is also very critical when considering the most suitable method for a survey. In this chapter, after a brief description of the types of errors that appear in surveying measurements, the main sources of errors in a UAV Laser Scanning system are discussed. What follows is the investigation of the 3D coordinates' accuracy of the Alpha AL3-32 aerial system with the use of an error model and the impact of certain flight parameters on it. Finally, the procedure for forming a flight plan is described.

5.1. Data quality considerations

The accuracy and the precision are one of the most important measures for the quality of a system, a dataset etc and they are closely linked to the error budget of a system. In this section, some background information is given on these two measures, but also on the three types of errors that can be found in surveying measurements.

5.1.1. Accuracy and Precision

Accuracy and precision are two terms that are often confused and erroneously used due to the similarity of their colloquial meaning. However, because we refer to them quite a lot in the following chapters, it is important that we clarify their meanings, according to how they are defined in the fields of science, engineering and statistics.

- *Accuracy* of a measurement system is the level of closeness between the best value of the measurements of a variable and the true value of it [79]. Therefore, when talking about a laser scanning system, accuracy is the degree of conformity of a measured position to its actual (true) value [85].
- *Precision* of a measurement system is the degree to which repeated measurements under unchanged conditions show the same results [79]. It is also called reproducibility or repeatability and it actually accounts for the variation in successive measurements [85].

In Fig. 5.1, these two terms are illustrated using the example of a round target.

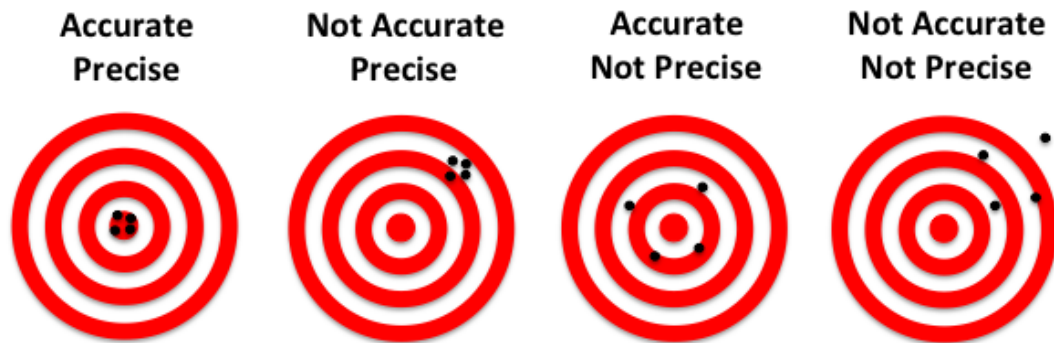


Figure 5.1: Accuracy vs. precision. The four different cases illustrated using round targets.

When a set of measurements is normally distributed, then the accuracy can be determined from the distance between the mean value and 'true' value - or reference value - on the x-axis. At the same time, the precision can be derived by computing the total spread of all the measurements on the x-axis. These are best depicted in Fig. 5.2.

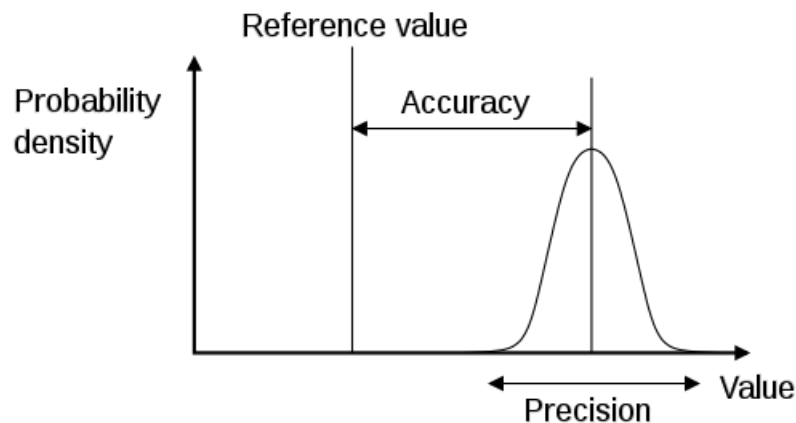


Figure 5.2: Accuracy and precision of a normally distributed set of measurements. Source: [79]

5.1.2. Types of errors

When talking about errors that are introduced during a measuring process, there are three main types that can be distinguished. These are: the *blunders*, the *random* and the *systematic* errors.

- **Blunders:** The blunders, which are also referred to as *outliers*, are the measurements that are quite different from the rest and introduce large errors in the final survey, if missed or ignored. However, exactly because they are significantly larger, they are the easiest errors to be identified with normal survey checks and eliminated, except for certain cases that some small blunders may remain undetected and therefore not removed.
- **Random errors:** The random errors are the errors generated by the imperfections of the instruments used - in our case the laser scanner, the GPS and the IMU - and they are influenced by diverse internal and external interferences during the measurements [75]. Their impacts are more complicated than

the ones from the other types of errors, since they don't follow a specific pattern. They are always present and can never be eliminated, however, when studied in depth, their contribution to the final uncertainty of the measurements can be minimised. There are different methods to quantitatively analyse these errors, the most popular of which is the least-square solution with redundant observations [76]. A characteristic example of such a study on ALS measurements is the one from Wang et. al [75], where the method of linear least squares regression was used to investigate the impact of random errors on the ALS accuracy.

- **Systematic errors:** This last type of errors is also introduced by the instruments as well as by possible misalignments between them or coordinate transformations. But, unlike random errors, systematic errors reproducible inaccuracies that appear consistently in the same direction. Systematic errors are often due to a problem that persists throughout the entire measurement process. To study the effect of an individual systematic error, the other systematic errors have to be kept unchanged. This method is demonstrated later in the chapter for the determination of the 3D coordinates systematic errors.

In the error investigation that follows, the positioning error budget is discussed by mainly focusing on the systematic errors. The blunders are obvious and easily eliminated, as it was mentioned before, and the random errors need an extensive study to be accurately determined. Therefore, we take a closer look into the systematic errors of our aerial system and we investigate their impact on the positioning accuracy of a point cloud.

5.2. Sources of error in UAV Laser Scanning systems

When evaluating a UAV Laser Scanning system, the first thing that future buyers (or clients) are interested in is its positioning accuracy. That is the accuracy of the 3D coordinates of a point cloud derived with this aerial system. Therefore, here we discuss the sources of (systematic) error that affect this accuracy and we try to quantify the errors coming from different sensors or procedures, from the acquisition of the raw data to the derivation of the final 3D coordinates.

The positioning accuracy of a UAV Laser Scanning system is affected by numerous factors, the most obvious of which are the performances of the different components of such a system, namely the laser scanner, the GPS and the IMU. More specifically, the laser beam range and incidence angle as well as the target reflectivity properties are significant sources of error that could affect the final accuracy, but quite critical factors are also the accuracy of the platform position and orientation derived from the carrier-phase differential GPS/INS data [76]. In addition to the previous, any misalignments between the instruments of the system reduce the accuracy by introducing systematic errors. Finally, in the case that the derived point cloud has to be transferred in another coordinate system, this transformation includes errors as well, sometimes small (or even negligible) and sometimes larger.

Fig. 5.3 summarises the major types of errors that determine the accuracy of the 3D coordinates, as reported from Baltsavias E. P., [5], followed by a more detailed description of them.

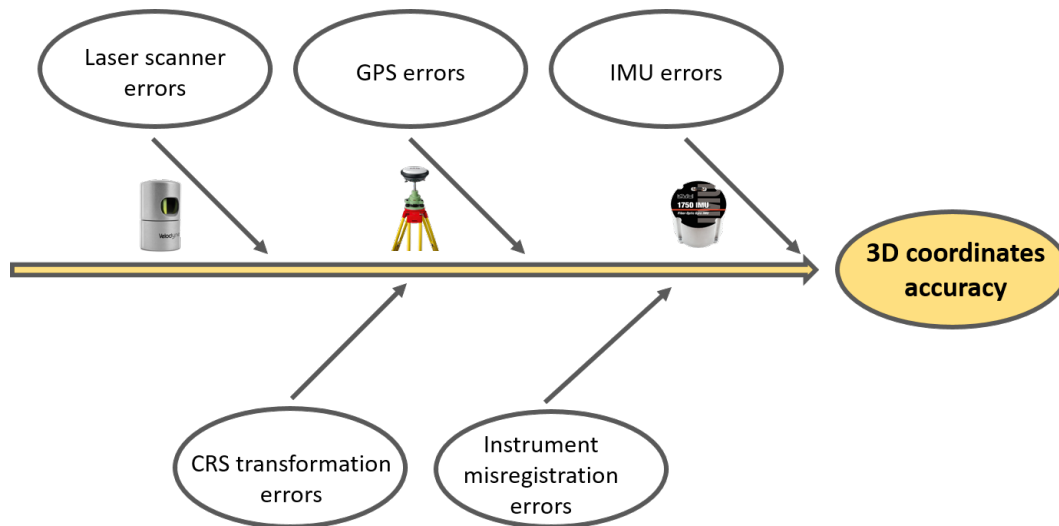


Figure 5.3: The major systematic errors that determine the 3D coordinate accuracy

5.2.1. Laser scanner errors

There are multiple factors that influence the accuracy with which the laser scanner subassembly is able to measure the distance and the angle from the LIDAR system to the ground target [22]. These factors introduce the two main errors that are associated with the laser scanner of an UAV LiDAR system and these are the *range error* and the *scan angle error*.

The range between the sensor and a point on the reflecting surface is determined by measuring the travelling time between the emitted and the received pulse. The uncertainty of this measurement (range error) depends mainly on two categories of factors and these are: the optical and electronical design and the target reflectivity [76]. So, on the one hand, aspects like the scanner mirror vibration, the laser firing point ambiguity, the laser transmitted time and receipt time determination etc. determine the magnitude of the range error, but on the other hand, the characteristics of the ground target are also very significant. The accuracy of the range measurement is highly related to the surface roughness, the terrain slope and any other kinds of disturbances, like e.g. water, that usually absorbs the light, or other terrain discontinuities and temporary objects such as pedestrian, cars and animals [82].

The second main laser scanner error is the scan angle error. The scan angle is defined as the angle between the vector that lays on the nadir direction and the laser beam vector. This error is also influenced by many elements. The most important of these is the laser beam divergence, which results in an incorrectly measured point position [54]. In addition, it may be affected by mechanical aspects, such as vibrations or oscillations caused by the interference with the UAV engine [36].

Fig. 5.4 illustrates the effects of these two errors in the determination of the position of the laser point.

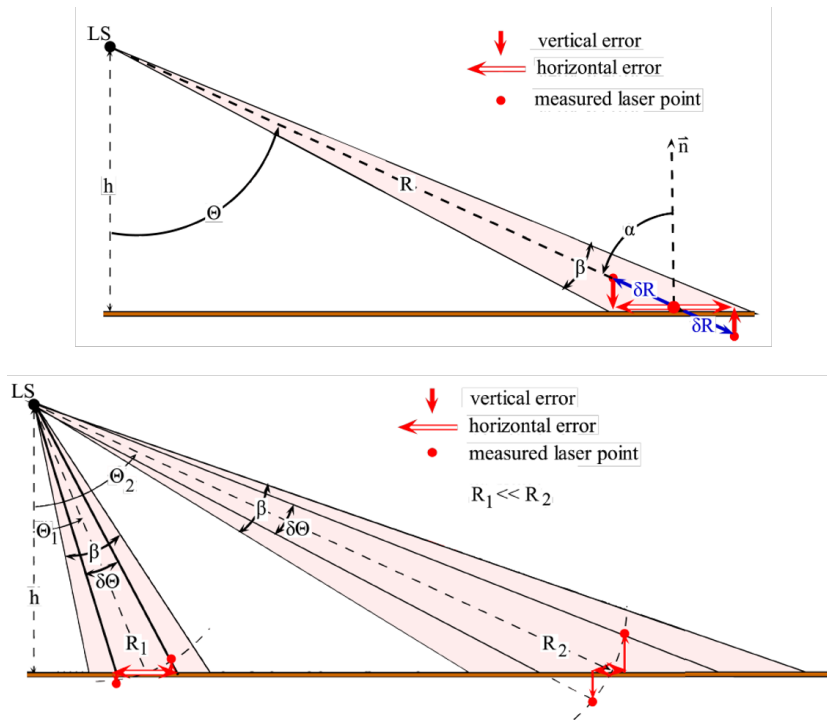


Figure 5.4: The effects of the range and the scan angle error on the final position of the laser point. Source:[7]

In the top image, the firing of a laser pulse from a laser scanner (LS) towards the target surface is depicted. h is the flight height, Θ is the scan angle, R is the range, β is the beam width, which is the dispersion of the highly directed laser beam, α is the incidence angle, and thus the angle between the normal vector n and the laser beam vector and finally δR is the range error. The range error δR lays on the laser beam vector and is added, when directed towards the target surface, or removed, when directed towards the laser scanner, to the range. This effect creates both a horizontal and a vertical error, on which the final position of the laser point depends.

In the bottom image, two laser pulse firings from the laser scanner are shown. The first one is fired with a scan angle Θ_1 , which results to a range R_1 , and the second one is fired with a larger scan angle Θ_2 , which consequently results to a larger range R_2 . Here, $\delta\Theta$ is the scan angle error and its effect is investigated in these two cases. It is observed that the positioning error of the laser point depends on the scan angle. More specifically, when the scan angle is smaller, the error created is mainly horizontal and thus the positioning error of the laser point is mostly on the y-axis. On the other hand, when the scan angle is larger, then the beam spreads more and now the vertical error is much larger. That results to a positioning error which is mainly on the z-axis.

These two laser scanner errors are most of the times mentioned and quantified by the laser scanner manufacturers in the manuals of their instruments and they are used to compare different models with each other, since they are a good measure of the absolute accuracy that can be achieved.

5.2.2. GPS errors

The GPS positioning error budget depends on diverse aspects, mainly regarding the atmosphere wherein the signal is transmitted, the available satellites as well as the mechanical part of it. The planimetric¹ error is

¹The term planimetric refers only to the *horizontal* features.

always lower than the vertical one and the most crucial factors are:

- the satellite configuration, i.e. the number of observable satellites, the baseline² geometry etc.
- the signal multipath, which is caused by the reflection of the signal from flat surfaces. The most characteristic example of this are the windows of the buildings.
- the satellite and the receiver clock biases
- and the atmospheric conditions, such as differential troposphere effects or ionosphere delay [54].

The GPS errors are usually combined with the IMU errors and they are referred to as navigation system error by the manufacturers of such aerial systems for UAV surveys. When it is necessary to know the exact error budget introduced only by the GPS system, we have to look into the specifications of the GPS antenna and receiver.

5.2.3. IMU errors

The IMU component of the aerial system computes the roll, pitch and yaw angles, which rotate the measurements from the body frame of the vehicle into the mapping frame [22]. The corresponding orientation errors of roll, pitch and yaw are determined for each axis individually and they change throughout the whole flight, having a tendency to decrease with time [54]. The major causes of these errors are initialisation errors, misalignment, and gyro drifts and measurement noise [82]. By integrating the GPS and the IMU measurements, mostly by using the Kalman filter, a better solution for the IMU orientation parameters can be derived, and as a result, the overall navigational accuracy increases.

5.2.4. Temporal interpolation errors

The three components of the UAV Laser Scanning system, the laser scanner, the GPS and the IMU, record measurements independently and with different time intervals. In order to derive the final 3D coordinates, the measurements of the position and orientation of the UAV (GPS and IMU records) have to correspond to the laser scanner measurements. Therefore, a temporal interpolation between the time gaps is required. This procedure introduces errors in the final values of the UAV position and orientation angles, which are then propagated into the positioning accuracy. However, this topic was not an objective of the current study, since there were not enough information about the recording patterns of the GPS and the IMU and is thus going to be neglected.

5.2.5. Instrument misalignment errors

All the main components of a UAV laser scanning system, namely the laser scanner, the GPS and the IMU, have different coordinate systems. Thus, another quite important source of systematic errors is the mounting between these components. The ones that are often mentioned in the literature and have been studied deeply are the *bore-sight error* and the *lever-arm error*.

The bore-sight error is associated with the imprecise alignment between the laser scanner and the IMU component. More specifically, these two components have independent coordinate systems. Typically, in the laser scanner's coordinate system, the x-axis is positive towards the head of the UAV, the y-axis towards the right side of it and the z-axis towards the ground. The two coordinate system axes should be parallel,

²A baseline is defined as the three dimensional vector between a pair of GPS stations, usually a base and a rover.

but in fact, small angles always exist between the IMU and laser scanner coordinate axes [87]. That is the bore-sight error and it can be distinguished into roll, pitch and heading error [24]:

- the roll error leads to a constant shift across the flight direction and a shift in the Z direction that varies linearly across the flying direction. The planimetric effect is dependent on the flying height and independent of the scan angle, while with the vertical effect the opposite happens.
- the pitch error results to a constant shift along the flight direction, which depends on the flying direction and the flying height, but it is independent of the scan angle.
- finally, the heading error is the most complicated one, since it causes a shift along the flying direction, but its magnitude varies linearly across the flight direction. This effect is independent of the flying height and direction, but it depends on the scan angle.

As shown in Fig. 5.5, bore-sight effects due to roll errors can be detected by projecting the cross-sections of different passes over the same area - when there is more than one. Quite often differences in the projected plane are noticed, which are due to different flying heights. However, bore-sight errors due to pitch and yaw cannot be observed from a cross-section view as easily [54]. Because the effect of this error cannot be neglected, the bore-sight angles must be estimated during an in-flight calibration procedure and be taken into account [76].

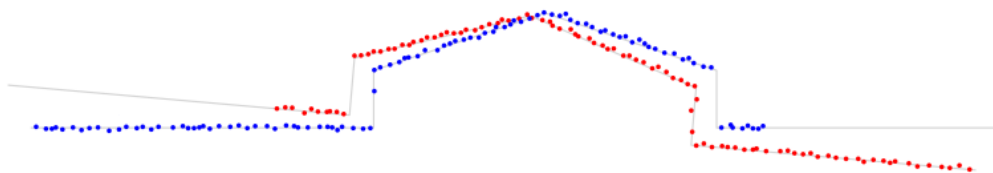


Figure 5.5: Discrepancies between the two point clouds due to bore-sight errors. Source: [46]

The lever-arm offset errors (or vectors) express the mounting errors between the laser scanner and the IMU, but also between the laser scanner and the GPS antenna. Unlike the bore-sight errors, these are not angular errors, but linear. They result to constant shifts in the derived point cloud to all directions. While the planimetric shifts are dependent on the flying direction, the shift in the Z-direction does not. In addition, both of them are independent of the flying height and scan angle [24].

The lever-arm offset between the laser scanner and the IMU can be usually measured quite accurately and therefore it is eliminated, but that is not the case for the offset between the laser scanner and the GPS antenna [76]. In order to achieve a correct geo-referencing, it is crucial that these offsets are measured. The method to do so is either through a calibration procedure or with physical measurements, which is often preferred [22].

5.2.6. Coordinate system transformation errors

Finally, the procedure of transferring a point cloud from a coordinate system to another - usually from a global to a local - introduces some extra errors that are mainly correlated with the accuracy of the transformation parameters and of course the method used.

5.3. Error analysis and accuracy estimation for the Alpha AL3-32

Now that the main sources of errors have been identified and discussed, the next task is to investigate their quantitative impact on the 3D coordinate accuracy.

5.3.1. Error model for ALS positioning accuracy

Peng et al., [50], investigated the influence of the motion errors on the positioning accuracy. They established an error model which is based on the geometry of the ALS measurements. Fig. 5.6 illustrates this geometry for the simplest case of a flat terrain and introduces the variables that are used in the motion error model of Peng et al.:

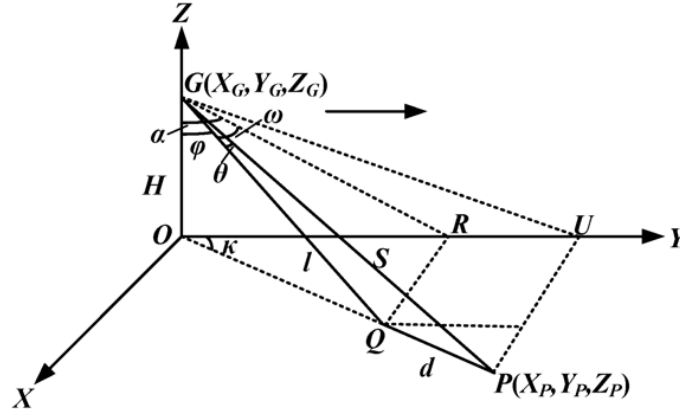


Figure 5.6: Positioning diagram of the airborne lidar for a flat terrain. Source: [50]

Based on the positioning diagram above, the 3D coordinate errors of an arbitrary laser point P (X_P, Y_P, Z_P) are given by the three following formulas [50]:

$$m_{X_P} = \sqrt{m_{X_G}^2 + \sin^2(\omega) m_l^2 + (l \cos(\omega))^2 m_\omega^2 + \sin^2(\kappa) m_d^2 + (d \cos(\kappa))^2 m_\kappa^2} \quad (5.1)$$

$$m_{Y_P} = \sqrt{m_{Y_G}^2 + \cos^2(\omega) \sin^2(\alpha) m_l^2 + (l \sin(\omega) \sin(\alpha))^2 m_\omega^2 + \sqrt{(l \cos(\omega) \cos(\alpha))^2 m_\alpha^2 + \cos^2(\kappa) m_d^2 + (d \sin(\kappa))^2 m_\kappa^2}} \quad (5.2)$$

$$m_{Z_P} = \sqrt{m_{Z_G}^2 + \cos^2(\omega) \cos^2(\alpha) m_l^2 + (l \sin(\omega) \cos(\alpha))^2 m_\omega^2 + (l \cos(\omega) \sin(\alpha))^2 m_\alpha^2} \quad (5.3)$$

where m_{X_G} , m_{Y_G} , m_{Z_G} are the GPS positioning errors, α , ω , κ are the attitude angles roll, pitch and yaw (heading), m_α , m_ω , m_κ are the attitude angles errors respectively (introduced by the IMU), S , l are the distances (ranges) between the sensor and the arbitrary laser points P and Q respectively - with Q being the adjacent point of P - and d is the distance between these two adjacent points (point spacing). Finally, m_S , m_l , m_d are the errors of S , l and d respectively. The last two are given by the formulas below [50]:

$$m_l^2 = \frac{\cos^2(\theta) - b^2 \cos(2\theta)}{1 - b^2} m_S^2 + \frac{S^2 \sin^2(\theta) + \cos(2\theta) b^2 S^2}{1 - b^2} m_\theta^2 + \frac{S^2 \sin^2(\theta)}{(1 - b^2)^3} (m_\alpha^2 + m_\omega^2 + m_\kappa^2) \quad (5.4)$$

$$m_d^2 = \frac{\sin^2(\theta)}{1 - b^2} m_S^2 + \frac{S^2 \cos^2(\theta)}{1 - b^2} m_\theta^2 + \frac{S^2 \sin^2(\theta) b^2}{(1 - b^2)^3} (m_\alpha^2 + m_\omega^2 + m_\kappa^2) \quad (5.5)$$

where θ is the angle between GP and GQ, or in other words the angular spacing between two adjacent planes, and m_θ is its error. The parameter b is calculated as: $b = \cos(\omega) \sin(\alpha) \cos(\kappa) + \sin(\kappa) \cos(\omega)$.

A more detailed description of the motion error model of Peng et. al as well as the solutions for other types of terrains can be found in [50].

5.3.2. Error budget

To calculate the a priori accuracy of the 3D coordinates of a point cloud derived with the Alpha AL3-32 aerial system, the uncertainties of each instrument that it consists of (as given by their manufacturers) will be used in combination with the previously described error model (see Fig. 5.7). The analysis above showed that the required values are:

- the ranging and the scan angle error of the laser scanner (Velodyne HDL-32)
- the horizontal and the vertical error of the GPS
- the attitude errors of the IMU (KVH 1750)

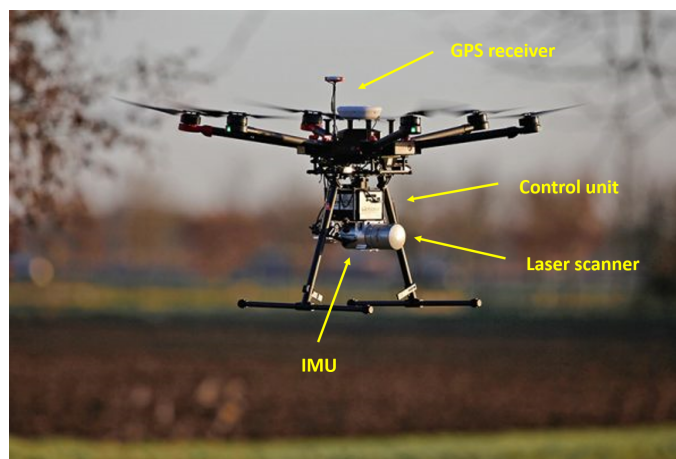


Figure 5.7: System components of the Alpha AL3-32 aerial system

According to the datasheets of the instruments and Phoenix LiDAR Systems that provided the aerial system, the required uncertainties are listed in the following table:

Table 5.1: Nominal errors of the instruments that the Alpha AL3-32 consists of

Instrument	Type of Error	Value
Laser Scanner	Ranging error	2 cm
	Scan angle error	0.01°
GPS	Horizontal error	1cm + 1ppm
	Vertical error	150% * horizontal error
IMU	Roll, Pitch angle error	0.015°
	Heading (Yaw angle) error	0.035°

Because the laser scanner and the IMU are fixed to each other through a single flat aluminium part (see Fig. 3.7), they are considered as perfectly aligned by the manufacturer (Phoenix LiDAR Systems) and it is expected that no misalignment error is introduced into the LiDAR measurements (neither static, nor - worse - dynamic, e.g. due to vibrations). In addition, the errors introduced by the coordinate system transformation are not taken into account here since no transformation was realised.

From the above it is concluded that the error budget of Alpha AL3-32 consists of the three components: the laser scanner, the GPS and the IMU. The contribution of these components as sources of error in the positioning accuracy is not constant and it depends on the range. The reason for that is because the magnitude of the angular errors that are introduced both by the laser scanner and the IMU depend on the range. So, what follows is an investigation of how much each component contribute to the positioning accuracy when the range varies.

5.3.3. Positioning accuracy

This investigation was performed for five different characteristic for a UAV flight values of range, which are 10 m, 20 m, 30 m, 40 m and 50 m, and the extreme value of 100 m range. The next figure illustrates these fluctuations in the form of pies. The orange part correspond always to the laser scanner contribution, the yellow one to the GPS and the green one to the IMU.



Figure 5.8: Percentage contribution of each one of the three components (laser scanner, GPS and IMU) to the positioning accuracy for different values of the range, 10 m, 20 m, 30 m, 40 m, 50 m and 100 m.

Looking at the six pies, it is clear that there is a specific pattern according to which the contributions of the three components fluctuate with the varying range. More specifically, for a range equal to 10 m the IMU contribution is very small (16 %), while the GPS contribution is quite large (52 %). However, this changes drastically with the range increase. At the range of 30 m, the two contributions are almost the same, but when it further increases, the IMU contribution is significantly larger than the one from GPS (47% and 29% respectively for 50 m range). At the same time, the laser scanner contribution changes too, but not that much, and more precisely, it decreases when the range increases. These observations are best illustrated in Fig. 5.9.

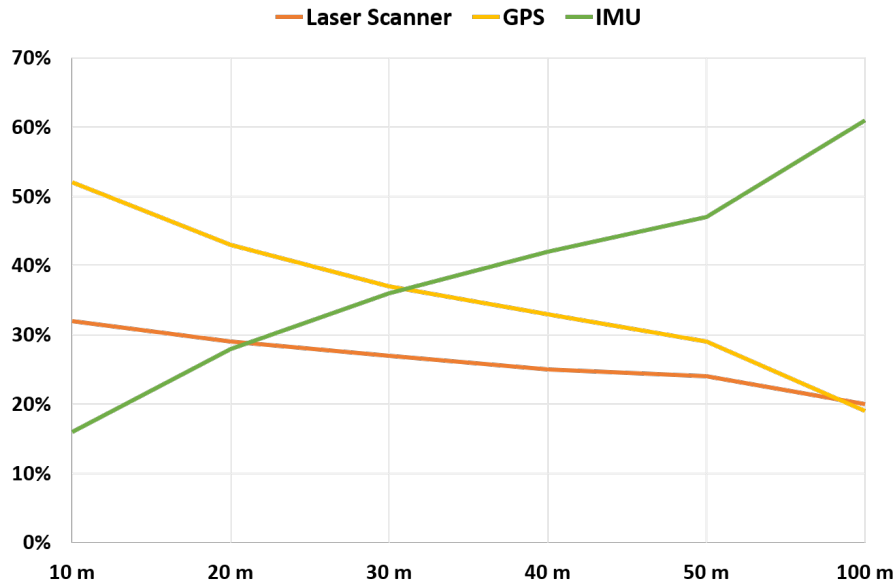


Figure 5.9: The fluctuating contributions of the laser scanner, the GPS and the IMU to the positioning accuracy.

Combining the two figures above, we can reach the conclusion that both the laser scanner and the GPS contributions as sources of error decrease while the range increases. On the other hand, the IMU contribution constantly increases.

What follows is the calculation of the 3D coordinate accuracy for typical values of the flight parameters as well as how it fluctuates when some of them change.

At first, we had to conclude on specific values for all of the variables of the error model. The ones that are given by the manufacturers are of course used, but for the rest some characteristic values that describe a typical drone flight are assumed. These are:

- $m_{X_G} = 0.0101m$, $m_{Y_G} = 0.0101m$ and $m_{Z_G} = 0.0152m$, which correspond to the horizontal error of $1cm + 1ppm$ when having a 0.5 Km baseline³ and the vertical error equal to 150% * horizontal error.
- $\alpha = 10^\circ$, $\omega = -20^\circ$, $\kappa = 0^\circ$. For the attitude angles, the simplest case of a slight tilt forward ($\omega = -20^\circ$) and to the left ($\alpha = 10^\circ$) is assumed.
- $m_\alpha = 0.015^\circ$, $m_\omega = 0.015^\circ$, $m_\kappa = 0.035^\circ$, the attitude angles errors according to Table 5.1.
- $\theta = 1.33^\circ$ and $m_\theta = 0.01^\circ$, which is the angular spacing between two adjacent planes as reported by the manufacturer of the laser scanner and its error that is essentially the scan angle error.

³By the corresponding law in the Netherlands, the distance between the UAV and the pilot is not allowed to be larger than 0.5 Km. So, assuming that the base station of the GPS is set somewhere close to the pilot, a typical baseline would be 0.5 Km.

- $m_S = 0.2m$, the range error according to Table 5.1.
- Finally, the range is assumed to be 50 meters.

Using these hypothetical values, the resulting 3D coordinate accuracy is:

Table 5.2: 3D coordinate accuracy using the parameters of a typical drone flight

m_{X_p}	0.0173 m
m_{Y_p}	0.0184 m
m_{Z_p}	0.0245 m

From the table above, it can be concluded that the a priori accuracy of the Alpha AL3-32 aerial system is 2 cm. At the same time, Phoenix LiDAR systems, which is the manufacturer of the system, suggests that for the range of 50 m the accuracy level is between 2.5 and 3.5 cm [53], so 3 cm in the general case. This value is quite close to the value of the a priori accuracy as determined above. However, the company has probably considered slightly larger errors for the system components so that they would be on the safe side. That results in the difference of approximately 1 cm.

3D coordinates accuracy with varying range

It is known that certain flight parameters have a high impact on the uncertainties of the 3D coordinates and thus it is quite important to investigate them. At first, we looked into the positioning accuracy changes when having a varying range. The parameters values of the error model are kept the same as in the previous application, except for the range that varies from 0 to 100 m - with 1 m interval. Using the values above, the 3D coordinate errors were calculated for every (integer) value of the range between 0 and 100 and the results were plotted in the following graph:

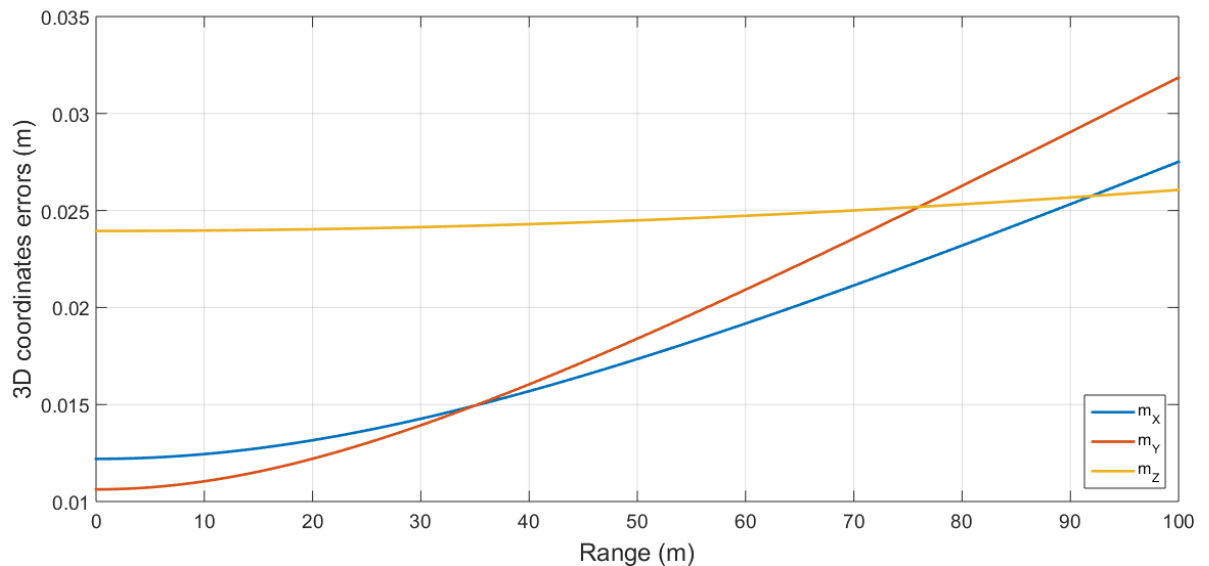


Figure 5.10: 3D coordinate errors dependency on the range

From Fig. 5.10, it can easily be concluded that the varying range influences mainly the uncertainties of the x and y coordinates, while the m_z changes slightly. More specifically, all of the three errors increase when the range increases. But while the vertical accuracy spans from 0.024 to 0.026 cm for a range equal to 0 and 100 m respectively, for the same range change the accuracy of the x-coordinate spans from 0.012 to 0.028 cm and

the accuracy of the y-coordinate spans from 0.011 to 0.032. So, the magnitude of the impact that the varying change has on the 3D coordinates is clearly not the same.

3D coordinates accuracy with varying orientation angles

The same procedure was followed also for the three orientation angles, the roll, pitch and yaw. In order to determine the impact of each one of them on the coordinates' uncertainties, the under investigation angle varies from 0° to 360° , while the two remaining angles are kept constant and equal to the decided value in the previous section. The results are shown in the three following graphs:

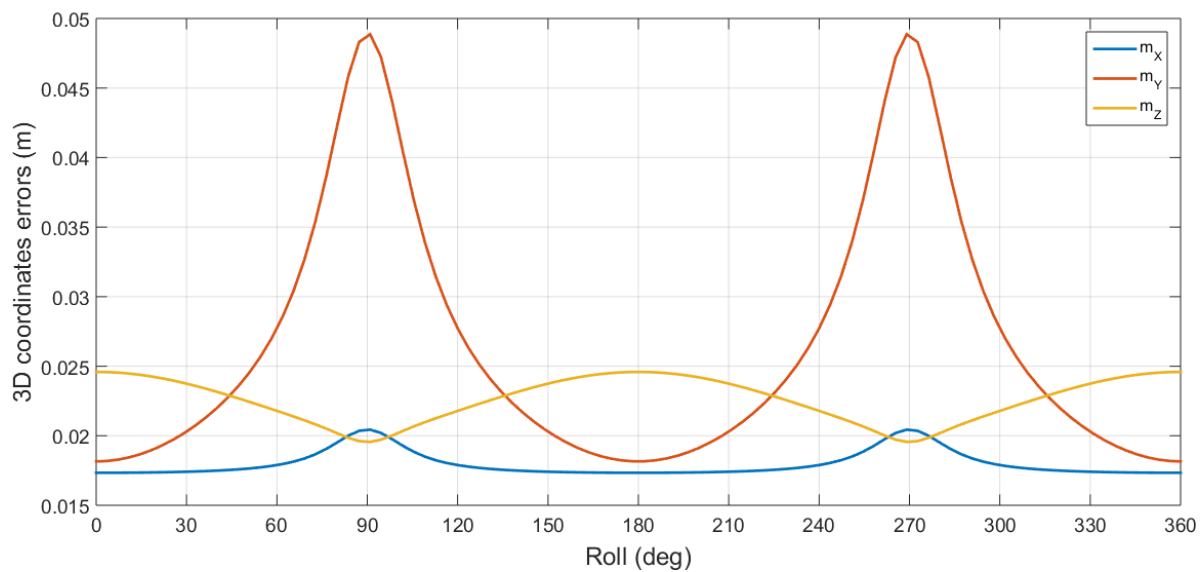


Figure 5.11: 3D coordinate errors dependency on the roll angle

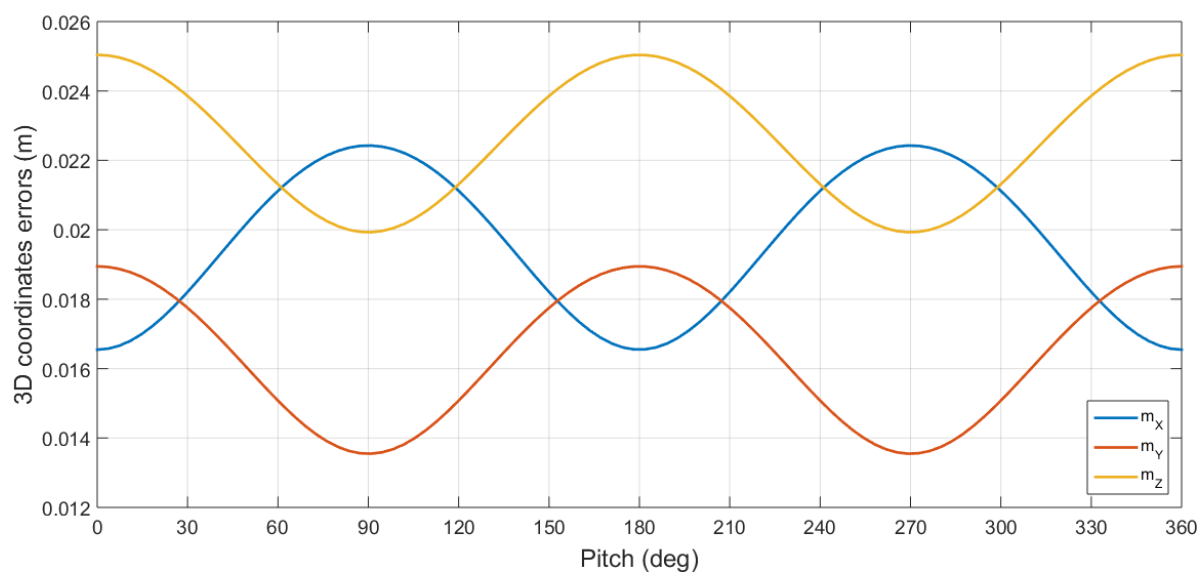


Figure 5.12: 3D coordinate errors dependency on the pitch angle

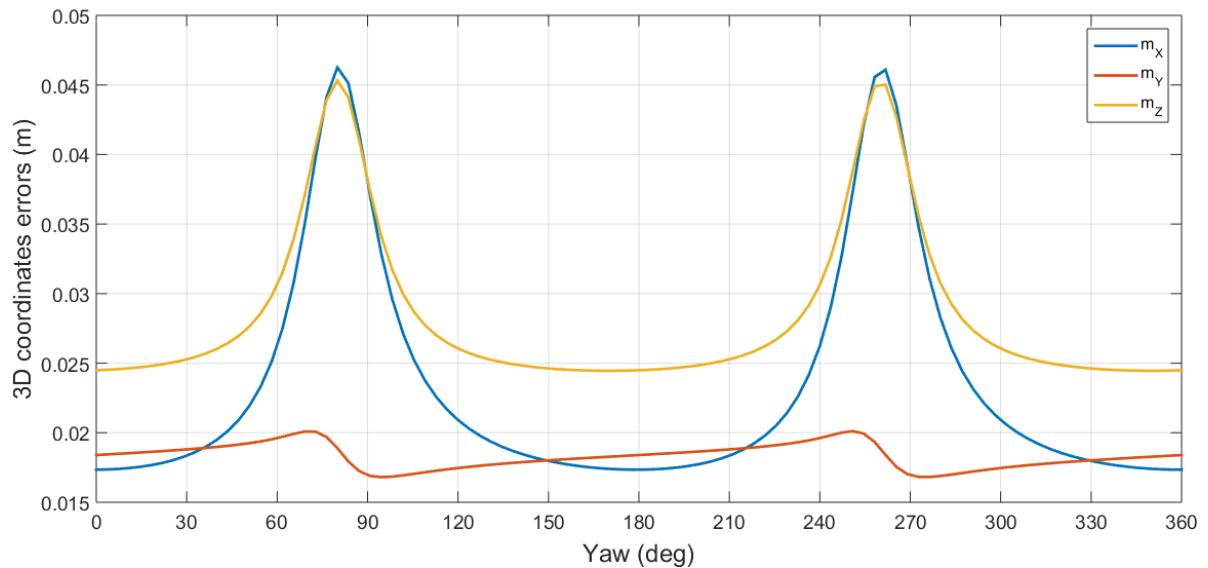


Figure 5.13: 3D coordinate errors dependency on the yaw angle

When the roll angle varies, the most influenced accuracy is the one of the y-coordinate, as presented in Fig. 5.11. The two other uncertainties do not remain unchanged either, but the magnitude of the change is significantly smaller. The lowest accuracy in the y-coordinate is achieved when the roll is either 90° or 270° . That was expected, since the roll angle expresses the rotation of the drone around the front-to-back axis, which means that for the values of 90° and 270° the drone would fly totally sideways. Regarding the varying pitch angle, the magnitude of the change in all three accuracies is the same. However, the x-accuracy behaves exactly the opposite from the y- and the z-accuracy. From 0° to 90° the uncertainty in the x-axis increases, while the other two decrease. The same fluctuation occurs every 90° . Finally, the x- and the z-accuracy decrease quite significantly when the yaw angle is around 90° and 270° . On the contrary to that, the y-accuracy decrease also but much less.

5.4. Flight planning

Every UAV Laser Scanning survey consists of three main phases. These are the flight planning, the survey campaign, during which the flight, the operation of GPS ground station(s) and the collection of ground control data take place, and finally the data processing and quality control [74]. This section is focused on the first phase. The major concerns when forming a flight plan are the point density that is required and the characteristics of the study area, assuming that the aerial system is always the same. If more than one systems are available, then the selection of the most suitable system for each survey is also part of the flight planning. In order to achieve the desired point density, but at the same time taking into account the quality that these points should have, an appropriate flight height and scan angle have to be chosen. These are the two most important flight parameters that determine the rest of the parameters, too. The aim is to find the largest values for both of these two flight parameters that would produce results that can still meet the requirements of the survey. That would lead to the full coverage of the study area in the most economical way. In general, larger scan angles can be used in flat terrains, but in urban areas or in densely vegetated areas smaller scan angles are preferred due to the shadowing effects.

A flight plan is organised in parallel flight lines that cover the whole study area. Typically, there is a 20% overlap between consecutive lines in order to avoid data gaps and make up for possible minor navigation difficulties. Cross flight lines at regular distances are also very useful for the quality control during data

processing. Using them a more reliable estimate of the internal accuracy⁴ can be achieved. In addition, there are usually some extra manoeuvres for the initialisation of the navigation system. The flight plan overlies a topographic map of the study area - or a satellite view of the region - to facilitate the planning.

Here, a flight plan for the UAV Laser Scanning survey of the same study area in Schelphoek will be presented. As seen in Fig. 5.14, the study area is approximately 1700 m long and 500 m wide (850000 m^2). To simplify the flight plan, we assume that the whole area has to be covered, although the water part, which is below the last breakwater during a low tide, is not going to return any data. Regarding the characteristics of the area, it is an open area, with no high vegetation, and mostly flat. The only height variations of a few meters can be found in the dunes. However, since they are not large, we can still use a constant flight height throughout the whole survey.

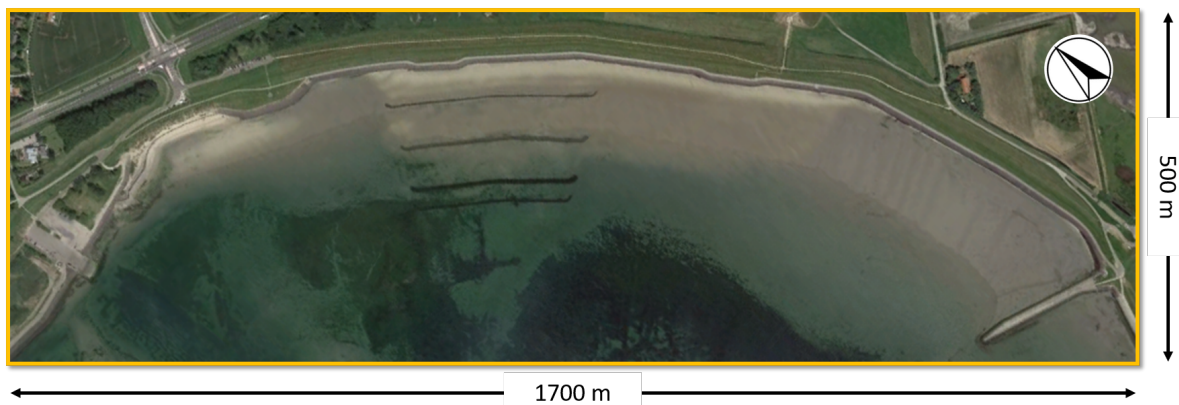


Figure 5.14: Study area in Schelphoek. For visualisation purposes, the satellite image has been rotated. The symbol in the top right corner shows the North. Source: Google Earth

The basis of the flight plan is the point density that we want to achieve. So, starting from that, all the flight parameters will be determined. Let's assume that we need a high point density of $500 \text{ points}/\text{m}^2$ for the generation of a very detailed and accurate DTM of the area. Starting with a hypothetical value for the flight height H and the scan angle ϕ , the swath B_s , which is the width of a flight strip on the ground, is given by the following formula [9]:

$$B_s = 2H \tan(\phi)$$

So, for a flight height equal to 50 m and a scan angle equal to 30° , the swath is 57.735 m. However, we should take into account the 20% overlap (P) between the consecutive strips. Thus, the effective swath B is expressed as [9]:

$$B = B_s(1 - P)$$

That means that the final width of each flight strip is going to be 46.188 m. Combining this information with the width of the area, we can determine the number of strips n needed:

$$n = \text{width}/B = 10.825 \approx 11$$

With 11 flight lines and two additional cross lines for validation purposes, the flight plan is illustrated in Fig. 5.15:

⁴Internal accuracy of a point cloud is the accuracy that is estimated using the point cloud itself.

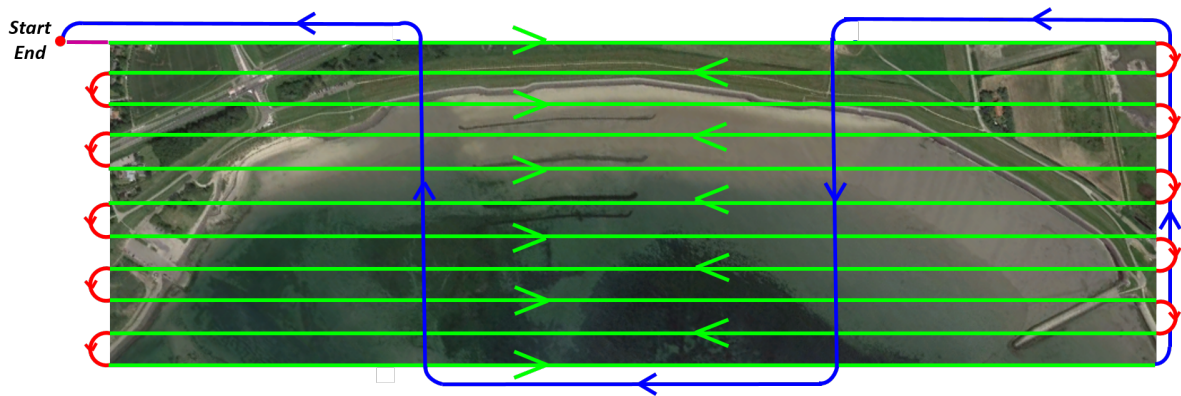


Figure 5.15: Flight plan with 11 flight strips and 2 cross strips. The magenta line is the distance that the UAV needs to get steady, the green lines represent the flight strips, the red lines the turns of the UAV and the blue lines are the route of the UAV for the two cross lines.

The UAV takes off outside of the study area (magenta line) so that it will have some time to get steady. Then, it starts scanning along the first strip (green line) that lays on the upper border of the study area. We will only make use of the data that is derived from the right side of it, since on the left side there will be no overlapping strip. Once the UAV has scanned all along this first strip, it turns outside of the study area again (red line), since we do not want to use the data derived during turning. This data usually has larger errors due to the higher attitude angles. This procedure continues till all the flight strips are scanned and finishes at the opposite corner of the start. Then, we want to add two cross lines, so the flight carries on with the blue lines. The UAV turns outside of the area and heads upwards. It crosses the study area vertically two times, as depicted in the image above, and finally it ends at the starting point.

However, we know that the flight duration can be maximum 15 min. So, what follows is to check whether the UAV can follow all this route in 15 min and with a speed that would give us the desired point density. For that purpose, at first we have to calculate the total distance. The total distance consists of:

- 65 m for the initialisation of the drone
- 11 flight strips of 1700 m each
- 10 turns of 72.55 m each
- the route for the cross lines, which is approximately 3,520 m in total.

and thus it is equal to approximately 23 Km. If the UAV has to fly 23 Km in 15 min, then it has to have a speed of 25.5 m/s. The maximum speed that the DJI Spreading Wings S1000 can fly with, though, is 20 m/s. That means that the first hypothesis for the flight height and the scan angle is not feasible and therefore we have to change it.

Since the terrain is mostly flat, we can increase the scan angle. That will result to a smaller number of strips and thus to a smaller distance for the UAV to fly. After some tests, and following the same methodology, we decided to keep the flight height the same (50 m) and change the scan angle to 45°. The new swath B_s is then 100.00 m, the new effective swath B is 80.00 m and the new number of strips is 7. The flight plan then changes as follows:

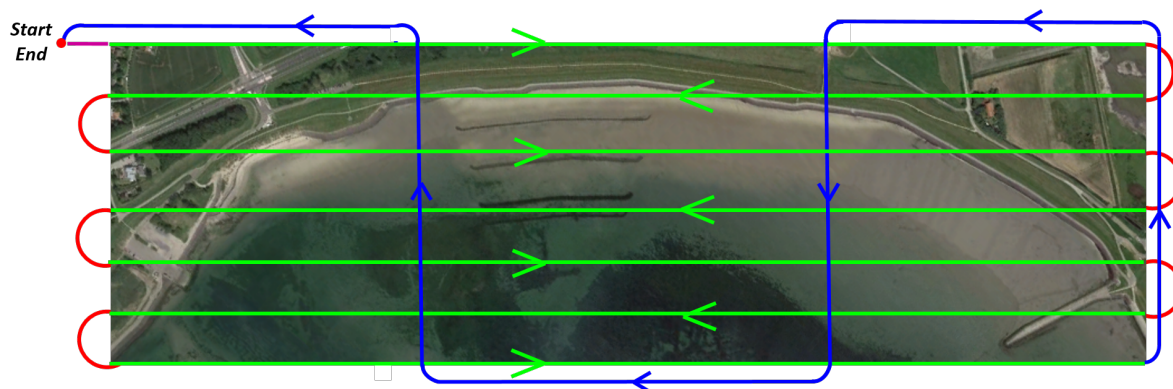


Figure 5.16: Flight plan with 7 flight strips and 2 cross strips. The magenta line is the distance that the UAV needs to get steady, the green lines represent the flight strips, the red lines the turns of the UAV and the blue lines are the route of the UAV for the two cross lines.

The new distance that the UAV has to fly is 16,240 m and, in 15 min, that can happen with a speed of 18 m/s. The Velodyne laser scanner that this aerial system is equipped with fires 700,000 shots per second at its highest (20 rotations/sec). When a homogeneous point distribution is assumed over the whole study area, then after flying along the 7 strips with a speed of 18 m/s (which takes 11 min), 462.7 million points are derived. That is a point density of 545 points/ m^2 . The rest 4 minutes of flight are used for the initialisation of the drones, the cross lines and its return to the starting points.

5.5. Summary

At first, the errors introduced in the 3D coordinates, and contribute to their final accuracy, had to be determined. The sources of error in a UAV Laser Scanning system are the three main components, namely the laser scanner, the GPS and the IMU, as well as possible instrument misalignments that cause bore-sight and lever-arm errors, coordinate system transformations and temporal interpolations between the three components. For the determination of the quantitative impact of them on the positioning accuracy, an error model was used. Using the uncertainties of the instruments that Alpha AL3-32 consists of, the a priori positioning accuracy of the system was estimated equal to 2 cm. In addition, an investigation on how the contribution of the three components as well as the 3D coordinates accuracy change with varying range and varying orientation angles was carried out. From that it was concluded that that both the laser scanner and the GPS contributions as sources of error decrease while the range increases, but, on the other hand, the IMU contribution constantly increases. Furthermore, it was found that the differences in range affect mostly the planimetric accuracy rather than the vertical one, while differences in the orientation angles affect both accuracies in different ways. Finally, a flight plan for deriving a point cloud with an average point density of 500 points/ m^2 was suggested. More specifically, using a flight height of 50 m and a scan angle of 45°, an effective swath of 80 m is resulted. Therefore, we need 7 flight strips to cover the whole study area and two extra cross lines for cross-validation purposes. All these add up to a distance of 16,240 m for the UAV to fly with a speed of 18 m/s in order to achieve the desired point density.

6

Post-processing methodologies

In this chapter, we start with the second important objective of our study, which is the generation of the final products, which, for coastal monitoring, is most commonly the DTM of the study area. Thus, in the following chapters the methods that are used during the post-processing of the point cloud are addressed. In our case, that is from the moment that a point cloud is delivered till the derivation of the DTM. In addition, the methodologies for the validation of the point cloud and the DTM are discussed.

6.1. Preparation of the point cloud

A raw point cloud that comes from a drone flight with a duration of 15-20 min usually contains over 100 - or even 150 - million points. That makes the file size quite large and consequently its post-processing quite slow and difficult - in some cases even impossible, if the specifications of the computer are not good enough. Because surveyors tend to scan the wider area around the study area, in order to be on the safe side, most of the times not everything in the initial point cloud is necessary. The preparation of the point cloud includes, thus, all these actions that are needed in order to select the study area and remove redundant parts of the point cloud that would drastically reduce the file size and facilitate the processing. When the derived point cloud contains no redundant points that could be removed, but the file size is still quite large for processing, then during the preparation of the data, the point cloud is divided into smaller point clouds that will be processed separately.

In the first case, when it is needed to select the study area in order to minimise the file size, we usually crop it in an interactive software (e.g. CloudCompare) or when working with a command-line software (e.g. LAStools, OPALS), we use the bottom-left and the top-right coordinates to define a tile that contains it. The former method is more precise in the sense that we can crop exactly the study area that we need and remove all the redundant points, but it is usually much slower, since the whole point cloud has to be loaded first. The latter method is quite faster, but it maintains some unnecessary points. Depending on the characteristics of the data and the resources (time etc.), one of the two methods is chosen.

In the second case, when we need to keep all the information of the initial point cloud, we tile it - either manually or automatically in a command-line software. In this way, we first conclude on the exact processing chain based on one tile and then apply it on the rest of the tiles.

6.2. Noise removal

Once we have converted the initial point cloud into a smaller dataset that can be more easily processed, we move on to the first actual step of post-processing, the noise removal. During noise removal, points are flagged as 'isolated' according to certain criteria that are specified by the user and depend on how strict we want this filtering to be. During the present study, the tool that was used for the noise removal was the *lasnoise* tool from LAStools. Of course, there are similar tools in other software too, but it can also be programmed.

The algorithm that *lasnoise* uses to determine which points must be flagged as isolated is essentially based on two parameters:

- for each point, a 3x3x3 grid of cells is considered, with the cell, where the query point falls into, being in the centre, as shown in Fig. 6.1. In the general case, the cells are cubes and thus all of their edges have the same length, called *step*, and this is the first parameter. It is possible, though, to specify different steps for the edges that lay in the z direction from the ones in the x,y direction. In this way, if the z - step is smaller (larger) than the x,y - step, that would result to a more (less) strict solution on the vertical than in the horizontal direction.
- the second parameter is the minimum number of neighbouring points that the query point should have so that it will not be considered as isolated. For instance, if that parameter is equal to 5, then a point that has five or fewer other points in their surrounding 3x3x3 grid is designated as isolated and flagged as such.

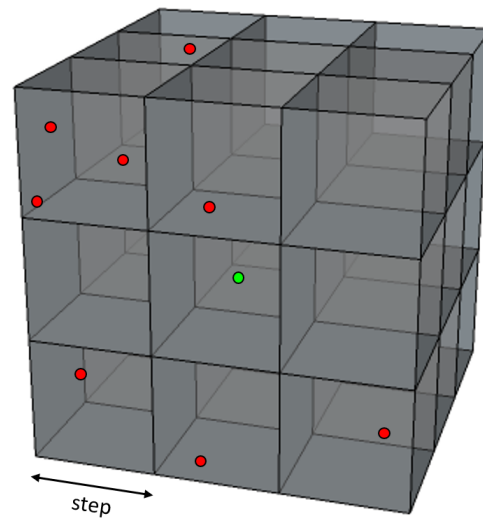


Figure 6.1: The 3x3x3 grid of cells that is used in the noise removal algorithm. The green point that falls into the central cell is the query point and the red ones are its neighbouring points.

This tool can be used differently depending on what we want to achieve. So, if we only want to remove some 'flying' points that we know are outliers, then we set a larger step and low minimum number of neighbouring points. But on the other hand, if we want to reduce the number of points and only keep the most accurate ones, then we can set a smaller step - so that the filtering is finer - and a larger number of minimum neighbouring points.

Another method that is often used for noise removal is the Statistical Outlier Removal filter (or SOR), which

is realised in PCL and a similar version of it can be used in CloudCompare. It was not used for this study, though, so it will not be further discussed. More information can be found in [49].

6.3. Above ground analysis

After deriving a 'clean' point cloud - and by the term 'clean' we mean the point cloud of the area of interest, having removed the noise and all the other unwanted points - the next processing step is the separation of the ground and the non-ground points, the so-called *above ground analysis*. This procedure is required for the creation of the Digital Terrain Model (DTM) of the study area, since for such a grid only the ground points must be used. The above ground analysis is essentially a classification with two classes: the ground and the non-ground. If required, the non-ground class can be further classified into more classes that would be related to the land cover, e.g. buildings, vegetation, etc., but this is not included in the objectives of the current study.

During this study, the tool that was used for the above ground analysis was *lasground*, provided by LAStools. This tool is basically a filtering algorithm based on Triangular Irregular Networks (TIN) that eliminates those points that do not belong to the ground surface. In Axelsson's approach, [3], the surface that is created by the TIN is initially derived from neighbourhood minima, as shown in Fig. 6.2, and then progressively densified to the laser point cloud. In each iteration, points are added to the TIN, if they are within defined thresholds [27]. This process depends on the complexity of the study area, i.e. whether it is a flat rural area or for example a city area with different building heights. More information on the criteria that are used during the method can be found in [3].

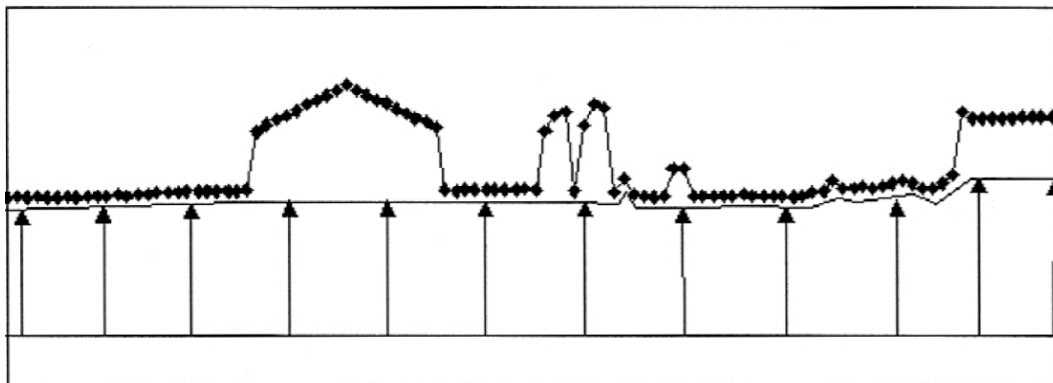


Figure 6.2: Axelsson's above ground analysis algorithm. Source: [3]

6.4. DTM and DSM generation

For monitoring purposes, it is very useful to know how the surface of the study area looks like at different time periods. That would mean to know its elevation, but also possible objects on it. More specifically for coastal monitoring, it is very important to have information about the elevation of the shore, the dunes and the nearby area as well as about the vegetation on the dunes and objects that may lay on the shore, e.g. beach houses. That can be achieved by creating a Digital Terrain Model (DTM) and a Digital Surface Model (DSM). As it can be seen in Fig. 6.3, the former is a mathematical representation of the bare earth surface in digital form. The bare earth is here defined as the boundary surface between the solid ground and the atmosphere or objects attached to it (e.g. buildings, vegetation). At the same time, the DSM describes the top surface that is visible from above. The DSM is equivalent to the DTM in open areas, but in contrast to the DTM it

describes the vegetation cover and the upper boundary surface of spatiotemporal fixed man-made objects [74]. During this study, we focused on the DTM generation, since the monitoring of the terrain was of the highest importance.



Figure 6.3: The difference between a Digital Surface Model (DSM) and a Digital Terrain Model (DTM). Source: [45]

The final processing step is, thus, the generation of the necessary DTM of the study area. Since the DTM is a model of the bare earth, for its generation only the terrain observations are used. These are the extracted (during the previous processing step) above-ground points. On the contrary, if the DSM of the study area was required too, all first echo points would be necessary. These points correspond to the surface of the study area as seen from above, which is the objective of a DSM representation. When there is redundancy of points, we can filter these first echoes in order to remove points that come from possible reflections from too high surfaces. These points are considered as 'flying points' and they can originate from e.g. birds or dust. In addition, points created from temporal objects that were present during the data acquisition - e.g. cars, tower cranes, people - are also unwanted and they should be eliminated.

A DTM is a 2.5D representation of the study area, i.e. a certain height value z is assigned to each 2D location (x,y) . The data format that is typically used is the grid, which represents the height information on discrete regularly arranged points. This height values are determined by surface interpolation methods. However, the generation of a DTM is also possible by using triangulation methods. In this case, the neighbourhood topology of the given terrain dataset is derived according to a certain geometric rule (e.g. Delaunay triangulation) [74].

The DTM can be generated in either interactive software, such as CloudCompare, or in command-line software. Throughout this study, OPALS was mainly used for that purpose, and more specifically its Grid module. This module provides us with the opportunity to specify the grid size, the interpolation method as well as other critical parameters for the creation of DTMs in a regular grid structure. While the grid size is usually associated with the nature of the application, the interpolation method that should be used depends on the available resources, since more complex algorithms need larger computation time. In the next chapter, the results of different interpolation methods are presented and compared. More details on the Grid module of OPALS can be found in [47].

6.4.1. DTM data redundancy

One of the strongest points of UAV Laser Scanning nowadays is the high density of points per square metre that it can provide, even over large study areas. That is achieved with the development of new laser scanners with much higher measurement rate, but mainly due to the significantly lower flight height - when compared to Airborne Laser Scanning. The increase in the volume of the original data leads to high resolution DTMs, which subsequently implies the need for larger storage spaces. Considering the DTM generation procedure, having a large number of points available for the interpolations is quite important. Above a certain limit of point density, though, we can consider some of these points redundant, in the sense that even if they didn't exist, the resulting DTM would be of the same quality.

The factor that often determines whether a data reduction should be carried out or not is the desired grid size of the DTM. Depending on the level of detail that is necessary of an application, a different grid size is decided. For coastal monitoring purposes, the grid sizes usually span from 10 cm to 1 m. So, it is obvious that the amount of points that is going to be used for the generation of a DTM with grid size 1 m can be much less than for a DTM with grid size 10 cm and still achieve the same quality, but with smaller file size. The data reduction is in any case an optional procedure, since if the resources for large datasets are available, then it can easily be skipped. However, it is always beneficial, especially when the resulting DTMs will be much further processed.

6.5. Validation

In this last part of the chapter, the validation techniques that were used throughout the whole study are described. These include the validation techniques used to check the precision and the accuracy of the point cloud of the measurements that were acquired with the drone, but also for the accuracy of the derived products.

6.5.1. A posteriori errors of the 3D coordinates

First of all, what follows after the calculation of the a priori positioning errors of a point cloud acquired with the Alpha AL3-32 aerial system (see Section 5.3.2) is the calculation of the corresponding a posteriori positioning errors. By comparing the two types of errors, we can reach conclusions about how close we can get with our measurements to the nominal accuracy of the system and of course about what is the actual precision of such a point cloud. However, our attention is focused on the vertical accuracy rather than on the planimetric one. The main reason for that is the fact that these point clouds are destined for the generation of digital terrain models. When working with raster data, the planimetric information is not maintained due to the interpolations and the filtering that are performed in order to end up to the final grid, so what we care about finally is the vertical information [36].

The most straight-forward method to determine the vertical precision of a point cloud - and the one that was also used here - is by calculating the standard deviation of it. However, because a point cloud can be quite diverse (in the Z-coordinate) depending on the nature of the study area, calculating the standard deviation of all the points would not give us a realistic measure of the precision. The way to deal with this problem is to detect a flat area - with the least vertical variations - and compute the standard deviation of it. In such a subset, the differences in height indicate the distribution (deviation) of the points in the vertical direction (and not the actual height differences), which is what we need in order to determine the vertical precision.

Along with the standard deviation of the points that are contained in the subset, the mean (height) value can also be computed. When this procedure is repeated for multiple subsets, then we can have a measure of the accuracy of the point cloud, too.

6.5.2. Point cloud validation with TLS data

To validate the accuracy of the point cloud, other kinds of laser scanning data may be used. For this study, Terrestrial Laser Scanning data were used for the validation of the 'clean' point cloud.

The accuracy that can be achieved with a terrestrial laser scanner is in general higher than with any airborne method. The main reason for that is the fact that the noise introduced in the TLS measurements is much reduced than in the ALS measurements, since in the latter the noise increases due to the flight and the extra devices that are necessary (IMU etc.). In addition, TLS offers higher resolution, since the range is shorter. Therefore, TLS data are often used for validation of other kinds of laser scanning data. In order to do so, a registration¹ between the two points clouds (the UAV LS and the TLS point clouds) has to be performed so that they are correctly oriented in a usually local coordinate system. After the procedure is completed, they can be compared.

6.5.3. DTM quality

The quality of a DTM depends on two main factors, the quality of the input dataset and the model quality [74]. At first, when talking about the data quality, the point density of the point cloud that is used as input is of the highest importance. Most of the times the point density of an ALS dataset is not the same throughout the whole study area, since it depends directly on the flight height and the scan angle. Fluctuations of these two parameters cause different point densities and that was also the case in our dataset. The reason why the point density is a very crucial factor for the final DTM quality is because it influences the result of the interpolation and thus the final height values assigned to the grid points. An effective way to get an overview of the point density throughout the whole input dataset is by creating a point density map in the form of a raster image. In order to do so, the number of points per square metre is at first determined and then this value is assigned to the corresponding cell of the raster file. In case there more than one returns resulted from a single pulse, only one of them must be kept, since in any other case the number of points counted in the grid cell will not be the real one. Similar to the point density map is the point distance map, which also allows the detection of areas with a low amount of input data.

Based on the above, Karel and Kraus [31] suggested that the vertical accuracy of a DTM can be estimated by taking into account the point density n (in points/ m^2) and the terrain slope α according to the formula below:

$$\sigma_z(cm) = \pm \left(\frac{6}{\sqrt{n}} + 30 \tan \alpha \right)$$

While the point density can be estimated according to what was described above, the terrain slope can be derived by using plane fitting in a neighbourhood of points. More specifically, a number of neighbours is chosen and then the plane that best fits through them is determined. What follows is the computation on the normal of this plane. Finally, using the normal, the slope is estimated as well.

The other very important factor that influences the DTM quality is the quality of the processing steps prior to the DTM generation. These are the noise removal and most importantly the above ground analysis. While the

¹Registration is the procedure during which the two point clouds are correctly oriented in a common coordinate system

classification of ground and non-ground points might be reliable in certain areas where the complexity of the terrain is low, significant classification errors can be present in built-up areas with a complex arrangement of buildings [65]. Therefore, that can be an important issue in certain cases. Last but not least is the accuracy of the input point cloud itself, meaning the uncertainty in the elevation determination.

Regarding the model quality, which is the second part of the DTM quality, it can be divided into interior and exterior quality. On the one hand, the internal quality describes the quality of the estimated DTM with respect to the input dataset. More specifically, by calculating the Root Mean Square Error (RMSE) between the input point cloud and the derived DTM, we can detect areas where there is a significant difference between the two and therefore get an idea about the precision of the DTM generation process. On the other hand, the external quality of a DTM describes the quality of the estimated DTM with respect to external control data. That means data that were not used during the DTM generation but will act only as validation data [74]. It is important that our confidence in the quality of the control data is higher than in the input dataset so that they can actually have the role of validation data. In our case, this data was GPS (RTK) measurements acquired by Shore Monitoring & Research B.V. during the day of the test flight.

6.6. Summary

In this chapter, the methodologies used during the post-processing of a UAV Laser Scanning dataset were described. More specifically, the preparation of the point cloud includes the selection of the study area and its tiling, if necessary. What follows is the noise removal using a filtering algorithm implemented in LAStools and the classification of the points in ground and non-ground (above ground analysis) using Axelsson's approach. Finally, DTMs and DSMs can be generated using only the ground points and only the first returns respectively. Regarding the validation methodologies, the validation of the derived point cloud is possible by using other types of laser scanning data. Here, the TLS data that were obtained during the fieldwork in Schelphoek were used for that purpose. Finally, the DTM quality depends both on the quality of the input dataset and the model quality. The former depends mainly on the point density and the characteristics of the area and thus the empirical formula by Karel and Kraus [31] was used for the estimation of the vertical DTM accuracy. The model quality is divided into interior and exterior quality. The interior quality describes the quality of the estimated DTM with respect to the input dataset and thus it is derived by calculating the Root Mean Square Error (RMSE) between the input point cloud and the DTM, while the exterior quality describes the quality of the estimated DTM with respect to external control data. In our case, this data was GPS (RTK) measurements acquired by Shore Monitoring & Research B.V. during the day of the test flight.

7

UAV Laser Scanning post-processing and validation results

In the previous chapters, the Alpha AL3-32 error budget was investigated and the a priori positioning accuracy that can be achieved using this system was estimated. In addition, all the methodologies that were used for the post-processing of the UAV Laser Scanning point cloud were described. This chapter, thus, focuses on the results derived with these methods. More specifically, these are the estimation of the a posteriori vertical accuracy and precision using a small dataset from the initial point cloud, the intermediate results from each post-processing step and the derived DTMs, and finally the validation of the point cloud using a TLS dataset acquired during the fieldwork and the estimation of the DTM quality.

7.1. Calculation of the vertical accuracy

After the determination of the a priori accuracies of the 3D coordinates - both the planimetric and the vertical one - with the use of the error model by Peng et. al, [50], the estimation of the a posteriori vertical accuracy follows in the next paragraphs. As already discussed in Section 6.5.1, that is possible by using a completely horizontal surface - or more realistically, in our case, with the least possible height variations. The bike path of the study area served this purpose really well, since it is almost entirely horizontal. So, assuming that the elevation of the points contained in this subset are the same, by detecting the existing height variations of neighbouring points, we could get insight into the effects caused by the imperfections of the components of the aerial system and consequently we could conclude to a magnitude of the accuracy that can be achieved.

Since the total length of the bike path is quite large, only the part of it that was flat in most of its extent was selected, with a length of approximately 50 m, as shown in Fig. 7.1. Along that, 25 adjacent boxes were extracted from the denoised point cloud - so the outliers were already removed - containing as much as possible the same number of points, so that any effects caused by that difference would be eliminated. The dimensions of the boxes were about 2x2 meters and the average number of points contained in each one of them was 3336 points (Fig. 7.2). That was realised in the environment of CloudCompare. It has to be mentioned that, although the dimensions of the 25 boxes were quite similar, the number of points in them spans from 2699 to 4237 points (see Table 7.1). The reason for that is the different way that the points are distributed in the point cloud due to the different flight characteristics. For instance, in areas where the

drone flew lower, the point cloud is denser. Similar effects are caused also by the differences in the incidence angle.



Figure 7.1: The part of the bike path that was used for the calculation of the vertical accuracy. Source: Google Earth

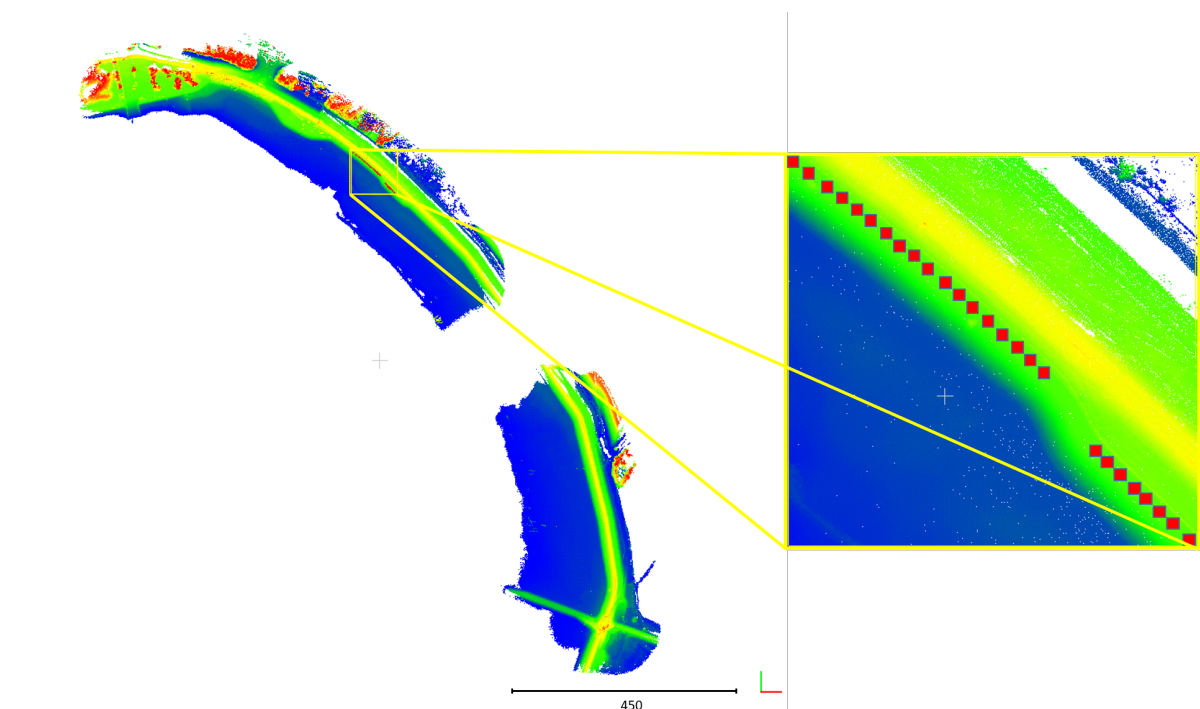


Figure 7.2: The locations of the 25 adjacent boxes on the bike path. The colour indicates the elevation in the dataset.

For each one of these boxes, the mean value and the standard deviation of all the contained points were calculated and listed in Table 7.1. From these, it can be seen that there are some variations of a few centimetres in the mean value, with the minimum value being 47.889 m and the maximum 47.968 m (~ 8 cm). These variations are due to the different point distribution, but there might be also some (quite small) actual height variations that are also included. However, there is no other area in the dataset that is more flat (more horizontal) than this one, so we will have to proceed with that.

Table 7.1: The mean value and the standard deviation for each one of the 25 boxes with varying and with constant number of points (2000 points). δ Mean and δ STD are the differences in the mean and the standard deviation respectively.

Box ID	Number of points	Mean with var. no. of points	STD with var. no. of points	Mean with const. no. of points	STD with const. no. of points	δ Mean	δ STD
1	3200	47.889	0.037	47.889	0.036	0.0001	0.0004
2	2827	47.902	0.032	47.902	0.032	0.0002	0.0001
3	3422	47.907	0.034	47.907	0.035	0.0004	-0.0006
4	2919	47.916	0.034	47.916	0.033	0.0002	0.0003
5	2866	47.924	0.034	47.924	0.033	-0.0006	0.0007
6	2699	47.925	0.036	47.925	0.035	-0.0003	0.0003
7	2868	47.921	0.035	47.921	0.035	-0.0002	0.0000
8	2821	47.920	0.033	47.920	0.034	0.0000	-0.0007
9	3044	47.922	0.034	47.923	0.034	-0.0001	-0.0002
10	3197	47.926	0.034	47.926	0.033	0.0000	0.0011
11	3184	47.940	0.030	47.940	0.030	0.0002	0.0007
12	3005	47.951	0.028	47.952	0.029	-0.0007	-0.0003
13	3068	47.943	0.033	47.944	0.034	-0.0002	-0.0009
14	3020	47.936	0.036	47.936	0.036	0.0003	-0.0001
15	3124	47.942	0.035	47.942	0.035	-0.0005	0.0005
16	3236	47.926	0.035	47.926	0.036	0.0002	-0.0005
17	3059	47.913	0.035	47.913	0.034	0.0002	0.0006
18	3609	47.935	0.033	47.935	0.032	0.0003	0.0007
19	3897	47.932	0.037	47.932	0.038	0.0000	-0.0007
20	4169	47.941	0.040	47.940	0.039	0.0011	0.0008
21	3975	47.953	0.038	47.953	0.038	0.0002	0.0001
22	3914	47.967	0.044	47.966	0.044	0.0006	-0.0007
23	4048	47.967	0.044	47.965	0.044	0.0014	0.0005
24	3992	47.968	0.041	47.968	0.040	0.0005	0.0004
25	4237	47.959	0.044	47.959	0.044	-0.0004	-0.0004
	<i>Mean: 3336</i>	<i>STD: 0.021</i>	<i>Mean: 0.036</i>	<i>STD: 0.021</i>	<i>Mean: 0.036</i>		

The standard deviation of all the calculated mean values gives the spread of the mean and that is in our case the relative vertical accuracy¹ of the point cloud. So, the computed vertical accuracy based on these 25 boxes and according to Table 7.1 is equal to 2 cm. This value is quite close to the value of the a priori vertical accuracy as calculated in Section 5.3.2 (a priori: 0.0245 m and a posteriori: 0.0194 m) and it is actually a bit smaller. This is due to the nature of the area that was chosen for this estimation. Although from this flat subset of the point cloud the vertical accuracy is estimated to be close to 2 cm, it expected that if the same analysis was performed in a more heterogeneous or rougher area, the final result would have been different and most likely larger (lower accuracy). It is still a good measure of the accuracy magnitude that can be achieved though.

In addition, the computed standard deviations can also be used as auxiliary information. More specifically, the standard deviation of each box gives a measure of precision. So, by calculating the average standard deviation, we can have an idea of the precision of our dataset. From Table 7.1, it can be seen that the average standard deviation of the boxes is equal to 0.036 m or more roughly 4 cm. It should also be mentioned that the manufacturer of the used aerial system (Phoenix LiDAR Systems) suggests that its precision is 3.983 cm, when a baseline of 1 Km is assumed [69], which is really close to the computed precision. In our study, a baseline of 0.5 Km was used and thus the precision according to the manufacturer would be slightly lower and equal to 3.893 cm, which is still close to the a posteriori precision. And although this value can fluctuate

¹It is called *relative* vertical accuracy, because it is estimated using the same dataset. In order for this accuracy to be absolute, the dataset should be compared with external (validation) data of higher reliability, which is then considered to be ground truth data.

quite a lot depending on the flight or the surface characteristics, it is good to investigate it so that we have an idea of its magnitude for an 'ideal' part of the point cloud.

However, by looking at Table 7.1 a relation between the number of points in a box and the corresponding standard deviation can be observed. It is noticeable that boxes with a smaller number of points (e.g. Box #5) have lower standard deviation than the opposite (e.g. Box #25). Therefore, there was the need for further investigation on whether the number of points actually influences the standard deviation or the cause of these discrepancies is something different. The way to achieve that was by randomly subsampling the boxes until they would contain the exact same number of points. That was performed in CloudCompare. The new values of the mean and the standard deviation are listed in Table 7.1 together with their differences ($\delta Mean$ and δSTD are the differences in the mean and the standard deviation respectively). We can see that the maximum difference in the mean is 1.4 mm for Box #23 and in the standard deviation it is 1.1 m for Box #10. Since the differences are so small, we can draw the conclusion that the number of points in the 25 boxes has no actual impact on their standard deviation. Instead, it probably has to do with slight actual height variations along the bike path.

Fig. 7.3 illustrates the statistical variables mentioned above, the mean values and the standard deviations both of the initial boxes and from the subsampled ones. More specifically, the solid lines represent the mean values, while the shaded areas represent the standard deviations. The blue colour indicates the initial values and the red colour the values coming from the subsampled boxes. Here, we can see again that the differences are very small, and thus negligible.

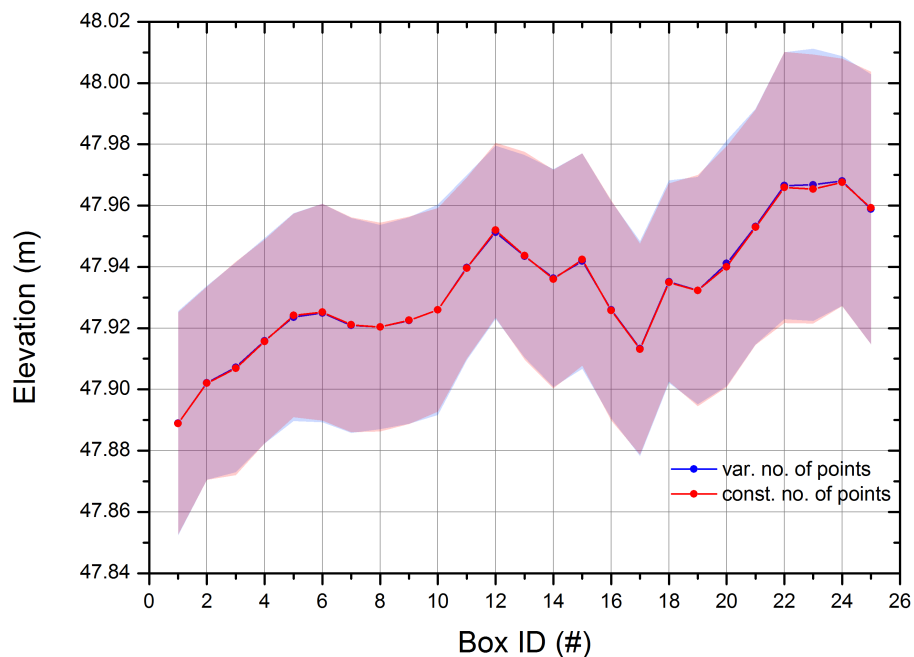


Figure 7.3: The mean value and the standard deviation for each one of the 25 boxes with varying and with constant number of points (2000 points). The mean value is indicated by the solid line the standard deviation by the shaded area.

However, by taking a closer look at this graph, a slight, but gradual, elevation increase can be noticed, when going from Box #1 to Box #25 (left side to right side of the graph). The reason for that is because the bike path is apparently not totally flat, as briefly mentioned earlier. This fact has certainly some effect on the a posteriori vertical accuracy and the precision as they were calculated above. But since we cannot be sure about what is noise introduced by the system components and what is actual elevation variations - and also since it is not

that significant - we keep the estimated values of the a posteriori vertical accuracy and the precision.

7.2. Preparation of the dataset and noise removal

After the point cloud was derived, and before we start with the processing for the DTM generation, we first had to bring it to a form that it could be easily and quickly processed. Since there were no unnecessary parts in the point cloud, but instead we needed the DTM of the entire study area, we couldn't remove any points. However, the file was quite large (~4.5 GB), because the point cloud in this initial phase consisted of 224,692,517 points. With the provided resources (software, computer etc.), it was not possible to process it as a whole and therefore it was divided into 73 square tiles, with dimensions 100x100 m. For that, the GUI of the *lastile* tool by LAStools was used. In Fig. 7.4, the green horizontal and vertical lines depict the tiling pattern, while the cyan square in the background represents the area that the point cloud covers. The number of points contained in each one of the tiles was not the same due to the different point density of the point cloud. The processing steps that followed were performed for each tile separately, but always with the same parameters.

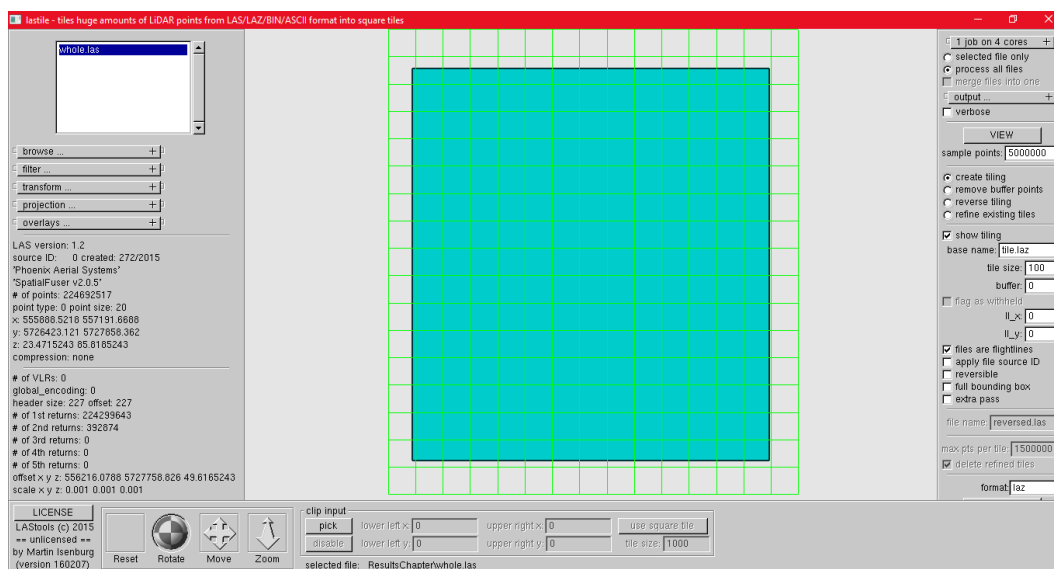


Figure 7.4: The Graphical User Interface of *lastile* while tiling the dataset into 100x100m tiles

What followed was the removal of the noise contained in the point cloud. The *lasnoise* tool by LAStools was used for that purpose, a detailed description of which is given in Section 6.2. The two main parameters that had to be specified were the *step*, i.e. the dimensions of each cube cell of the 3x3x3 grid, and the *isolated*, i.e. the minimum number of neighbouring points that the query point should have so that it will not be considered as isolated. In order to conclude to the optimal combination of these two parameters multiple test runs were performed with varying values. Taking into account the characteristics of the dataset, meaning that it is a very dense point cloud since it was derived with UAV and not Airborne Laser Scanning, some conclusions were reached that also led us to the final selection of the parameters. These are the following:

- when the specified *step* is larger than a couple of meters (the default value by LAStools is 4 meters), the noise filtering is coarse. That happens because the algorithm is searching for the required number of neighbours that is needed in order to maintain a point in a larger space and thus it is more easily for the criterion to be satisfied.

- on the contrary, when it is smaller than 0.5 m, then it is too strict and many points are removed, among which useful points are also excluded. This is certainly undesirable since, although in some areas the point density is high and even if some of the points are removed, they are still enough for an accurate grid, in other areas there may be no redundant points to be filtered out.
- regarding the *isolated*, when it is close or smaller than the default value, which is 5 points, then the filtering is not effective. The reason for that is the high point density of the point cloud. If, for instance, the *isolated* is set equal to 3, there is a really small number of points in the dataset that has less than 3 neighbouring points. So, that is again a very coarse filtering.
- on the other hand, when the specified *isolated* is too high, e.g. larger than 50, then there is the same effect as when the step is too small, useful points are also removed.

Finally, after all the different runs and the different combinations of the two parameters, it was decided that for this specific dataset the optimal values are:

- *step*: 0.5 m
- *isolated*: 10

While the initial point cloud consisted of 224,692,517 points, in the denoised point cloud 224,606,123 points remained. That means that 86,394 points were classified as noise and consequently they were removed. As it can be seen in Fig. 7.5, the majority of these points were laying at the edges of the point cloud, where it naturally becomes sparser due to the larger scan angles. In these areas, the criterion regarding the minimum number of neighbouring points could not be satisfied. The rest of the points that were classified as noise were some 'flying' points, i.e. points with unreasonably high elevation caused by dust or other particles in the air, or even birds, and a few vegetation points in the north part of the study area.

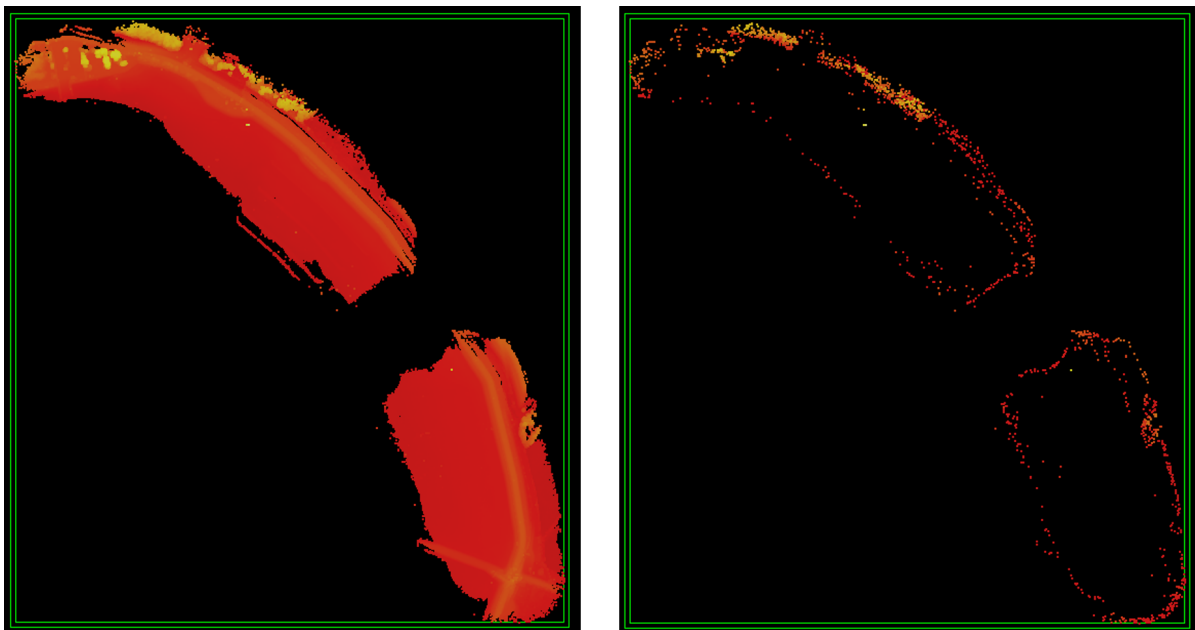


Figure 7.5: Left: The initial point cloud. Right: Only the points that were classified as noise and later removed. The green boxes around each point cloud represent the bounding boxes. For the visualisation, the GUI of the *lasview* was used and the point size was increased in order to make it more clear.

For the rest of the processing, only this denoised point cloud is used and it is referred to as 'clean' point cloud. When the DSM of the study area is required, the clean point cloud is used for the grid generation. However, we will proceed with the above ground analysis, which will lead us to the DTM generation.

7.3. Above ground analysis

Following the noise removal, the above ground analysis was realised also in LAStools, and more specifically using the *lasground* tool, which was described in Section 6.3. The main aim of this processing step is to separate the points that belong to the ground from those that do not for the generation of a DTM. A classification between the ground and the non-ground points is essentially performed, assigning the classification code '2' to the ground points and '1' to the rest of them ('unassigned' points), according to the LiDAR point classification codes defined by ASPRS ([2]). In urban areas, the non-ground points belong usually to buildings or other constructions, cars and sometimes to vegetation, while in rural areas they belong almost exclusively to vegetation. In our study area, the majority of the above ground points are vegetation points - both high grass and trees and points that belong to some concrete structures that are located at the north part of it, cars and objects that stick out from the sand, e.g. metal poles, traffic cones etc.

During the use of *lasground*, two were the critical parameters that had to be specified. These were the *step* and the *spike*. The former refers to the spacing used by the algorithm of the tool and the latter to the positive elevation difference of a spike with respect to the reference surface. Similarly to the use of *lasnoise*, different test runs were realised during this processing step in order to conclude to the values of the parameters that would result to the most satisfying ground extraction and the following conclusions were reached:

- the spacing ('step') is highly dependent on the nature of the study area and the type of objects that lay on the ground (and thus they have to be removed). That implies that if the study area is part of a forest or a mountain, the default value by LAStools, 5 meters, can give quite satisfying results. However, if it is part of an urban area, the user must make sure that even the bigger objects (buildings or other man-made constructions) can be detected by the algorithm and removed. So, for instance, for a study area in a town, the *step* should be increased to 10 meters, in a bigger city, it should be 25 meters and finally in a really big city, like a European capital, it could even be up to 50 meters.
- furthermore, the value of the *step* defines the level of detail in the ground extraction. So, even though the default spacing of 5 meters would detect and remove most of the major (above-ground) objects, some smaller ones could be missed. In case we really want to have a very detailed ground extraction, then the spacing should be set quite low (less than couple of meters).
- the specification of the *spike* value is very critical, although it is not mandatory for running the tool. The most characteristic example to understand and prove this fact is the case of low grass (some tens of centimetres high). When there is low grass in the study area - which is usually the case for all the dunes adjacent to the Dutch coasts, it is very difficult to detect and remove it, since it appears in the point cloud like noise, meaning that it is represented by points with systematic higher elevations. In the way it is laser scanned, though, spikes are created. So, by setting a value of e.g. 50 cm, all the grass points that protrude more than 50 cm from the reference surface will be removed. This is one of the most efficient ways to remove really fine objects that they would be missed in any other case.

After the test runs and their results, it was concluded that for this study area the optimal values for the ground extraction are:

- *step*: 1 m
- *spike*: 0.4 m, which implies that up-spikes above 40 cm and down-spikes below 4 meters will be removed.

Regarding the *spike*, although someone would think that by setting an even lower value (than 0.4 m) that would result to a more accurate ground extraction, this is in fact not true. The reason is that, together with

some really low above ground objects (e.g. very low grass) that are correctly classified as non-ground points, a lot of ground points that have slightly higher elevations due to the instruments imperfections are also erroneously removed, something that is undesired, unless we aim to decimating the point cloud. In this study, however, we wanted to make use of the strong point of the method of UAV Laser Scanning, the high point density, for the DTM generation, so we didn't want to remove any ground points.

After the above ground analysis was successfully performed, the ground points were separated from the non-ground points by creating two new point clouds. The only-ground point cloud consists of 218,999,070 points (see Fig. 7.6) and the non-ground point cloud of 5,607,053 points. That means that the 97.5% of the points of the denoised points cloud was classified as ground and the remaining 2.5% was classified as non-ground. The low percentage of non-ground points was expected, since the largest part of the study area is the sandy beach, where all of the scanned points are ground points.

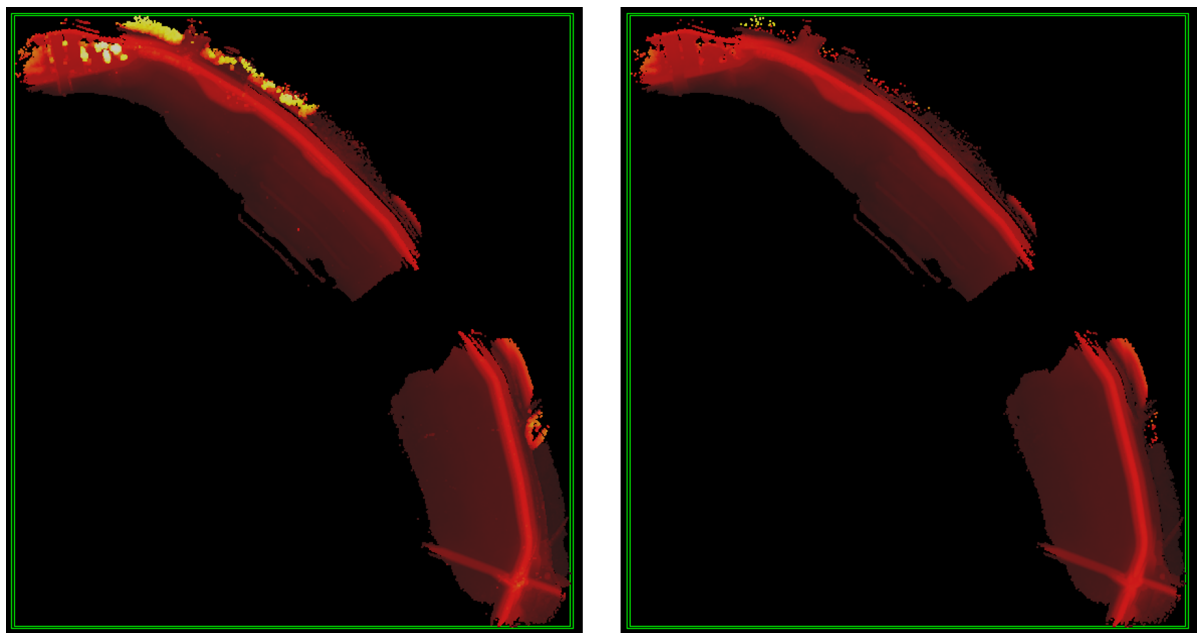


Figure 7.6: Left: Denoised point cloud. Right: Denoised *only-ground* point cloud.

In order to determine whether the above ground analysis was successful or not, we need to take a closer look at the resulted only-ground point cloud and make sure that all the above ground objects have been removed. Here, we will use as examples the two areas that contain the majority of these objects and they are illustrated in Fig. 7.7 and 7.8.

Starting from the most northern part of the study area, which is depicted in the Google Earth screenshot in the top left image of Fig. 7.7, it is concluded that the *lasground* tool was quite successful, since all sorts of above ground objects were removed. At first, it can be observed that the trees in the middle and the top right corner of the area were very accurately removed, keeping untouched only some points that were derived by the laser penetration through them and they actually belong to the ground. These points are second returns - since we know that the Velodyne laser scanner can give only up to two returns. In the grass area, there were also some points removed - but not everything - which apparently protruded by more than 40 cm from the ground. Furthermore, on the left side of the image, we can see some concrete objects (cubes) that are placed next to each other as a roadblock for the parking area. It is very clear in both point clouds, in the only-ground and in the only-nonground, that they were all classified as above ground and consequently removed. The

same happened also with a couple of cars that happened to be parked there during the drone flight. It is noted that the cars that appear in the Google Earth image are not the same as during the flight.

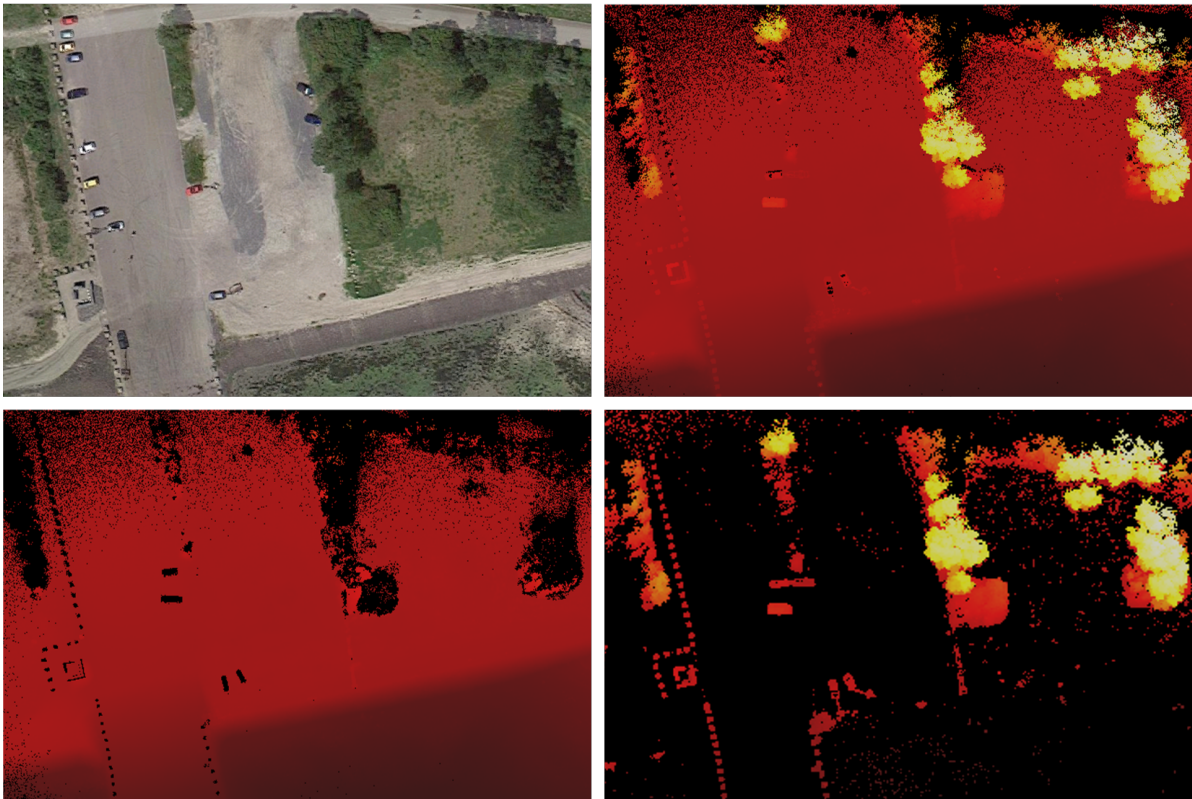


Figure 7.7: First example of the above ground analysis results. Top left: Picture of the northern part of the study area. Source: GoogleEarth. Top right: Denoised point cloud, bottom left: Denoised *only-ground* point cloud and bottom right: Denoised *only-nonground* point cloud of the same area.

For the second example, the area right next to the first one was chosen to be shown due to the variety of objects in it. By looking at the only-ground point cloud (see the bottom left image in Fig. 7.8), which is completely 'clean' of any above ground objects, we can conclude again on the good quality of this processing step. The high vegetation (next to the intersection) has been entirely recognised as such and removed, as it depicted in the only-nonground point cloud (see bottom right image of Fig. 7.8). Some low vegetation that is located before the start of the sand was also removed, but partly, since there are some gaps where really low vegetation alternates with short bushes (about 0.5 m tall). Finally, the man-made structures next to the street have been correctly classified as above ground points.

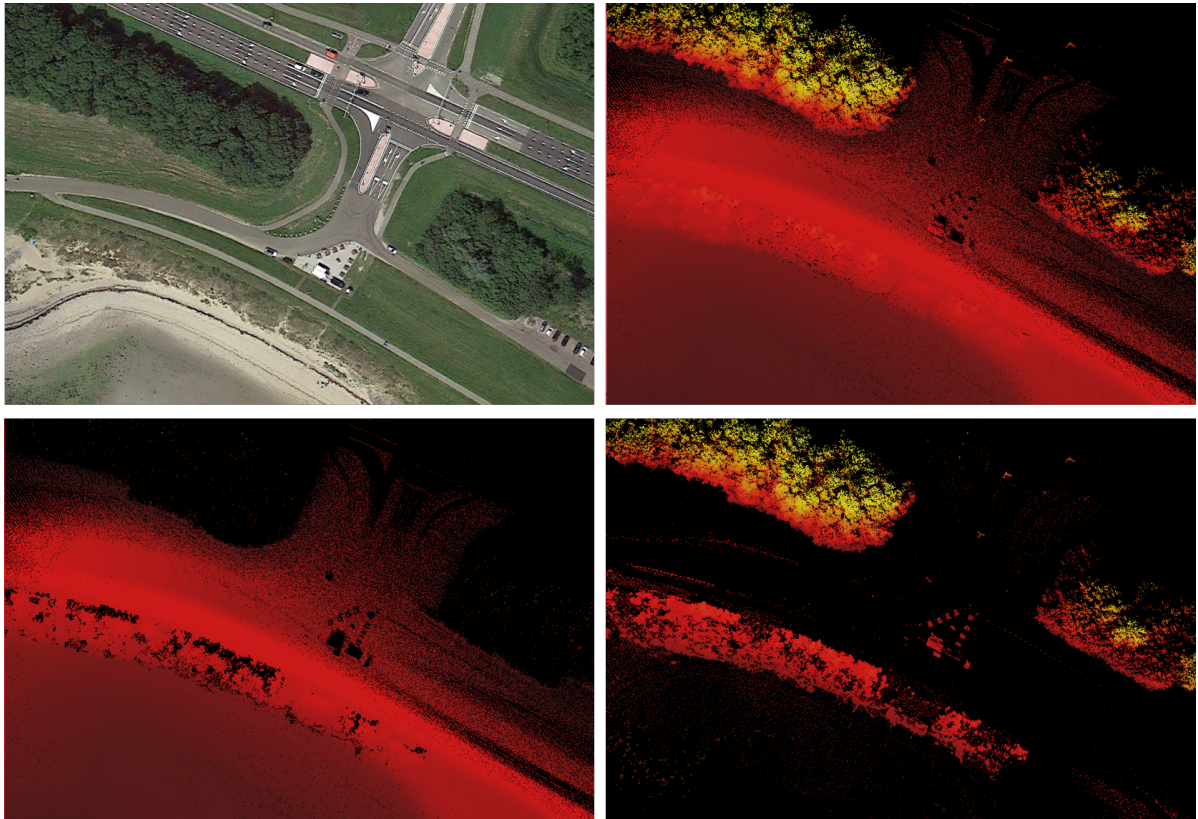


Figure 7.8: Second example of the above ground analysis results. Top left: Picture of the second region of the study area. Source: GoogleEarth. Top right: Denoised point cloud, bottom left: Denoised *only-ground* point cloud and bottom right: Denoised *only-nonground* point cloud of the same area.

The quality of the above ground analysis is similarly high throughout the entire denoised point cloud, something that allows us to continue with the processing and derive the grids, the DTMs. In case there are areas of erroneous classification during this step, usually that would be above ground points that have not been classified as such. Then the point cloud should be manually processed too by importing it in an interactive software (e.g. CloudCompare) and removing all the remaining above ground objects. Sometimes this is necessary in order to remove cars from the dataset. With this combination, both automatic and manual ground extraction for the details, the desired result can be achieved.

7.4. Generation of Digital Terrain Models

The last of the basic processing steps is the generation of the Digital Terrain Models (DTM) and it requires that all the previous steps are completed successfully, or in other case the derived grids will not be accurate. The software that was mainly used for that was OPALS, and more specifically the *Module Grid*, [47], mostly because it enables the processing of quite large datasets - in a reasonable time - due to its special data structure (OPALS Datamanager, ODM). More information regarding ODM can be found in [48]. However, grids can be also generated also in other command-line software, e.g. LAStools, or in interactive software, such as CloudCompare, although in the latter the user does not have the opportunity to control as many parameters as in the command-line software.

The parameters that concern us the most for the generation of a DTM are the grid size, the interpolation method and the number of neighbours -the last one only applies to some interpolation methods. Multiple DTMs were created by varying the parameters settings so that the differences between the resulting grids, as

well as their advantages and disadvantages, could be detected. In this way, we could conclude to the optimal parameters during a grid generation for an application like ours (the parameters can vary a lot depending on the application). For that, a subset of the study area with the most possible different elements in it was chosen, since when using the entire dataset for that purpose the computation time and the size of the raster file are quite large and not handy for further processing. This subregion is the most northern part of the study area (it was also used earlier during the above ground analysis) and it contains both ground and non-ground objects.

7.4.1. Grid size

The *grid size* (or resolution), which indicates the size of each cell that the resulting grid will consist of, is the most critical parameter to be decided, since it determines the level of detail of the grid and thus also the size of the corresponding raster file. Depending on the requirements of the survey, the grid size may vary from a few centimetres to a couple of meters. For coastal monitoring purposes, the typical grid sizes that are usually required span from 5 cm and up to 1 m.

In this study, six different DTMs of the selected region were generated with varying grid size. The largest one is 1 m and the smallest is 1 cm. In between, grid sizes of 0.5 m, 0.20 m, 0.10 m and finally 0.10 m were used. The interpolation method that was used for their generation was Moving Planes with 20 neighbours and the results are presented in Fig. 7.9. On the title of each DTM, the selected grid size is mentioned together with its RMSE. The latter is the computed Root Mean Square Error between the point cloud and the derived DTM and it expresses the magnitude of the deviation between the two - and thus the quality/reliability of the grid.

From these test DTMs, there are some important conclusions that can be reached regarding the parameter of the grid size. At first, the most obvious observation is that with the given point cloud - or any other point cloud derived with the method of UAV Laser Scanning and with similar flight parameters - the DTM cannot have a grid size lower than 5 cm. As seen in the last image of Fig. 7.9, the DTM with 0.01 m grid size is full of gaps (missing data) and it is barely visible. A grid size of, for instance, 4 cm might also have worked, but we usually tend to use rounded grid size values. So, a general conclusion about the minimum grid size that could give an accurate DTM is that this is the 5 cm.

When looking that the RMSE values of the six DTMs, it is easy to notice - and it was also highly expected - that the smaller the grid size, the lower the RMSE, which means the more accurate. More specifically, the DTM with grid size 1 m has the largest RMSE (4.4 cm). A square meter of this DTM is assigned with one single value, while in a square meter of the point cloud there are hundreds of points with a range of different values. Therefore, it is reasonable that there are a lot of differences. As the grid size decreases, the number of points contained in each grid cell are less, something that makes the RMSE to lower. Going from 0.50 m to 0.05 m, the RMSE decreases gradually getting the value of 3.9 cm for a grid size of 0.50 m, 3.5 cm for for a grid size of 0.20m, 3.4 cm for a grid size of 0.10 m and 3.3 cm for a grid size of 0.05 m. Finally, when a grid size of 0.01 is used, the grid cells are very small (one square cm) and thus the value assigned to them is very close to the values of the points. This DTM, however, is not usable due to the lack of data in it, so we will not further discuss it.

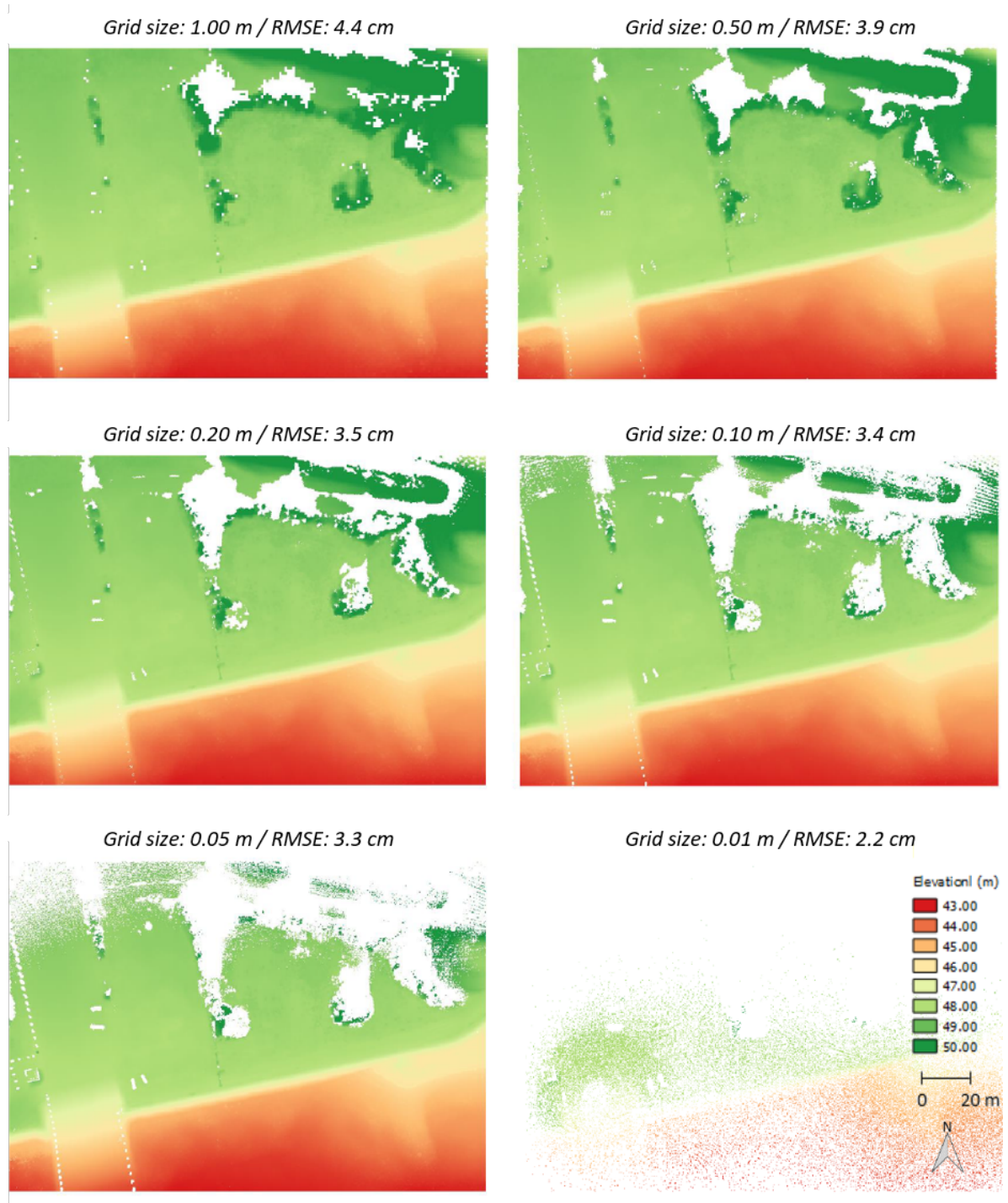


Figure 7.9: DTMs of the selected subregion of the study area with six different grid sizes, 1 m, 0.5 m, 0.20 m, 0.10 m, 0.05 m and 0.01 m.

In addition, in all of the DTMs we can see that there are some gaps, mostly in the north-east part of the region. These are the result of the removal of the non-ground points with the procedure of the above ground analysis. These gaps, however, are quite different between the six images. It can be observed that the largest the grid size, the more the gaps are filled with data. Another characteristic example is also the concrete cubes (roadblock), which have been classified as non-ground and removed. Someone would expect to see (almost) square gaps at their locations, but, especially in the first two images (1 m and 0.5 m grid sizes), these are almost entirely covered. As the grid size decreases, then the gaps due to the roadblock appear. That is

reasonable, since when the grid size is large, then the interpolation occurs in a wider area. Because we know from before, though, that these areas have mostly non-ground objects, we do not want them to be filled with data (in a DTM). The 5 cm and the 10 cm DTMs serve this purpose quite well, because the grids in these cases are quite fine and the interpolations are performed in smaller areas, without influencing the neighbouring cells.

Finally, as stated above, the grid size represents the level of detail in the grid. That means that going from the first to the fifth image of Fig. 7.9 (the sixth is not even visible), the grids are more and more detailed and thus fine characteristics of the study area can be visible. These details are in certain cases necessary, in other cases useful and in other redundant. So, depending on the requirements of the survey, a different level of detail has to be chosen.

7.4.2. Interpolation method

For the generation of a grid, an *interpolation* is always performed, with which the available information, here the z-coordinate of the points, is converted into grid information. That means that each cell gets a value of the selected attribute through this procedure. There are many different interpolation methods, but among them, there are several ones that are more suitable for DTM generation due to their combination of high quality and short processing time.

The ones that were decided to be presented in this section are the following:

The Inverse Distance to a Power method

The Inverse Distance Weighted method is a weighted average interpolator. When this technique is applied, data are weighted so that the influence of one point, relative to another, declines with distance from the grid node. At the same time, the weighting power controls how the weighting factors drop off as the distance from the grid node increases. More specifically, the more the weighting power increases, the less effect the points that lay further from the grid node have during the interpolation. Thus, as the power increases, the grid node value approaches the value of the nearest point (Nearest Neighbour interpolation), while as the power decreases, the weights are more evenly distributed among the neighboring data points [83].

The Kriging method

Kriging is a geostatistical interpolation method that is used in diverse fields and deal with irregularly spaced data very efficiently. The unknown value at a certain location is calculated by weighting the observations at known locations by a list of weight coefficients. These coefficients are computed based on a spatial dependence function, which describes the relationship of the observed values as a function of their separation distance [71]. In general, Kriging performs better in terms of accuracy than many other methods. However, its algorithm is more complex - which implies lower computation performance - and thus usually it is not preferred for DTM generation, where there is a large number of points.

Nearest Neighbour

Each grid cell gets its value (height, in the case of a DTM) from the nearest point. The quality of the derived surface is most of the times low because of the simplicity of the algorithm, but for the same reason the computation performance is very high.

Delaunay Triangulation

At first, all the points of the point cloud are triangulated, according to the rules of Delaunay Triangulation, and then the grid values are interpolated using the created TINs. It is one of the fastest methods for triangulating point cloud and it is mostly used for the creation of terrain models.

Natural Neighbour

This technique finds the closest subset of input samples to a query point and applies weights to them based on proportionate areas to interpolate a value. Its basic properties are that it's local, using only a subset of samples that surround a query point, and interpolated heights are guaranteed to be within the range of the samples used [63].

Moving Average

For each grid cell, n neighbouring points, the number of which is specified by the next parameter (number of neighbours), are used. The value that is assigned to the cell is equal to the average height of all these n points. The computation performance of this method is quite high and at the same time the quality is improved too.

Moving Planes

For each grid cell, n neighbouring points are again used. The algorithm estimates a best fitting tilted plane, meaning a plane that minimises the vertical distances from the used points to it. The value that is assigned to the cell is the value of the derived plane at the specific grid position. This is the most accurate method of the ones discussed here, but at the same time is the most complicated and thus it needs more computation time.

Out of the seven interpolation methods discussed above, only four of them are going to be investigated here through the generation of test DTMs. These are the Nearest Neighbour, the Delaunay Triangulation, the Moving Average and the Moving Planes method. The reason for that is because each one of these four technique presents certain advantages that are good to be looked into:

- Nearest Neighbour is one of the interpolation methods that have quite simple algorithm and thus they are very fast.
- Delaunay Triangulation assigns values to grid cells using TINs and it is a very popular method for the representation of terrains.
- Moving Average usually gives a smoothed result, which is very useful in the case of a noisy dataset.
- finally Moving Planes is a quite reliable method since the value assignment is based on best fitting tilted planes.

For these test DTMs a grid size of 0.05 m was chosen, so that more details could be observable, and 20 neighbours (for Moving Average and Moving Planes). Fig. 7.10 illustrates the results.

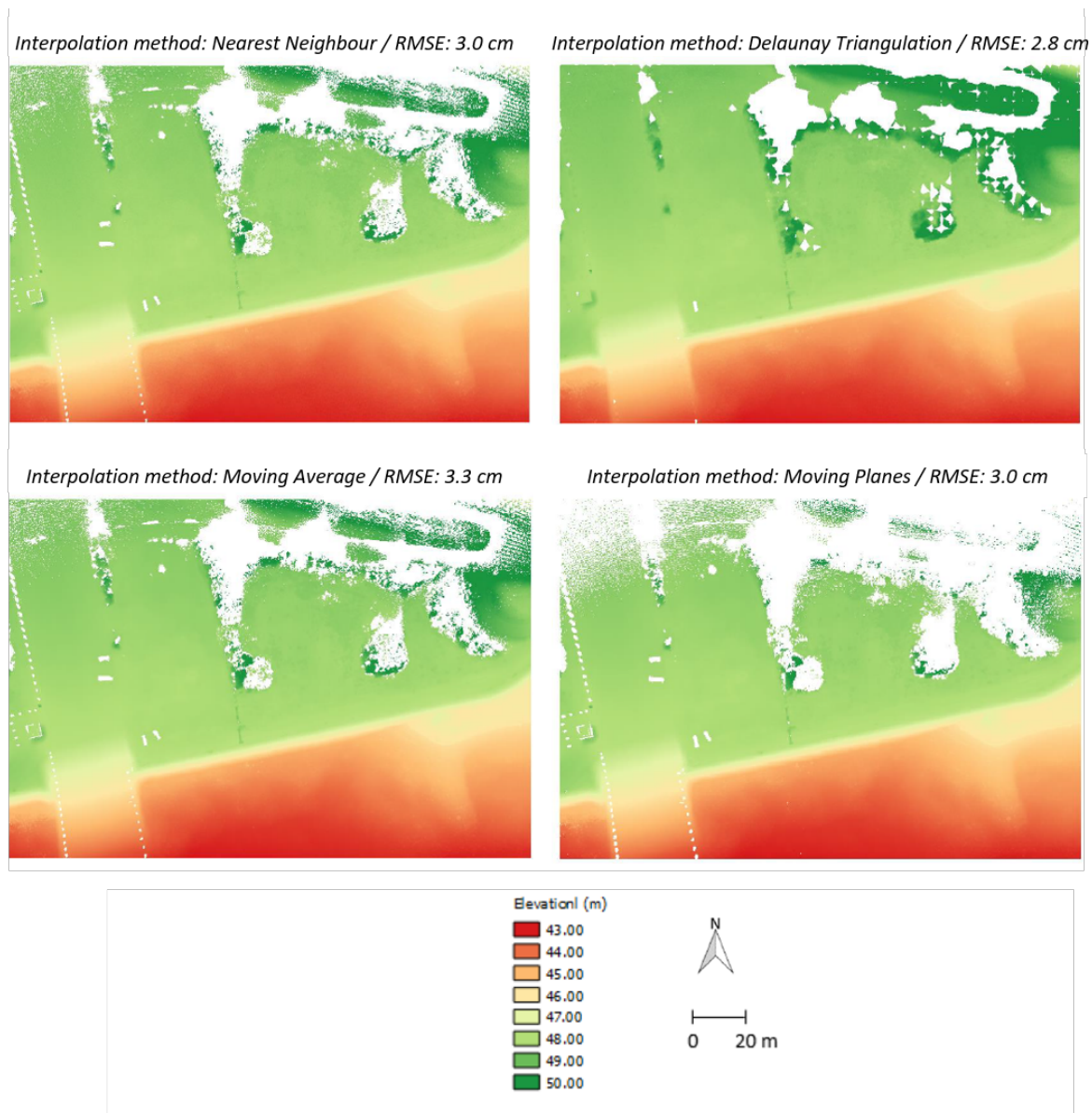


Figure 7.10: DTMs of the selected subregion of the study area with four different interpolation methods, Nearest Neighbour, Delaunay Triangulation, Moving Average and Moving Planes.

Looking at the results of the four different interpolation methods, the most obvious conclusion is that the Delaunay Triangulation is not the most suitable method for this kind of surveys, although its RMSE is the lowest between all them. The grid cells that are located in the gaps (resulted by the removal of the non-ground objects) get filled in through the triangulation that precedes the interpolation. For the reasons that were discussed in the previous section, that is undesired. The second observation is that the DTM derived with the method of Moving Planes has more gaps at the northern part (due to the low point density), something that is associated with the grid size according to the previous section. Between the other two methods, it is noticed that there are not many differences. And more specifically, although the Nearest Neighbour method is expected to be of low quality in comparison to the others, in this case the result was quite satisfactory.

Regarding their RMSE values, the lowest is the one of Delaunay Triangulation, as noted above. However, this DTM gives an unrealistic idea of the terrain by filling in the no data cells and therefore we move on to the rest. More specifically, the two methods, Nearest Neighbour and Moving Planes, have equal RMSE (3

cm) and Moving Average has a bit larger (3.3 cm). Nearest Neighbour performs quite well when the point density is high and the study area is relatively flat. For that reason, we see a quite accurate result here. On the other hand, Moving Planes does not depend so much on the nature of the terrain, since its algorithm is based on fitting planes. However, it does depend on the point density. In cases that there are not many points around the query points, the estimation of the fitting planes is not possible and that results to a no data cell. According to this fact, the RMSE of our Moving Planes DTM could be lower if the northern part had a higher point density.

The runtime of each method, however, is also of high importance, especially when the dataset is large. Therefore, the runtime of these methods was recorded, too, and is presented in Table 7.2. It is noted that all of the DTM derivations were performed in OPALS and thus the runtime here corresponds to the OPALS runtime.

Table 7.2: Runtime in OPALS for the four interpolation methods

Method	Runtime (sec)
Nearest Neighbour	16
Delaunay Triangulation	53
Moving Average	36
Moving Planes	32

The first conclusion that is drawn from this table is that Nearest Neighbour is the fastest method (16 seconds). That was expected - and it is actually the strongest advantage of the method, since it has the simplest algorithm when compared to the other three methods (time complexity: $O(\log n)$). On the other hand, it is observed that Delaunay Triangulation is the most time-consuming method (53 seconds) with a significant difference from Nearest Neighbour. That is also demonstrated by its time complexity, which is $O(n \log n)$, and it can be explained from the fact that a triangulation has to be performed at first. Finally, Moving Average and Moving Planes are quite close regarding their runtime, with the latter being slightly faster (36 seconds for Moving Average and 32 seconds for Moving Planes). They both have a reasonable runtime, even for large datasets, but at the same time they perform better when it comes to more complex terrains due to their moving window algorithms².

7.4.3. Number of neighbours

The last parameter to be investigated is the *number of neighbours*. From the four interpolation methods that were used earlier, the number of neighbours is used in the last two, the Moving Average and the Moving Planes. It determines how many points (nearest neighbours) are used for grid point interpolation and it influences the computation time and the result.

In Fig. 7.11, the DTMs of the selected region with 5, 10, 20, 50 and finally 100 neighbours are presented respectively. The interpolation method that was used here was Moving Planes and the grid size was 0.05 m.

²A moving window algorithm takes into account the values of a certain number of neighbours, specified by the user, around the query point. For a more accurate result a small number of neighbours is chosen (5-10) and for a smoothed result a larger number of neighbours is preferred (>10).

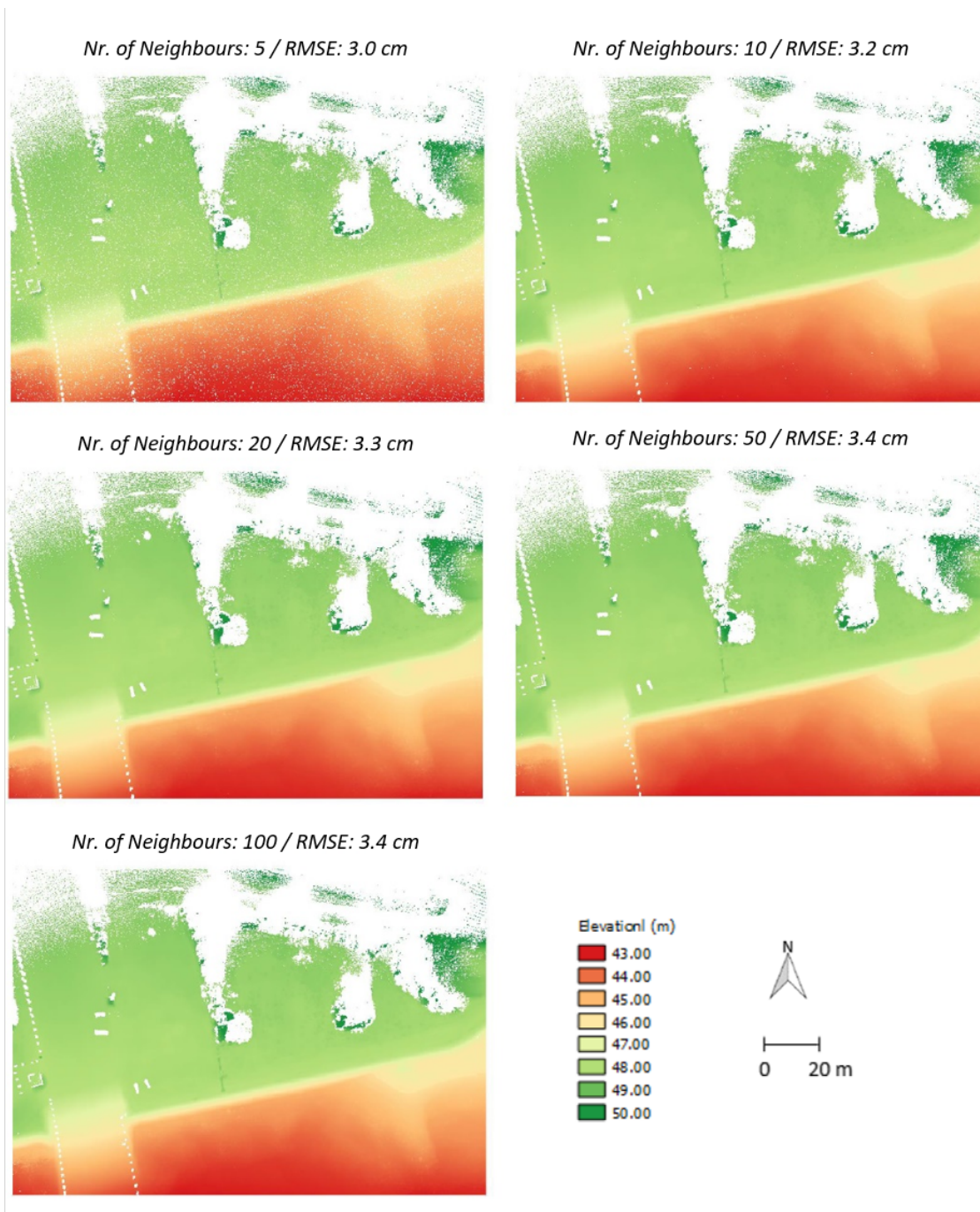


Figure 7.11: DTMs of the selected subregion of the study area with five different numbers of neighbours, 5, 10, 20, 50 and 100 using the Moving Planes method.

The general conclusion that can be drawn from the figure above is that the lower the number of neighbours, the more gaps in the form of missing data (white dots) appear in the resulting grids. From a certain number, though, and on, the result remains the same (there are no gaps) and here this number is 20 neighbours. This effect can be explained by the fact that when a low number of neighbours is used, there may be grid cells with no points in the specified search radius (that is specified by the software depending on the point density of the point cloud). In this case, the grid cell remains empty and it gets the no-data value. However, we can also see that the more neighbours we use, the larger the RMSE gets. This is due to the fact that when more neighbours are used, the result is more smoothed and thus it deviates more from the real value. In order

to achieve a uniform grid (no missing data) but accurate at the same time, we have to choose the smallest number of neighbours possible that would give us no gaps. Here, that is between 10 and 20 neighbours.

In order to decide on the three significant parameters, the grid size, the interpolation method and the number of neighbours, the results from all the test DTMs above are combined and the final conclusions are the following:

- the grid size of the DTM can vary from 5 cm to 1 m (or even larger when necessary, although it is rarely used). However, when the point cloud is large, then a DTM of 5 cm resolution would also be a quite large raster file. So, if there is no requirements for such a high level of detail, it is preferable to use a larger grid size, such as 20 or 50 cm.
- the choice of the interpolation method can also vary depending on the point density, the type of terrain and time available. When the input dataset is quite dense - which is usually the case for point clouds coming from UAV Laser Scanning - and at the same time the study area is relatively flat, then the best choice would be to use the Nearest Neighbour method, since it gives quite fast an accurate result. However, when the study area is more complex, including slope and/or man-made structures, then it is preferable to use Moving Planes. It is more time-consuming than Nearest Neighbour, but due to its moving window algorithm, it is can approach the real terrain in a more reliable way. Finally, Delaunay Triangulation is a very accurate method too, but it requires that no gaps due to the above ground analysis are present. For instance, if we want to generate the DTM of a beach area, with no above ground objects, that could be a useful method.
- finally, the number of neighbours specified when using either the Moving Average or the Moving Planes interpolation methods should be between 10 and 20 for a point cloud with a point density similar to the one of our study - around $550 \text{ points}/\text{m}^2$. At the same time, though, there is no need to use too many neighbours (more than 20), since the results remains almost the same, but with the need for longer computation time.

7.5. Validation

7.5.1. Validation of the UAV LS point cloud with TLS data

As already mentioned in Chapter 4, during this study Terrestrial Laser Scanning measurements were carried out in the study area in Schelphoek. The main purpose for that was to use them for the validation of the laser scanning data acquired with the drone. Since the TLS measurements took place on a different date than the UAV measurements - and more specifically several months after, the only parts of the study area that could be compared were the time-invariant ones, such as the parking area, the bike path, the rock slope etc. For the acquisition of the data, the instrument was placed in four different stations, as illustrated in Fig. 4.7. In this way, four different point cloud were derived (see Fig. 4.8). From these, the fourth one, which is the one derived from the parking space, was used for the validation of the UAV LS point cloud.

For the validation of the UAV LS point cloud, three profiles were extracted both from the UAV LS and the TLS point cloud using CloudCompare. For that, three polylines were drawn and then the underlying point cloud of thickness 1 meter along these polylines was extracted. These profiles connect specific objects in the study area and thus no registration of the point clouds is needed. More specifically:

- Profile 1 connects the square structure with the first concrete cube on the lower side.

- Profile 2 connects the first concrete cube on the upper side with again the first one on the lower side.
- Profile 3 connects the ninth concrete cube on the upper side with the fifth one on the lower side, as shown in Fig. 7.12.

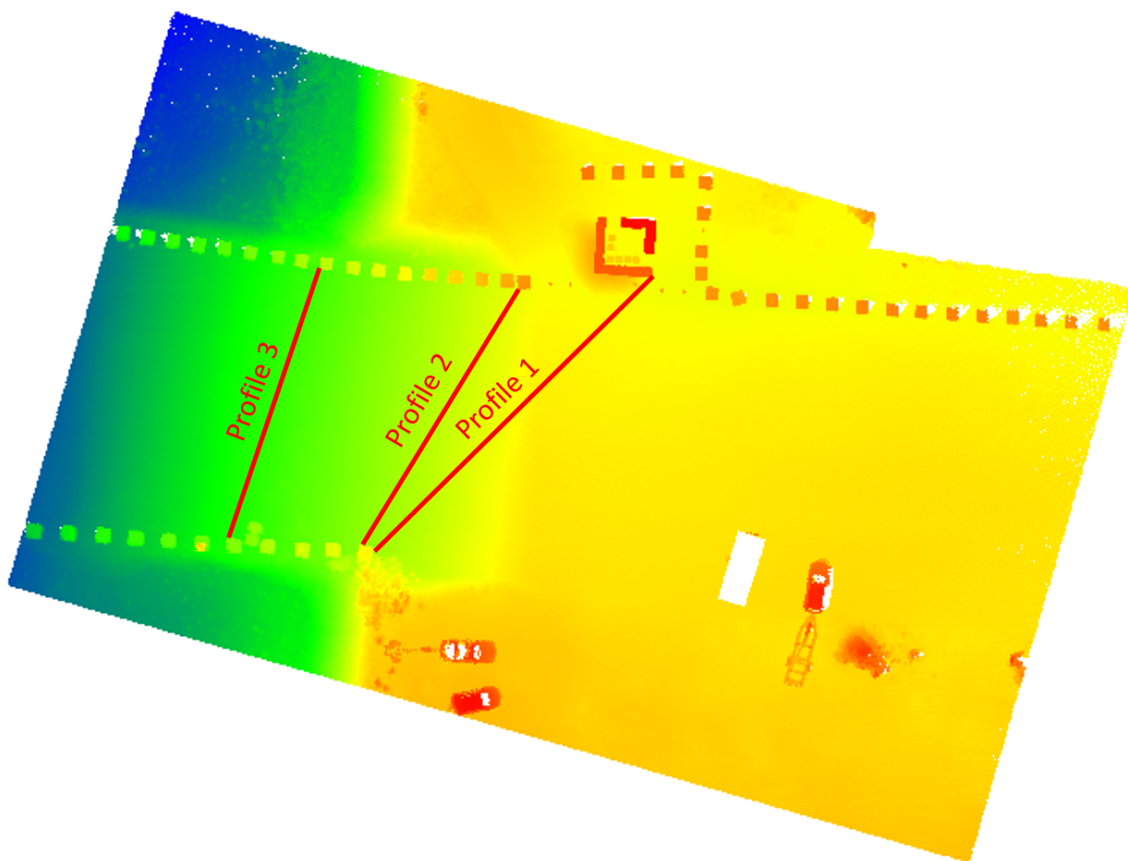


Figure 7.12: The three profiles having as background the UAV LS dataset

After the six profiles were extracted, three from each point cloud, they were matched - placed on top of each other - in order to detect the differences. The *distance from cloud to cloud* tool of CloudCompare was used and in this way the absolute distances in all these axes, X, Y and Z were determined. Since we mostly care about the vertical accuracy of the dataset, in the following figure the the histogram of the absolute distances in the Z are presented for each profile.

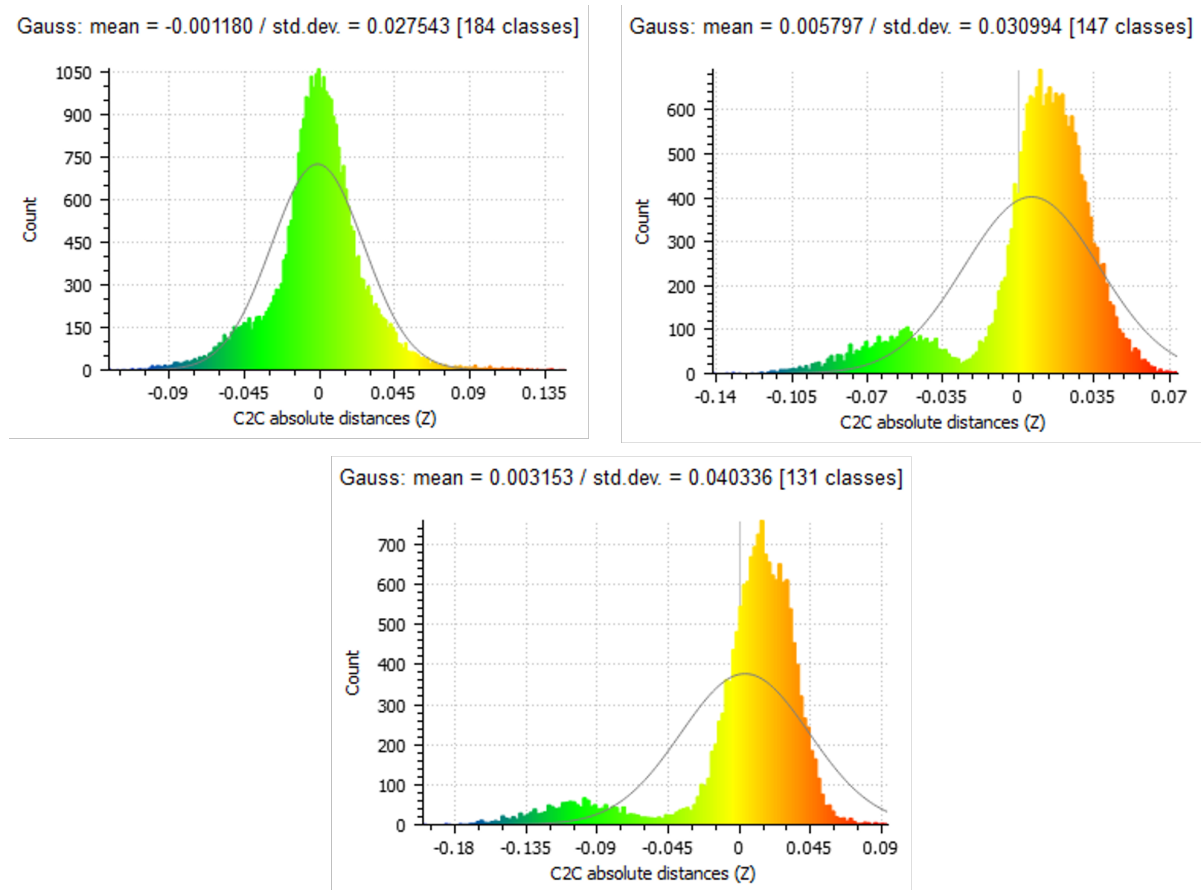


Figure 7.13: Histograms of the absolute differences in Z. Top left: for Profile 1, top right: for Profile 2 and bottom: for Profile 3.

At the same time, and as it can be seen in Fig. 7.13, a Gaussian distribution was fitted to the three histograms and their main statistics, the mean value and the standard deviation, were calculated. The peak of bell of the Gaussian distribution in Profile 1 is almost over zero and thus the mean value of the absolute differences in Z is 1 mm, while the standard deviation is close to 3 cm. That means that the vertical differences over this profile are quite small. However, the vertical differences in the other two profiles are a bit larger, with a mean value of 6 mm for Profile 2 and 3 mm for Profile 3.

In addition, 10 distances were measured both in the UAV LS and the TLS point cloud and compared. All of these distances were from and to known objects in the study area. Fig. 7.14 illustrates them and Table 7.3 contains the results.

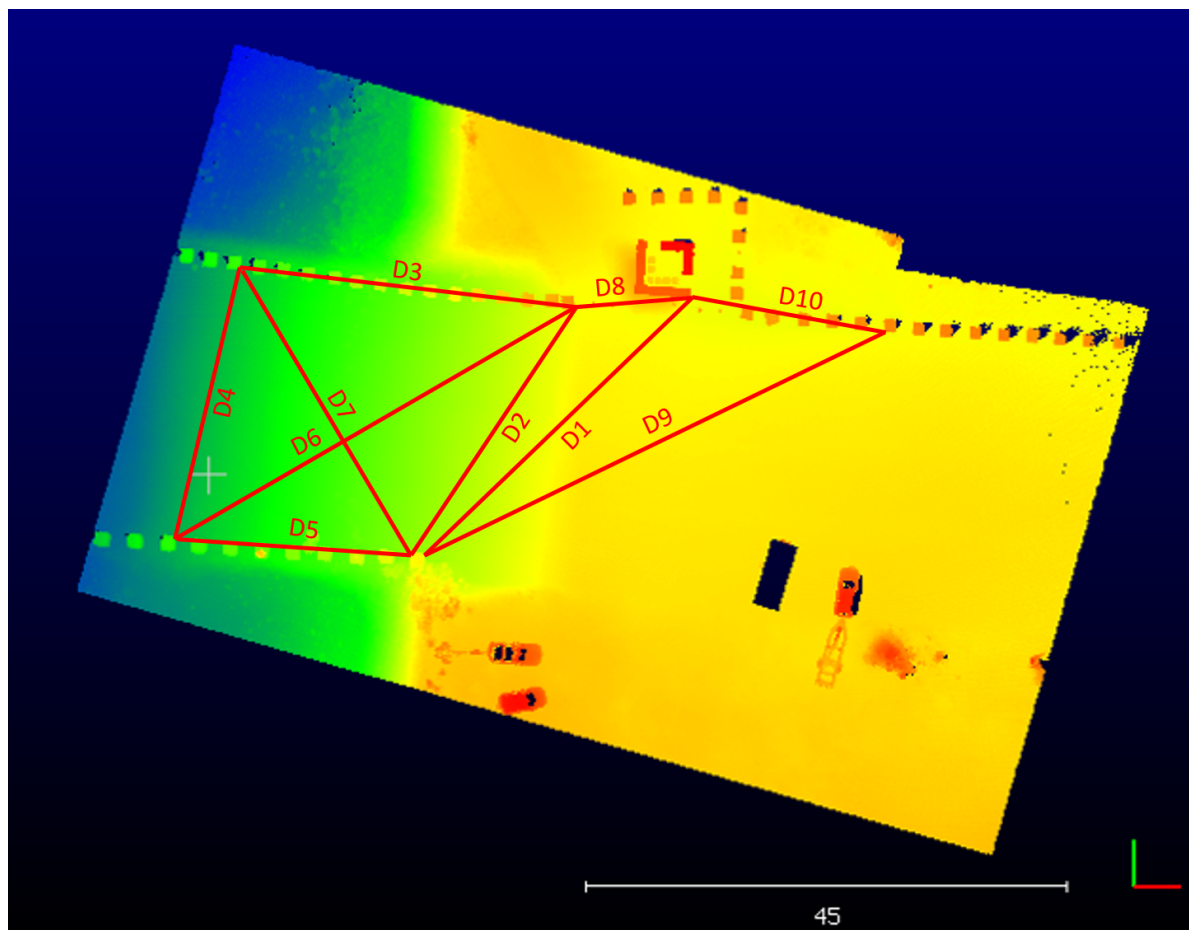


Figure 7.14: Measured distances in the UAV and the TLS point clouds

Table 7.3: Measured distances in the UAV and the TLS point cloud

Distance	Description	UAV point cloud	TLS point cloud
<i>D1</i>	1st cube down to rectangle structure	34.883	35.089
<i>D2</i>	1st cube down to 1st cube up	27.008	27.225
<i>D3</i>	1st cube up to 15th cube up	30.741	30.965
<i>D4</i>	9th cube down to 15th cube up	25.980	26.132
<i>D5</i>	9th cube down to 1st cube down	22.521	22.825
<i>D6</i>	9th cube down to 1st cube up	42.437	42.821
<i>D7</i>	1st cube down to 15th cube up	32.289	31.701
<i>D8</i>	1st cube up to rectangle structure	10.953	10.988
<i>D9</i>	1st cube down to 10th cube up (to the right)	48.091	48.486
<i>D10</i>	Rectangle structure to 10th cube up (to the right)	18.610	18.833

The differences between the ten distances in both point clouds are quite large according to the table. More specifically, the measured distance with the maximum difference is *D7* with -0.588 m, while the minimum is *D8* with -0.035 m. The mean value of this differences is almost 16 cm. Another observation is also that the differences in the UAV point cloud are always smaller than the ones in the TLS.

7.5.2. DTM quality estimation

The last part of this chapter is all about DTM quality. As mentioned earlier, the DTM quality depends on two main factors, the quality of the input dataset and the model quality. At the same time, the model quality can be divided into interior and exterior quality. Therefore, in the following paragraphs the DTM quality based on the input dataset, and the interior and exterior model quality are going to be estimated and discussed.

DTM quality based on the input dataset

The first DTM quality measure that is going to be estimated is the vertical accuracy of the derived DTM using the formula by Karel and Kraus [31]. For that, the point density and the terrain slope of the selected region had to be estimated at first. That was realised in OPALS. Using the *Module Cell*, the number of points per square metre was determined and then this value was assigned to the corresponding cell of the raster file. The resulting point density map is presented Fig. 7.15:



Figure 7.15: Point density map of the selected region in points/m²

In this figure, we can see that the point density varies a lot throughout the area. The highest values are under the trajectory that the drone followed in order to turn (dark purple colours). This fact is due to the lower speed that it has during turning. In addition, it is noticeable that the point density decreases when the distance from the trajectory increases (to both sides).

Next, the terrain slope was derived with the *Module Grid* [47] and with the same grid size (1 m) so that the vertical accuracy could later be calculated per square meter. Fig. 7.16 shows the result:

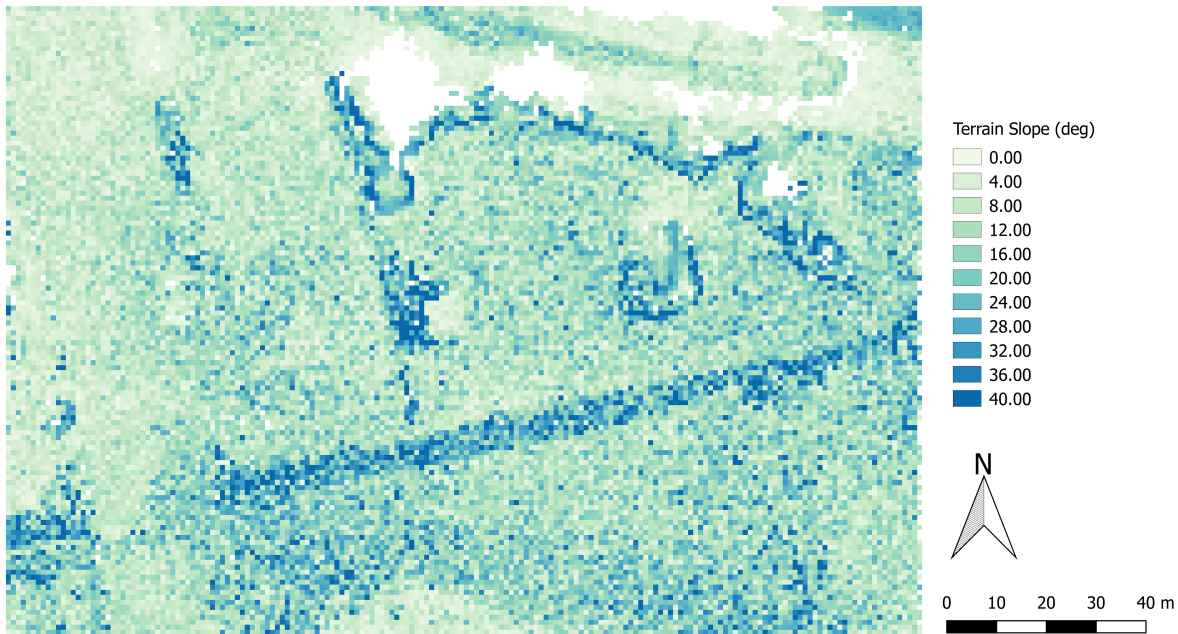


Figure 7.16: Terrain slope in degrees of the selected area.

This image suggests that the terrain slope varies from almost 0° to 40°. The highest values of the slope appear next to the removed vegetation areas, probably because there are still some remaining points with higher elevations after the above ground analysis. In addition, high values appear also in along the natural slope that exists in the study area. We can see a line of dark blue pixels that goes from the left to the right side.

Using the values of each 1x1m grid cell of these two maps, the vertical accuracy of the DTM is determined using the following formula and is illustrated in Fig. 7.17:

$$\sigma_z(cm) = \pm \left(\frac{6}{\sqrt{n}} + 30 \tan \alpha \right)$$

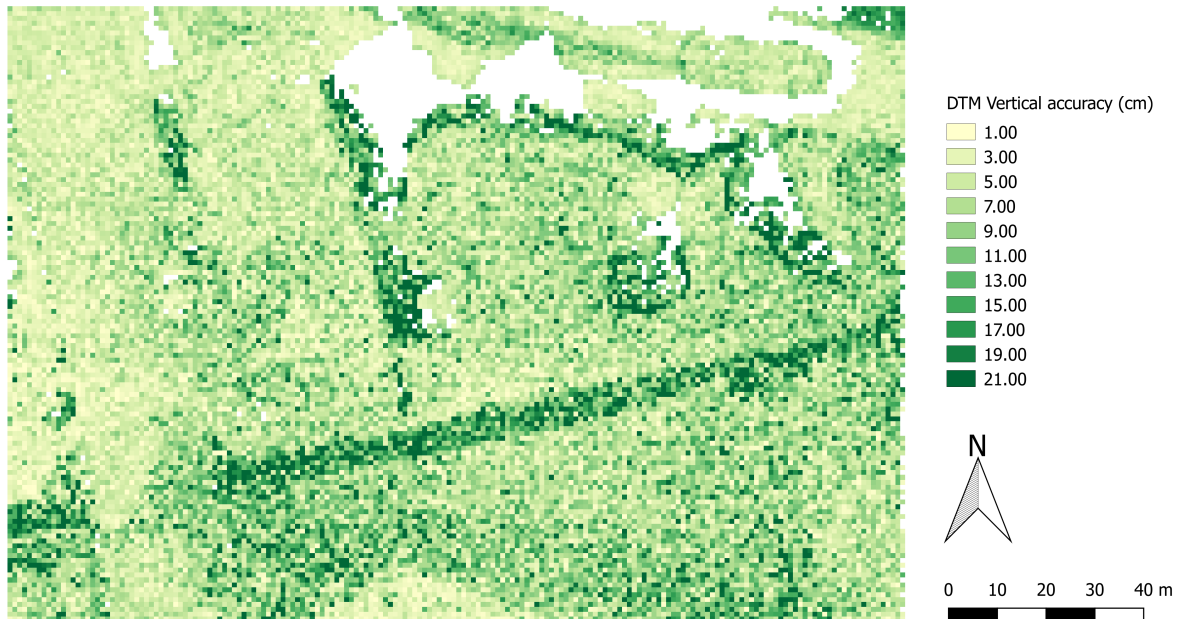


Figure 7.17: DTM vertical accuracy in cm.

From the figure, we can see that the vertical accuracy depends a lot on the slope. If we compare the terrain slope map and the vertical accuracy map, then we can see that the areas of higher values are the same. The area has an average vertical accuracy of approximately 8 cm. However, the same formula allows us to determine the DTM quality for different point densities in order to improve our flight planning. Therefore, assuming that the terrain slope of the area is the same and using its average value which is equal to 13° , we can change the point density and get different vertical accuracies as shown in Fig. 7.18:

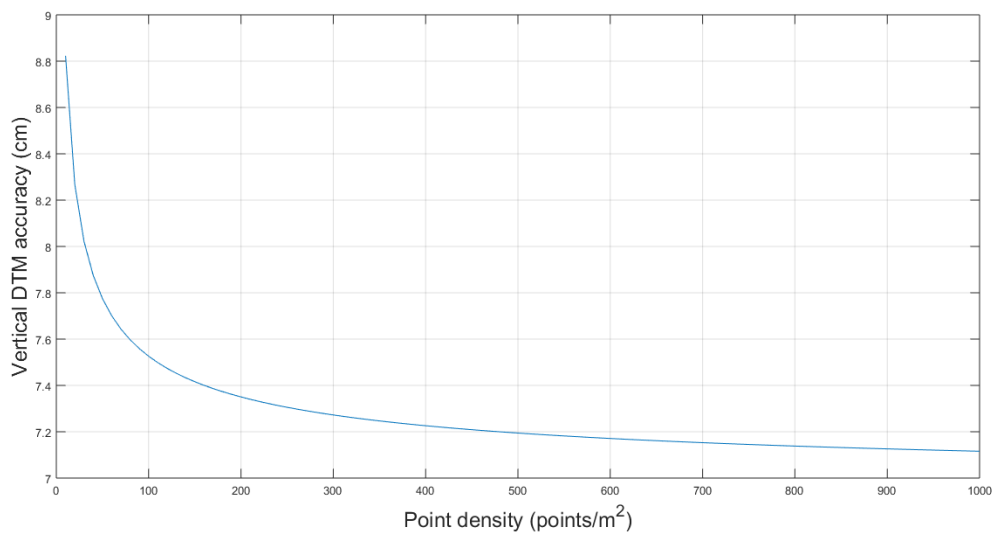


Figure 7.18: Dependency of the vertical DTM accuracy on the point density.

From this plot, we conclude to the fact that after a certain point density (here approximately $300 \text{ points}/m^2$) the vertical accuracy does not change much. The improvement in the accuracy for a point density of 300 and $1000 \text{ points}/m^2$ is only around 1.5 mm. That means that it is preferable to have a lower point density, e.g. around $300\text{-}400 \text{ points}/m^2$, which would make it easier to process the dataset and would keep the size of the

files smaller.

Interior and Exterior DTM quality

Next, we move to the model quality of the DTM. That is the interior and the exterior quality. At first, the interior quality describes the quality of the estimated DTM with respect to the input dataset. Thus, we calculated the differences between the only-ground point cloud and the previously derived DTM in OPALS and then the Root Mean Square Error (RMSE) of these differences. This procedure was carried out for all of the derived DTMs, but since their RMSEs are already mentioned and discussed above, we will go into detail only with one of them, the DTM that was derived with the Moving Planes method with 20 neighbours and with grid size 5 cm. This one was one of the best DTMs derived according to the criteria described in the previous section and this is the reason why it was selected. Fig. 7.19 shows the result of the comparison between the aforementioned DTM and the only-ground point cloud.

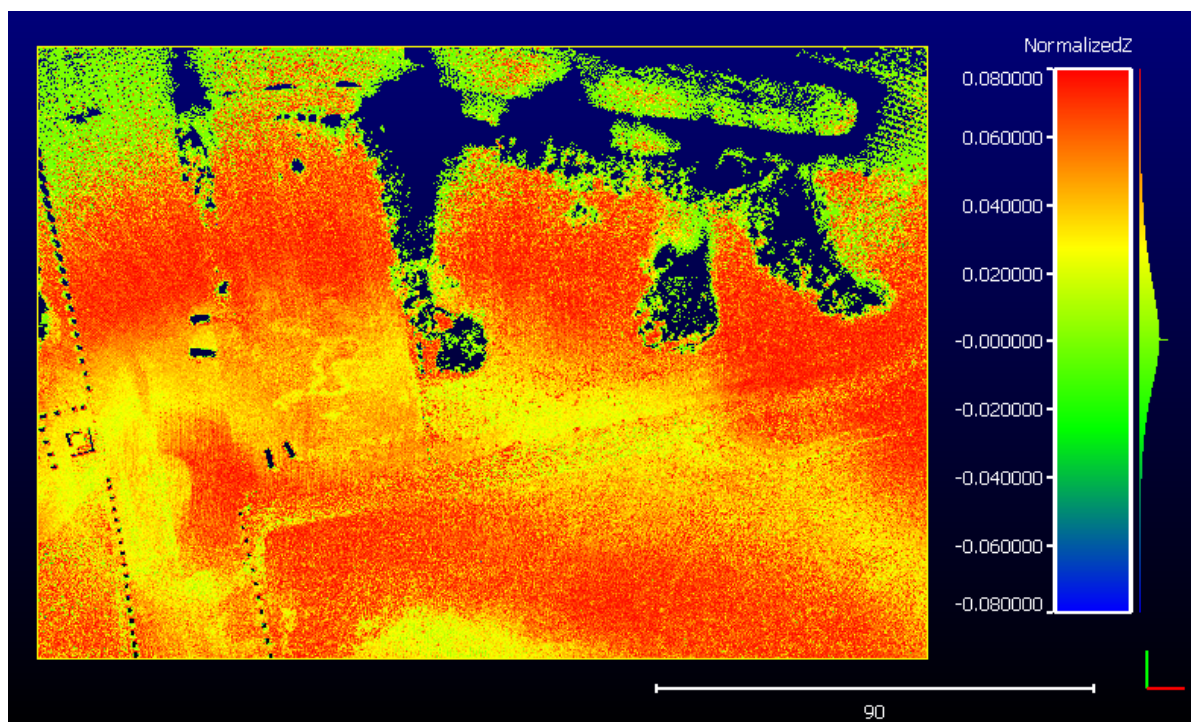


Figure 7.19: Differences between the only-ground point cloud and the Moving Planes DTM with grid size 5 cm.

What we notice on the first sight is an extend red area, which is translated to a difference of 6-8 cm. However, this impression is given due to the visualisation in CloudCompare. More specifically, CloudCompare shows the points with higher elevations on top of the other. So, what we see at the end is the top layer of points which indeed has the largest differences from the DTM. For that reason, it was necessary to look at the histogram (Fig. 7.20) of the differences.

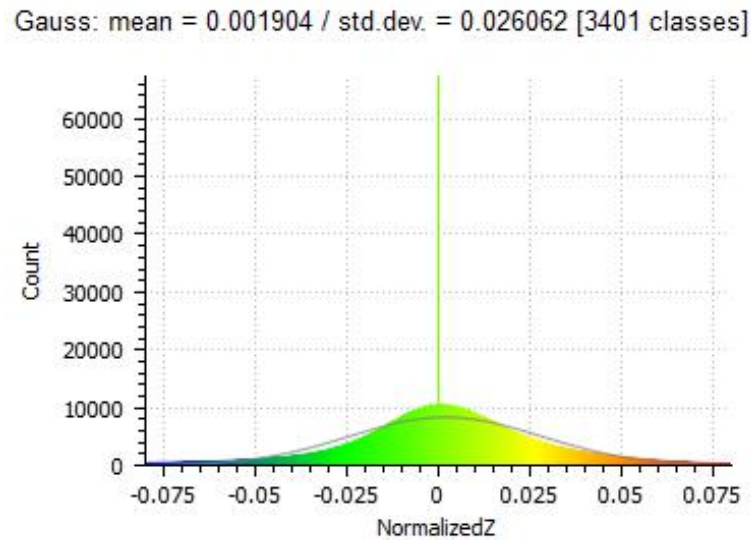


Figure 7.20: Histogram of the differences between the only-ground point cloud and the Moving Planes DTM with grid size 5 cm.

In order to get an idea of the statistics of the differences, a Gaussian distribution was fitted to the data. We can see that the mean difference is almost 2 mm, which is a very low value, and the standard deviation is 2 cm due to the standard deviation of the point cloud (which was also found to be around 2 cm earlier). Finally, the RMSE of these differences is 3.3 cm.

Finally, the exterior quality of the same DTM was investigated. For that, the GPS measurements that Shore Monitoring & Research B.V collected during the test flight were used. However, there were no GPS data for the area that has been used up to now (parking area) and therefore another area had to be selected. That was the part of the beach where the breakwaters are, since the density of the GPS measurements there was high and so we would have a large amount of validation data. This validation process was performed in QGIS. More specifically, the DTM and GPS data were at first imported into the software. Then, using the sampling tool of QGIS, a new point layer was created right on the same locations as the GPS data but with the value of the DTM assigned. Finally, these two point layers were subtracted from each other and visualised as shown in Fig. 7.21.

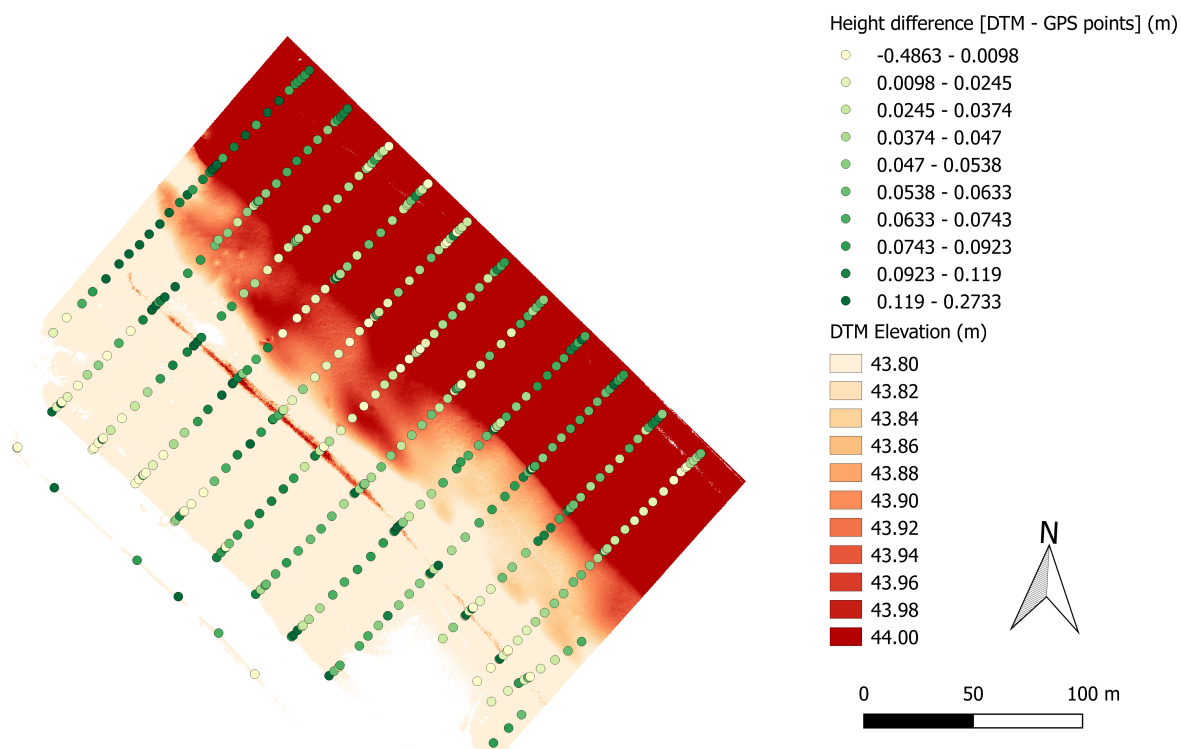


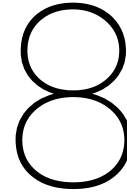
Figure 7.21: Differences between the GPS validation points and the Moving Planes DTM with grid size 5 cm.

As it can be seen in that Figure, the differences span from 0 to almost 12 cm, with the highest differences appearing close to the breakwaters, due to the wet vegetation that covers them, and near the borders of the DTM. The mean value of these differences is close to 6 cm.

7.6. Summary

This chapter was dedicated to the presentation of all the results from the post-processing of the UAV LS point cloud. It started with the calculation of the vertical accuracy and precision by using a small flat dataset from the initial point cloud. The accuracy was estimated equal to 2 cm and the precision to 4 cm. What followed was the preparation of the point cloud and the noise removal, after which 86,394 points were removed. Then, the above ground analysis was performed for the separation of the ground and non-ground points. After its successful performance, 218,999,070 points were classified as ground points and 5,607,053 points as non-ground. With the denoised and only-ground point cloud we proceeded to the DTM generation, for which the three most important parameters had to be at first investigated. These are the grid size, the interpolation method and the number of neighbours. From multiple test DTMs that were generated, we found out that the grid size of the DTM can vary from 5 cm to 1 m, the choice of the interpolation method varies depending on the point density, the type of terrain and time available and finally the number of neighbours should be between 10 and 20 for the Moving Average and Moving Planes methods. Finally, the validation of the UAV LS point cloud and the DTM had to be performed. For the former, three profiles were extracted both from the UAV LS and the TLS point cloud and compared by calculating the distance from the one point cloud to the other. Their differences were found to be from 1 mm to 3 mm. Regarding the DTM quality, at first the vertical accuracy of the derived DTM using the formula by Karel and Kraus was estimated to be equal to 8 cm. The interior DTM quality was derived by computed the RMSE of the differences between the only-ground point cloud and the DTM. These differences are 1 mm on average and their RMSE is 3.3 cm. The exterior quality

was estimated by using GPS data from the study area. The two datasets were compared and their differences were found to be 6 cm on average.



Conclusions and recommendations

The objective of the present Master thesis was the evaluation of the performance of UAV Laser Scanning as a technique for monitoring the changes in the coastal zones. For that purpose, the error budget, and consequently the quality, of the 3D laser points derived with this method were investigated. In addition, a post-processing chain, starting from the initial point cloud and till the final DTM generation, was determined and the quality of the products was evaluated. In this final chapter, the conclusions of this study are presented followed by some recommendations for future work.

8.1. Conclusions

In the Introduction of this report, the main research question was divided into six sub-questions. In the following paragraphs, the answers to these questions are going to be given as conclusions drawn from all the previous chapters. At the end, this will enable us to answer the main research question.

1. What are the sources of error introduced in a point cloud coming from UAV Laser Scanning and what is the error budget of such a system? A UAV Laser Scanning system consists of three components. These are the laser scanner, the GPS receiver and the IMU. All these three instruments are sources of error during their operation. More specifically, the laser scanner introduces a range and a scan angle error into the measurements. The range error depends mainly on the optical and electrical design as well as on the target reflectivity and surface roughness, while the scan angle error is influenced by the laser beam divergence and mechanical aspects, such as vibrations or oscillations caused by the interference with the UAV engine. Secondly, the magnitude of the GPS positioning error depends on the satellite configuration, the signal multipath, clock biases, atmospheric conditions etc. The vertical positioning error is always larger than the planimetric one and can be determined as a function of the used baseline. Finally, the IMU introduces some extra error through the calculation of the orientation angles roll, pitch and yaw, which mainly depends on initialisation errors, misalignment, and gyro drifts and measurement noise.

However, apart from these three instruments, sources of error are also possible misalignments between them. The most studied such errors are the bore-sight error and the lever-arm error. On the one hand, the bore-sight error is associated with the imprecise alignment between the laser scanner and the IMU component and more specifically the small angles that always exist between the IMU and laser scanner coordinate axes. The

bore-sight effects due to roll errors can be detected by projecting the cross-sections of different passes over the same area - when there is more than one. The bore-sight errors due to pitch and yaw, though, cannot be observed from a cross-section view as easily and therefore they must be estimated during an in-flight calibration procedure. On the other hand, the lever-arm offset errors (or vectors) express the linear mounting errors between the laser scanner and the IMU and they result to constant shifts in the derived point cloud to all directions. It can be usually measured quite accurately and therefore it is eliminated. In addition, coordinate system transformations and the temporal interpolation between the laser scanner, the GPS and the IMU are also sources of error.

In this study, the Alpha AL3-32 aerial system by Phoenix LiDAR Systems was used, which consists of the Velodyne HDL-32E laser scanner, a dual-frequency GNSS receiver and the KVH 1750 IMU. According to the manufacturers of these three instruments, the error budget of the system is broken down in the table that follows:

Table 8.1: Error budget of the Alpha AL3-32

Instrument	Type of Error	Value
Laser Scanner	Ranging error	2 cm
	Scan angle error	0.01°
GPS	Horizontal error	1 cm + 1ppm
	Vertical error	150% * horizontal error
IMU	Roll, Pitch angle error	0.015°
	Heading (Yaw angle) error	0.035°

The misalignment errors are neglected by the manufacturer, because the laser scanner and the IMU are fixed to each other through a single flat aluminium part and thus they are considered as perfectly aligned. In addition, the errors introduced by the coordinate system transformation are not taken into account here since no transformation was realised and the temporal interpolation errors were also not investigated due to lack of information.

2. How can the a priori and a posteriori quality of a UAV LS point cloud be derived? With the term quality of a point cloud, the accuracy of its 3D coordinates is implied. The a priori quality can be derived even before the measurements are carried out and is based on the error budget of the system, as suggested by the manufacturers. On the other hand, the a posteriori quality is derived after the flight and is based on the measurements themselves. During this study, for the determination of the a priori positioning accuracy, the error model by Peng et al., [50], was used. This model is created according to the geometry of the ALS measurements and it gives us insight into the quantitative impact of the different sources of error on the 3D coordinate accuracy in the form of x-, y- and z-uncertainties. For the derivation of this accuracy, apart from the error budget of the system, arbitrary values had to be assigned to the range and the orientation angles. For that reason, some typical values for a drone flight were chosen and thus roll was set equal to 10°, pitch equal to 20°, yaw equal to 0° and the range was set 50 metres. With these hypothetical values, the resulting 3D coordinates accuracy was computed as: $m_{X_p} = 0.0173m$, $m_{Y_p} = 0.0184m$ and $m_{Z_p} = 0.0245m$. So, it is concluded that the a priori accuracy of the Alpha AL3-32 aerial system is 2 cm, which is very close to the accuracy level that Phoenix LiDAR systems suggests for this system (2.5-3.5 cm for 50m range).

The a posteriori accuracy was derived using a small dataset of the UAV Laser Scanning point cloud. More specifically, there was the need for a surface with the least possible height variations. The bike path of the study area served this purpose really well. Assuming that the elevations of the points are the same, any height deviations between them are caused by the imperfections of the components of the aerial system

and consequently the vertical a posteriori accuracy can be determined. For that, 25 adjacent boxes were extracted from the denoised point cloud along the 50 m bike path. The dimensions of the boxes were about 2x2 meters and the average number of points contained in each one of them was 3336 points. For each one of these boxes, the mean value and the standard deviation of all the contained points were calculated and some centimetre variations in the mean value were detected, with the minimum value being 47.889 m and the maximum 47.968 m. The standard deviation of all the calculated mean values gives the spread of the mean, and thus the vertical accuracy, which was computed here equal to 2 cm (0.021m). This value is quite close to the value of the a priori vertical accuracy, and it is actually a bit smaller, which means that the accuracy that was achieved in reality was a bit better than predicted. In addition, by calculating the mean of all the standard deviations of the boxes a measure of precision can be derived. That was equal to 0.036 m or more roughly 4 cm. The manufacturer of the system suggests that its precision is approximately 4 cm, when a baseline of 1 Km is assumed, which is really close to the computed precision.

3. How can an accurate Digital Terrain Model (DTM) be generated from such a point cloud? DTMs are among the most useful products that can be derived from a UAV Laser Scanning point cloud, especially when it comes to coastal monitoring. For their generation, at first the point cloud has to be filtered, so that any possible outliers (flying points) and noise can be removed. During this study, that was realised by using the *lasnoise* tool by LAStools, which looks for isolated points according to the criteria *step* and *isolated*. These were set 0.5 m and 10 respectively. What follows is the classification of the remaining points into ground and non-ground. Since a DTM is the representation of the bare earth, only the ground points must be used for its generation. For that, the *lasground* tool was used by specifying the two most important parameters, the *step* and the *spike*. The optimal values for the ground extraction in this study were 1 m for the step and 0.4 m for the spike. Finally, the DTM is generated by performing interpolations between the points with available height information. For that, the *Module Grid* by OPALS was used. The grid size, the interpolation method and the number of neighbours (for the interpolation) are the most critical parameters. Given a point cloud derived with UAV Laser Scanning, which is known to be of high point density, the minimum grid size can be 5 cm and the maximum as required from the application. Regarding the interpolation method, there is a number of different ones. Here, the Nearest Neighbour, the Delaunay Triangulation, the Moving Average and the Moving Planes methods were decided to be presented. Nearest Neighbour is the fastest method, but it is also the simplest, which means that if the study area is complicated, it might not give accurate results. Delaunay Triangulation is concluded to be an unsuitable method, because it is quite slow and it fills in areas that should have no data (due to the triangulation). Finally, the two remaining methods, Moving Average and Moving Planes combine accurate model results with short runtime and thus they are preferred.

4. How can the results derived from the processing of the UAV Laser Scanning dataset be validated with external measurements? The external quality of the derived point cloud as well as the DTM generated from it has to be validated using other kinds of measurements with better accuracy. For that reason, the point cloud is validated with Terrestrial Laser Scanning data of the study area and the DTM using GPS (RTK) data. The TLS data was acquired several months later than the drone flight in the study area and therefore only the data from stable/unchanged objects could be used for validation purposes, while the GPS dataset was provided by Shore Monitoring & Research B.V. and it was acquired on the same day as the test flight.

At first, for the validation of the UAV Laser Scanning point cloud, the parking area of the study area was used, since it is mostly concrete and thus remained unchanged. Three profiles were extracted both from the UAV LS and the TLS point clouds using CloudCompare. These profiles connect specific objects in the study area and thus no registration of the point clouds was needed. After they were matched, the absolute distances in all the axes, X, Y and Z were determined. The absolute differences in Z, which is the axis that we care about

the most, have a mean value of 1mm, 6mm and 3mm for Profile 1, 2 and 3 respectively. These values are quite small, which implies that the two point clouds are almost identical.

Regarding the external quality of the DTM, the GPS data and the selected DTM (grid size:5 cm, interpolation method: Moving Planes and number of neighbours:20) were compared in the environment of QGIS and their differences were found to span from 0 to almost 12 cm, with the highest differences appearing close to the breakwaters, due to the wet vegetation that covers them, but also near the borders of the DTM. The mean value of these differences was close to 6 cm.

As a general conclusion, UAV Laser Scanning is a very suitable technique for coastal monitoring. It can provide us with a very dense point cloud with maintaining high accuracy and precision. In addition, we can derive DTMs with a high level of detail and good accuracy. Other advantages are the fact that it does not depend on the weather or the available light and it does not require GCPs. This fact makes it time- and cost-efficient when compared to the other remote sensing techniques currently used for coastal monitoring.

8.2. Recommendations

The present thesis fulfils the initial goals set for the investigation of UAV Laser Scanning as a tool for coastal monitoring. However, with certain additional studies we could get even more insight into the method and its potential for highly accurate results. The main ideas for future research are discussed in the paragraphs below.

Analysis of random errors in UAV Laser Scanning measurements. As mentioned in Section 5.1.2, except for the blunders and the systematic errors, random errors are also present in the UAV Laser Scanning measurements. They are introduced by the instruments that such a system consists of, namely the laser scanner, the GPS and the IMU, and they are affected by a variety of complex internal and external interferences during the measurement procedure. Random errors cannot be fully eliminated, but they can be minimised by least-square solution and redundant observations. Through their investigation and the quantitative evaluation of their impact on the 3D coordinate accuracy, the UAV LS accuracy can be further improved and therefore it is quite important to look into them.

Strip adjustment of UAV Laser Scanning data. When a UAV flight is carried out, the different flight strips that it follows have always an overlap - usually 20% but it can vary depending on the survey. That happens in order to ensure there are no gaps in the derived point cloud, but also in order to use this overlapping areas for systematic errors compensation. Using these areas in combination with Ground Control Points a re-calibration of the aerial system is possible. Fig. 8.1 shows an example of a part of a point cloud before and after the strip adjustment.

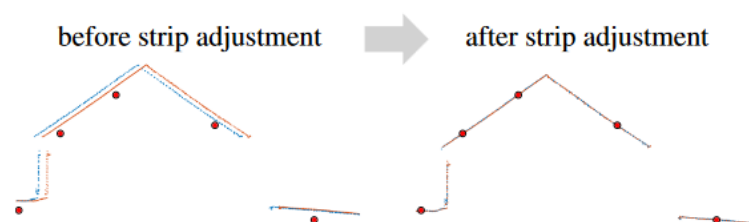


Figure 8.1: The discrepancies between overlapping strips (blue/orange) and between strips and ground control points (red) are minimised simultaneously by strip adjustment. Source:[23]

The left image illustrates the differences between two adjacent flight strips and their deviation from the ground truth data and the right one the result after the adjustment. This procedure can result to more accurate results and thus it is highly recommended to be investigated.

Investigation of temporal interpolation errors. During the operation of a UAV Laser Scanning system, its different components record data with different frequencies. When talking in particular for the Alpha AL3-32 aerial system, the Velodyne HDL-32e laser scanner can operate with a frequency of 5-20 Hz. That is specified by the user and it is usually set to 10 Hz. At the same time, the sampling rate of the KVH 1750 IMU can vary from 1 to 1000 Hz, which is also set by user, but the default frequency is 1000 Hz. Finally, the GPS receiver operates with a sampling rate of 20 Hz. The fact that all three main components record with different frequencies means that interpolations have to be performed for generating the ready to use file. This procedure introduces some additional errors to the data that add up to the total error budget of the system. For that reason, it would be useful to take a closer look into the raw data of each components, find out how the interpolations are performed so that these additional errors can be identified and quantified.

Generation of Vegetation Height Map. One of the strongest points of UAV Laser Scanning that its capability to penetrate through vegetation. This characteristic makes it a very useful technique for vegetation mapping. More specifically, when one laser pulse is emitted, multiple echoes (returns) are received by the laser scanner. These returns correspond to different layers of the vegetation and the last one correspond to the terrain. In this way, apart from the ground, we also get information about the vegetation and its form. Analysing the different characteristics of the echoes, we can even distinguish different types of vegetation (different types of trees). For the derivation of a Vegetation Height Map, all the points that belong to the ground are filtered out from the point cloud and only the above ground points are mapped. An example of such a map derived with ALS data is illustrated in Fig. 8.2. The production of a high-resolution Vegetation Height Map can be a very useful tool for mapping the vegetation on the dunes, and by comparing Vegetation Height Maps from different epochs, we can get insight into the evolution and the seasonal changes of the vegetation on the dunes.

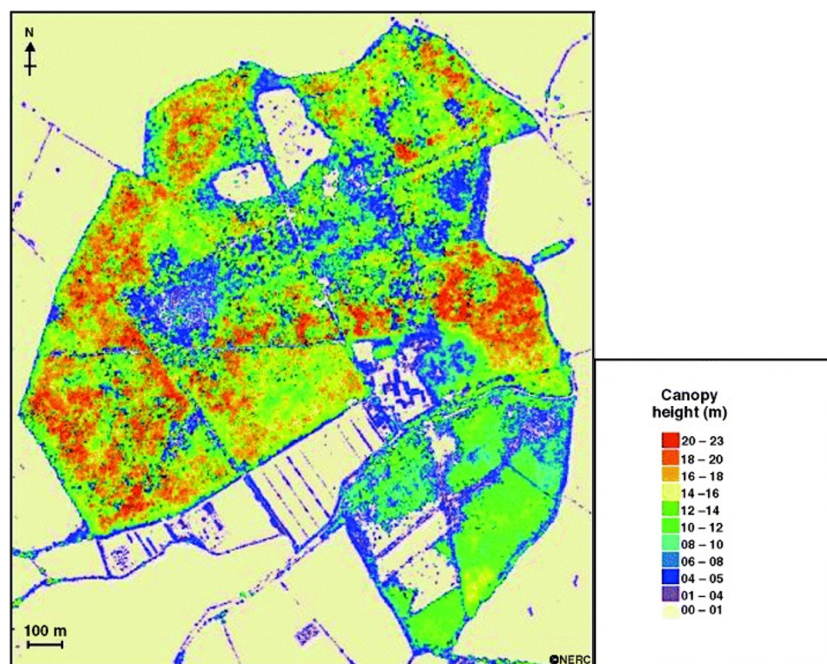


Figure 8.2: Vegetation height map of Monks Wood derived from the ALS data. Source:[25]

Bibliography

- Airborne Drones (2017). SENTINEL + LiDAR. <https://www.airbornedrones.co/products/sentinel-lidar>. Retrieved on May 15, 2017.
- ArcGIS (2016). Lidar point classification. <http://desktop.arcgis.com/en/arcmap/10.3/manage-data/las-dataset/lidar-point-classification.htm>. Retrieved on April 2, 2017.
- Axelsson, P. (2000). Dem generation from laser scanner data using adaptive tin models. *International Archives of Photogrammetry and Remote Sensing*, 33(B4/1; PART 4):111–118.
- Baily, B. and Nowell, D. (1996). Techniques for monitoring coastal change: a review and case study. *Ocean & Coastal Management*, 32(2):85 – 95.
- Baltsavias, E. P. (1999a). Airborne laser scanning: basic relations and formulas. *ISPRS Journal of Photogrammetry and Remote Sensing*, 54(2–3):199–214.
- Baltsavias, E. P. (1999b). A comparison between photogrammetry and laser scanning. *ISPRS Journal of photogrammetry and Remote Sensing*, 54(2):83–94.
- Bitenc, M. (2010). Evaluation of a laser land-based mobile mapping system for measuring sandy coast morphology.
- Corrigan, F. (2015). UAVs In The LiDAR Applications Sector Increases Substantially. <https://www.dronezon.com/learn-about-drones-quadcopters/uav-lidar-applications-services-technology-systems/>. Retrieved on May 14, 2017.
- Dashora, A., Lohani, B., and Deb, K. (2013). Two-step procedure of optimisation for flight planning problem for airborne lidar data acquisition. *International Journal of Mathematical Modelling and Numerical Optimisation*, 4(4):323–350.
- Deltares (2015). ARGUS Video monitoring for coastal management and engineering. Brochure.
- Deltares (2017). ARGUS video systems. <https://www.deltares.nl/en/projects/argus-video-systems/>. Retrieved on May 23, 2017.
- Dent, S. (2014). What you need to know about commercial drones. <https://www.engadget.com/2014/06/13/commercial-drone-explainer/>. Retrieved on May 15, 2017.
- DJI (2017). Spreading Wings S1000. www.dji.com/spreading-wings-s1000/feature. Retrieved on May 16, 2017.
- Doneus, M. and Briese, C. (2006). Full-waveform airborne laser scanning as a tool for archaeological reconnaissance. *BAR International Series*, 1568:99.
- dos Santos, A. L. S., Amaro, V. E., and Santos, M. S. T. (2014). Terrestrial laser scanner applied to monitoring beach morphological changes in a high energy coastal zone in northeast brazil.
- Dronelife (2014). CybAero Receives \$100M Contract for UAV helicopters. <http://dronelife.com/2014/07/09/cybaero-receives-100m-contract-uav-helicopters/s>. Retrieved on May 15, 2017.

- Edelman, T. and Eggink, D. (1962). Some characteristics of the dutch coast. *Coastal Engineering Proceedings*, 1(8):41.
- Eisenbeiss, H. (2004). A mini unmanned aerial vehicle (UAV): System overview and image acquisition. *International Archives of Photogrammetry, Remote Sensing and Spatial Information Sciences*, 36(5/W1).
- Environmental Agency and Authorities, Maritime Local (2010). The coastal handbook.
- Geosystems, L. (2016). Leica scanstation c10 – the all-in-one laser scanner for any application. <http://leica-geosystems.com/products/laser-scanners/scanners/leica-scanstation-c10>. Retrieved on February 5, 2017.
- GIM International (2017). UAS-based Lidar: A Market Update. <https://www.gim-international.com/content/news/uas-based-lidar-a-market-update>. Retrieved on May 16, 2017.
- Glennie, C. (2007). Rigorous 3d error analysis of kinematic scanning lidar systems. *Journal of Applied Geodesy jag*, 1(3):147–157.
- Glira, P., Pfeifer, N., Briese, C., and Ressel, C. (2015). Rigorous strip adjustment of airborne laserscanning data based on the icp algorithm. *ISPRS Annals of Photogrammetry, Remote Sensing & Spatial Information Sciences*.
- Habib, A. and Rens, J. (2007). Quality assurance and quality control of lidar systems and derived data. In *University of Northern Iowa, Advanced Lidar Workshop*.
- Hinsley, S., Hill, R., Gaveau, D., and Bellamy, P. (2002). Quantifying woodland structure and habitat quality for birds using airborne laser scanning. *Functional Ecology*, 16(6):851–857.
- Hoffmeister, D., Tilly, N., Curdt, C., Aasen, H., Ntageretzis, K., Hadler, H., Willershäuser, T., Vött, A., and Bareth, G. (2012). Terrestrial laser scanning for coastal geomorphologic research in western greece. In *International Archives of the Photogrammetry, Remote Sensing and Spatial Information Sciences. XXII ISPRS Congress, Melbourne*. <http://dx.doi.org/10.5194/isprsarchives-XXXIX-B5-511-2012>.
- Hyypä, H., Yu, X., Hyypä, J., Kaartinen, H., Kaasalainen, S., Honkavaara, E., and Rönholm, P. (2005). Factors affecting the quality of dtm generation in forested areas. *International Archives of Photogrammetry, Remote Sensing and Spatial Information Sciences*, 36(3/W19):85–90.
- Isenburg, M. (2015). Clone wars and drone fights. <https://rapidlasso.com/category/uav/>. Retrieved on January 04, 2017.
- Julius, A., Parks, M., Unit, R., and Jonsson, S. (2005). Monitoring programme for resource condition, environmental and biological parameters for mnazi bay-ruvuma estuary marine park (mbrem) tanzania. *Reykjavik, Iceland*.
- Kabat, P., Fresco, L. O., Stive, M. J., Veerman, C. P., Van Alphen, J. S., Parmet, B. W., Hazeleger, W., and Katsman, C. A. (2009). Dutch coasts in transition. *Nature Geoscience*, 2(7):450–452.
- Karel, W. and Kraus, K. (2006). Quality parameters of digital terrain models.
- KVH (2017). 1750 IMU. <http://www.kvh.com/Military-and-Government/Gyros-and-Inertial-Systems-and-Compasses/Gyros-and-IMUs-and-INS/IMUs/1750-IMU.aspx>. Retrieved on May 16, 2017.
- Lemmens, M. (2011). *Geo-information: technologies, applications and the environment*, volume 5. Springer Science & Business Media.

- LiDAR-UK.com (2017). The uses of LiDAR. What applications are there for LiDAR systems? <http://www.lidar-uk.com/usage-of-lidar/>. Retrieved on May 15, 2017.
- Low, C. (2016). You can buy Parrot's fixed-wing Disco drone in September. <https://www.engadget.com/2016/08/23/you-can-buy-parrots-fixed-wing-disco-drone-in-september/>. Retrieved on May 15, 2017.
- Maas, H.-G. (2003). Planimetric and height accuracy of airborne laserscanner data: User requirements and system performance. In *Proceedings*, volume 49, pages 117–125. Citeseer.
- Malthus, T. J. and Mumby, P. J. (2003). Remote sensing of the coastal zone: An overview and priorities for future research. *International Journal of Remote Sensing*, 24(13):2805–2815.
- Mapix Technologies Ltd (2017). UAV LidarPod. <http://www.routescene.com/products/product/uav-lidarpod/>. Retrieved on May 16, 2017.
- Marchand, M. (2010). Concepts and science for coastal erosion management.
- Mills, J. P., Buckley, S. J., Mitchell, H. L., Clarke, P. J., and Edwards, S. J. (2005). A geomatics data integration technique for coastal change monitoring. *Earth Surface Processes and Landforms*, 30(6):651–664.
- NASA. Glenn Research Center (2015). Aircrafts rotations - Body Axes. <https://www.grc.nasa.gov/WWW/K-12/airplane/rotations.html>. Retrieved on May 16, 2017.
- National Oceanic and Atmospheric Administration (NOAA) (2015). What is lidar? <http://oceanservice.noaa.gov/facts/lidar.html>. Retrieved on January 04, 2017.
- Navigation, T. (2003). *Trimble® R7 GPS Receiver*. Trimble Navigation, 5475 Kellenburger Road Dayton, Ohio 45424-1099, U.S.A.
- (NHV), N. H. S. and of the International Association of Hydrological Sciences (IAHS), N. N. C. (1998). Water in the netherlands.
- OCAD (2016). Dem. <http://www.ocad.com/wiki/ocad11/en/?title=DEM>. Retrieved on March 18, 2017.
- OPALS (2015). Module icp. <http://www.ipf.tuwien.ac.at/opals/html/ModuleICP.html>. Retrieved on March 14, 2017.
- OPALS (2016). Module grid. <http://geo.tuwien.ac.at/opals/html/ModuleGrid.html>. Retrieved on March 18, 2017.
- OPALS (2017). Opals datamanager. http://www.ipf.tuwien.ac.at/opals/html/ref_odm.html. Retrieved on April 5, 2017.
- PCL (2016). Removing outliers using a statisticaloutlierremoval filter. http://pointclouds.org/documentation/tutorials/statistical_outlier.php. Retrieved on March 13, 2017.
- Peng, T., Lan, T., and Ni, G. (2013). Motion error analysis of the 3d coordinates of airborne lidar for typical terrains. *Measurement Science and Technology*, 24(7):8.
- Phoenix Aerial Systems (2014). Introducing the AL3-32. <http://old.phoenix-aerial.com/products/lidar-systems/al3-32/>. Retrieved on May 16, 2017.
- Phoenix Aerial Systems (2017). Alpha Series AL3-32. <https://www.phoenixlidar.com/al3-32/>. Retrieved on May 16, 2017.

- Phoenix LiDAR Systems (2016). Alpha series al3-32. <https://www.phoenixlidar.com/al3-32/>. Retrieved on December 2, 2016.
- Pilarska, M., Ostrowski, W., Bakula, K., Górski, K., and Kurczyński, Z. (2016). The potential of light laser scanners developed for unmanned aerial vehicles—the review and accuracy. *International Archives of the Photogrammetry, Remote Sensing & Spatial Information Sciences*, 42.
- RIEGL Laser Measurement Systems GmbH (2017a). BathyCopter. <http://www.riegl.com/products/unmanned-scanning/newbathycopter/>. Retrieved on May 16, 2017.
- RIEGL Laser Measurement Systems GmbH (2017b). RiCOPTER. <http://www.riegl.com/products/unmanned-scanning/ricopter/>. Retrieved on May 16, 2017.
- RIEGL Laser Measurement Systems GmbH (2017c). RiCOPTER with VUX-SYS. <http://www.riegl.com/products/unmanned-scanning/ricopter-with-vux-sys/>. Retrieved on May 16, 2017.
- RIEGL Laser Measurement Systems GmbH (2017d). RIEGL miniVUX-1UAV. <http://www.riegl.com/products/unmanned-scanning/new-riegl-minivux-1uav//>. Retrieved on May 16, 2017.
- RIEGL Laser Measurement Systems GmbH (2017e). RIEGL VUX-1UAV. <http://www.riegl.com/products/unmanned-scanning/riegl-vux-1uav/>. Retrieved on May 16, 2017.
- RIEGL Laser Measurement Systems GmbH (2017f). *Riegl VUX-SYS*. RIEGL Laser Measurement Systems GmbH, Riedenburgstraße 48, 3580 Horn, Austria.
- Schmidt, A., Rottensteiner, F., and Sörgel, U. (2013). Monitoring concepts for coastal areas using lidar data. *International Archives of the Photogrammetry, Remote Sensing and Spatial Information Sciences-ISPRS Archives 40 (2013)*, 40(1W1):311–316.
- Shorelines, M. E. and on Nearshore Areas, S. I. (2005). A case study documenting coastal monitoring and modelling techniques in the netherlands.
- Sibson, R. (1981). A brief description of natural neighbor interpolation. *Interpreting multivariate data*, pages 21–36.
- SISTERMANS, P. and NIEUWENHUIS, O. (2004). Holland coast (the netherlands). *EUROSION Case Study. DHV group*.
- Sithole, G. and Vosselman, G. (2004). Experimental comparison of filter algorithms for bare-earth extraction from airborne laser scanning point clouds. *ISPRS journal of photogrammetry and remote sensing*, 59(1):85–101.
- Srinivasan, S., Popescu, S. C., Eriksson, M., Sheridan, R. D., and Ku, N.-W. (2015). Terrestrial laser scanning as an effective tool to retrieve tree level height, crown width, and stem diameter. *Remote Sensing*, 7(2):1877.
- Stive, M. J., Aarninkhof, S. G., Hamm, L., Hanson, H., Larson, M., Wijnberg, K. M., Nicholls, R. J., and Capobianco, M. (2002). Variability of shore and shoreline evolution. *Coastal Engineering*, 47(2):211 – 235. Shore Nourishment in Europe.
- Sutherland, J. (2007). Inventory of coastal monitoring methods and overview of predictive models for coastal evolution.
- Systems, P. A. (2014). Accuracy explained. <http://old.phoenix-aerial.com/information/accuracy-explained/>. Retrieved on March 27, 2017.

- Tang, L. and Shao, G. (2015). Drone remote sensing for forestry research and practices. *Journal of Forestry Research*, 26(4):791–797.
- Van der Graaf, S. (2016). Natural neighbour kriging and its potential for quality mapping and grid design.
- Velodyne LiDAR (2016). *HDL-32E. High-definition LiDAR Sensor*. Velodyne LiDAR, 345 Digital Drive Morgan Hill, CA 95037, USA.
- Velodyne LiDAR (2017). PUCK.VLP-16. <http://velodynelidar.com/vlp-16.html>. Retrieved on May 15, 2017.
- Vosselman, G. and Maas, H.-G. (2010). *Airborne and terrestrial laser scanning*. Whittles Publishing, Dunbeath.
- Wang, J., Xu, L., Li, X., and Tian, X. (2011). Impact analysis of random measurement errors on airborne laser scanning accuracy. In *Instrumentation and Measurement Technology Conference (I2MTC), 2011 IEEE*, pages 1–4. IEEE.
- Wang, Z., Shu, R., Xu, W., Pu, H., Yao, B., et al. (2008). Analysis and recovery of systematic errors in airborne laser system. *International Archives of the Photogrammetry, Remote Sensing and Spatial Information Sciences*, 37(B1):289–294.
- Wehr, A. and Lohr, U. (1999). Airborne laser scanning—an introduction and overview. *ISPRS Journal of photogrammetry and remote sensing*, 54(2):68–82.
- Wikipedia (2016). Intertidal zone — Wikipedia, the free encyclopedia. https://en.wikipedia.org/wiki/Intertidal_zone. Retrieved on February 2, 2017.
- Wikipedia (2017a). Accuracy and precision — Wikipedia, the free encyclopedia. https://en.wikipedia.org/wiki/Accuracy_and_precision. Retrieved on May 25, 2017.
- Wikipedia (2017b). Estuary — Wikipedia, the free encyclopedia. <https://en.wikipedia.org/wiki/Estuary>. Retrieved on April 24, 2017.
- Wikipedia (2017c). Inertial measurement unit — Wikipedia, the free encyclopedia. https://en.wikipedia.org/wiki/Inertial_measurement_unit. Retrieved on May 15, 2017.
- Xiaohong, Z. and Jingnan, L. (2004). Analysis of systematic error influences on accuracy of airborne laser scanning altimetry. *Geo-spatial Information Science*, 7(3):218–224.
- Yang, C.-S., Kao, S.-P., Lee, F.-B., and Hung, P.-S. (2004). Twelve different interpolation methods: A case study of surfer 8.0. In *Proceedings of the XXth ISPRS Congress*, volume 35, pages 778–785.
- YellowScan (2017a). What is all-integrated LIDAR systems for UAV? <http://www.yellowscan.fr/products>. Retrieved on May 15, 2017.
- YellowScan (2017b). YellowScan Mapper. <http://www.yellowscan.fr/products/yellowscan-mapper>. Retrieved on May 16, 2017.
- YellowScan (2017c). YellowScan Surveyor. <http://www.yellowscan.fr/products/yellowscan-surveyor>. Retrieved on May 16, 2017.
- Yuan, F., Li, G., Zuo, Z., Li, D., Qi, Z., Qiu, W., and Tan, J. (2014). Airborne lidar borsight error calibration based on surface coincide. In *IOP Conference Series: Earth and Environmental Science*, volume 17, page 012185. IOP Publishing.